CIRCULAR RNA FUNCTIONS IN VASCULAR SMOOTH MUSCLE PHENOTYPIC MODULATION AND VASCULAR REMODELING

by

XIAOHAN MEI

(Under the Direction of Shi-You Chen)

ABSTRACT

Vascular remodeling resulting from the smooth muscle cell (SMC) phenotypic switching from a quiescent state to a proliferative state is a crucial pathological process following vascular injury, which often occurs after percutaneous coronary intervention, cardiac transplantation, and bypass surgery. Therefore, identifying novel targets that regulate SMC phenotypic modulation and vascular remodeling is pivotal for developing new therapeutic strategies. Recently, circular RNA (circRNA), a novel type of non-coding RNA with closed-loop structure, has been discovered, displaying high stability and cell- and disease-specific expression patterns. The objective of this study is to determine the role and mechanism of circular Superoxide Dismutase 2 (circSOD2) and circular Cysteine-Rich Motor neuron 1 (circCRIM1) in SMC phenotypic modulation and vascular remodeling.

Using next-generation sequencing (NGS), we have identified circSOD2 and circCRIM1 as our targets highly expressed in platelet-derived growth factor-BB (PDGF-BB)-induced SMC. Blockade or forced expression of circSOD2 suppresses and promotes SMC proliferation, respectively. Mechanistically, in SMC, circSOD2 can act as a micro RNA 206 (miR-206) sponge which is an upstream inhibitory factor of NOTCH3 and consequently boosts phosphorylation of

extracellular signal-regulated protein kinase 1/2 (ERK1/2), leading to the increase of SMC G1-to-S cell cycle transition and eventually promotes SMC proliferation. In vivo, suppression of circSOD2 decreases injury-induced neointimal formation, indicating targeting circSOD2/miR-206/NOTCH3 axis may be a promising strategy to hinder injury-induced vascular remodeling in proliferative vascular diseases.

We also demonstrate for the first time that circCRIM1 is involved in SMC phenotypic modulation and has the capability of continuous loop-translation encoding a protein. Knockdown or overexpression of circCRIM1 restores and further suppresses PGDF-BB induced downregulation of SMC marker genes, respectively. Mechanistically, circCRIM1 can bind with miR-16 to modulate SMC phenotypic modulation. Using liquid chromatography-mass spectrometry (LC/MS), we have identified circCRIM1 encoded protein. Furthermore, circCRIM1 translation is found to be driven by N^6-Methyladenosine (m^6A) modification and recognized explicitly by YTH domain-containing family protein 3 (YTHDF3). Our results suggest that circCRIM1 is a novel regulator for SMC phenotypic modulation with continuous loop translation ability.

INDEX WORDS: Vascular remodeling, Smooth muscle cell, phenotypic modulation, circRNA, circSOD2, circCRIM1, platelet-derived growth factor-BB, miR-206, cell cycle, NOTCH3, ERK1/2, neointima formation, continuous loop-translation, miR-16, m^6A modification, YTHDF3, Smooth muscle cell differentiation.

CIRCULAR RNA FUNCTIONS IN VASCULAR SMOOTH MUSCLE PHENOTYPIC MODULATION AND VASCULAR REMODELING

by

XIAOHAN MEI

BS, NANJING FORESTRY UNIVERSITY, CHINA, 2013

A Dissertation Submitted to the Graduate Faculty of The University of Georgia in Partial Fulfillment of the Requirements for the Degree

DOCTOR OF PHILOSOPHY

ATHENS, GEORGIA

2021

CIRCULAR RNA FUNCTIONS IN VASCULAR SMOOTH MUSCLE PHENOTYPIC MODULATION AND VASCULAR REMODELING

by

XIAOHAN MEI

Major Professor: Shi-You Chen

Committee: Wan-I Oliver Li
Rabindranath De La Fuente

Electronic Version Approved:

Ron Walcott

Dean of the Graduate School

The University of Georgia

May 2021

ACKNOWLEDGEMENTS

It has been a long journey for me in pursuit of a doctoral degree at the University of Georgia. This would not have been possible without the support of many great individuals.

I first would like to pay my special regards and deep gratitude to my supervisor, Dr. Shiyou Chen, who has always been inspiring and supportive and encouraging me to be professional. His scientific attitude and the passion for work is the most precious gift I received from him. I am honored and grateful to be given the opportunity to work with Dr. Chen in an incredible lab that is always helpful and warm. His generous and genuine personality benefit people being around him.

I wish to express my sincere appreciation to my committee members, Dr. Wan-I Oliver Li and Dr. Rabindranath De La Fuente. Their insightful comments and valuable suggestions throughout the years not only have benefited my research but also broadened my horizon. I am honored to have the privilege of having them served on my advisory committee.

I would also like to acknowledge my lab members and lab alumni, Xiaobing Cui, Ning Shi, Wei Jia, Yung-Chun Wang, Dunpeng Cai, Ruimei Zhou, Gui Zhang, Kun Dong, Rui Tang, Sisi Chen, Li Li, Xia Guo, and Chengming Sun, for their pleasant collaborations and enlightening discussions.

Finally, I would like to give my most sincere gratitude to my beloved family. I am deeply grateful to my parents. Without the education they taught me and the continuous, selfless supports, I cannot make this accomplishment today. Also, I want to thank my lovely wife, Dr. Yiran Li, who has always supported me without a doubt. Your love is the fresh breath and starry night in the time of difficulties. “We have no idea where we're going / Lodged in life / Like branches in a river/ Flowing downstream / Caught in the current / I carry you / You'll carry me /.” And, thanks to my cat, Peaches, and dog, Chagall, for their devoted companion.

TABLE OF CONTENTS

Page

LIST OF TABLES

Page

LIST OF FIGURES

Page

CHAPTER 1

INTRODUCTION

Problem Statement

Cardiovascular diseases (CVDs) are the leading causes of morbidity and mortality worldwide and the significant factors to impact the quality of life. Despite recent declines in CVD morbidity and mortality due to the improvement in public health care and advances in precision medicine, for all groups, the decline of CVD mortality rate is showing a deceleration trend. Cardiovascular intervention, such as percutaneous coronary intervention (PCI), is a widely used technique for treating obstructive coronary artery disease. However, the procedure of PCI and the application of the intervention device cause a relatively high rate of restenosis, majorly due to vascular remodeling and neointimal hyperplasia.

Neointimal hyperplasia (NH) is a pathological response after the intervention. It is caused by the proliferation and migration of vascular smooth muscle cells (VSMCs) from the media layer into the tunica intima layer, thickening the vascular wall, depriving luminal patency, and eventually leading to the return of vascular insufficiency symptoms. Many cardiovascular diseases are provoked by NH, such as hypertension, atherosclerosis, abdominal aortic aneurysm, and diabetic vascular complications. Upon vascular injury, denudation of endothelium exposes VSMCs in the media layer to various growth factors and inflammatory cytokines, causing the de-differentiation of VSMC from a contractile to a proliferative phenotype and contributing to neointimal

thickening and vessel narrowing. Therefore understanding the underlying mechanism of VSMC phenotypic modulation and vascular remodeling is crucial for identifying therapeutic targets. Recently, a novel type of non-coding RNA, circular RNA (circRNAs) with covalently closed-loop, has been elucidated widely expressed in eukaryotes and exhibits surprisingly high stability, diverse biological functions, and disease-specific expression patterns. However, the role of circRNAs in VSMC phenotypic modulation and vascular remodeling is largely unknown.

Objective, Hypotheses and Specific Aims

Currently, circRNAs have been implicated in vast numbers of species and diseases. But the expression profiles and molecular regulatory roles of circRNAs in VSMCs are still unknown.

Our first aim is to generate VSMC genome-wide profiling of circRNAs by next-generation sequencing (NGS) and identify circRNA candidates involved in VSMC phenotypic modulation and vascular remodeling.

Our second aim is to test the hypothesis that a circRNA candidate, circular Superoxide Dismutase 2 (circSOD2), regulates VSMC proliferation and injury-induced neointimal hyperplasia. We will determine if circSOD2: 1) is involved in platelet-derived growth factor-BB (PDGF-BB) induced VSMC proliferation; 2) mediates balloon-injury neointimal formation. We also will investigate the underlying molecular mechanism and signaling pathways of circSOD2 regulation of VSMC proliferation and neointima formation.

Our third aim is to test the hypothesis that another circRNA candidate, circular Cysteine-Rich Motor neuron 1 (circCRIM1), regulates VSMC phenotypic switching, injury-induced neointimal hyperplasia, and can perform loop-translation to encode a novel protein. We will determine if

circCRIM1: 1) is involved in platelet-derived growth factor-BB (PDGF-BB) induced VSMC phenotypic switching; 2) mediates balloon-injury neointimal formation. We also will investigate the underlying molecular mechanism and signaling pathways of circCRIM1 regulation of VSMC phenotypic switching and neointima formation. Moreover, we will reveal the mechanism of circCRIM1 loop-translation and identify the circCRIM1-encoded protein.

CHAPTER 2

LITERATURE REVIEW

In eukaryotes, precursor mRNAs produce a unique class of biologically active molecules, namely circular RNAs (circRNAs) with a covalently closed-loop structure via back-splicing. Because of this unconventional circular form, circRNAs exhibit much higher stability than linear RNAs due to the resistance to exonuclease degradation and thereby play exclusive cellular regulatory roles. Recent studies have shown that circRNAs are widely expressed in eukaryotes and display tissue- and disease-specific expression patterns, including in the cardiovascular system. Although numerous circRNAs are discovered by in silico methods, a limited number of circRNAs have been studied. This review intends to summarize the current understanding of the characteristics, biogenesis, and functions circRNAs and delineate the practical approaches for circRNAs investigation. Moreover, we discuss the emerging roles of circRNAs in cardiovascular diseases.

Introduction

Transcriptomic analyses have revealed that human genome can transcribe ~90% of the genomic DNA, but only 1-2% of transcripts encode proteins, whereas a large amount of the transcripts are categorized as noncoding RNA (ncRNAs)[1]. Emerging evidence has shown that aberrant ncRNA expression is associated with a number of diseases, including developmental, oncological,

neurological, cardiovascular, autoimmune, and cutaneous disorders[2-11]. Recently, a novel class of ncRNA, circRNA, has drawn much attention from researchers in different fields, ascribed to its unusual structure and diverse biological features. The first circular form of RNA molecule was reported in 1976, due to the discovery of plant viroids that are covalently closed circular RNA molecules. Two ends of viroids were ligated by host cellular enzymes[12]. Since then, sporadic studies have identified a number of circRNAs in different species such as humans, mice, and rats, although most of them were considered as byproducts of RNA splicing or so-called "scrambled exons"[13-18]. In the 2000s, advances in next-generation sequencing (NGS) and computational pipelines led to an explosion of RNA-related researches and the scale of NGS datasets[19]. However, due to the lack of polyadenylation tail (poly-A tail), circRNAs have not caught the attention of scientists in the first wave of NGS, which has mainly focused on the polyadenylated transcriptomes. Starting in the early 2010s, new pre-sequencing approaches were developed to preserve non-polyadenylated RNAs, which revealed that circRNAs are expressed in many species, including mice, rats, pigs, monkeys, humans, zebrafish, and fruitflies, as well as plants, fungi, and protists, etc[20-33]. So far, more than 183,000 circRNAs have been identified in human tissues/cells[34]. Unlike linear mRNAs that are generated from precursor mRNAs (pre-mRNAs) and undergo normal splicing following RNA polymerase II (Pol II)-mediated transcription, circRNAs are formed via back-splicing, in which a downstream 5′ splice site is ligated to an upstream 3′ splice site across exon or exons[35, 36]. Besides, intron lariats derived from the normal splicing process erratically escape from debranching at times and cause a circular formation and are referred as circular intronic RNAs (ciRNAs)[37]. Additionally, another type of circRNAs called exon-intronic circRNA or exon-intron-containing-circular-RNAs (EIciRNAs) are predominantly localized in the nucleus and retrain intronic information. This type of

circRNAs is largely caused by escaping of EIciRNAs from decompression of debranching enzymes following splicing based on the nucleotide information in these introns[38, 39].

Given the unique characteristics, circRNAs exhibit excellent stability compared to the linear mRNA transcripts because they are resistant to exonucleolytic decay by the exosome ribonucleases[40]. The average half-life of circRNAs ranges from 19 to 48 hours, whereas linear RNA transcripts only have a life time of 4-9 hours [21, 41, 42]. Therefore, despite a relatively low expression level compared to the linear RNAs, circRNAs have shown disease- and tissue-specific expression patterns and extraordinary potential in modulating the pathogenesis of diseases, such as oncological, cardiovascular, neurodegenerative, and immune disorders[43-46]. In this review, we provide an overview of the recent progresses in circRNA biology, including characteristics, biogenesis, and functions of circRNAs, as well as strategies for investigating circRNAs and up-to-date available online resources. Moreover, the emerging roles of circRNAs in cardiovascular diseases are discussed.

Characteristics of circRNAs

circRNAs are considered to be very diverse and referred as a heterogeneous class of RNAs. The co- or post-transcriptional back-splicing processes the circularization of RNA molecules[47]. A circRNA typically consists of exons only, introns only, or a mixture of exons and introns. Using NGS, Zhang et al. revealed several key genomic features of circRNAs. Even though particular motifs are not required, single exon circularization has to meet the minimal length requirement. The median exon length of single exonic circRNAs is 353 nucleotides, which is much longer compared to the exon length of muti-exon circRNAs, which is 112 to 130 nucleotides in

human[29]. In addition, the vast majority of human circRNAs contain more than one exon, usually two or three, and most of these exons are not derived from the first and last exon, but exons located in the middle of reference genes[29]. The median length of circRNAs containing multiple exons is about 500-700 nucleotides[21, 48, 49], which is confirmed by a cryo-electron microscopy structural study of the yeast spliceosomal E complex[50]. The study shows that back-splicing is catalyzed by exon-definition complexes (such as spliceosomal E complex) on long exons (more than 300 nucleotides) or multiple exons which are not remodeled to intron-spanning complexes[50]. Generally, circRNAs are expressed at a relatively low level[25, 26, 29, 36], mainly because the efficiency of back-splicing of circRNAs is lower than that of canonical splicing although the kinetics of back-splicing may change under certain circumstances[51]. Additionally, during the circularization, the ligation pattern, i.e., a downstream 5′ splice site joining with an upstream 3′ splice site, is sterically unfavorable, which may also cause the low efficiency of back-splicing[21, 51].

It is well-known that humans and mice share nearly all their genes and, on average, 85% of genes are identical[52]. However, there are much fewer circRNAs in common between humans and mice. Only 5% to 30% of mouse circRNAs have human orthologs[21, 49]. Similarly, about 15% to 20% of porcine circRNAs in pig brain share orthologous splice sites with circRNAs in the mouse brain. Likewise, 5 to 10% of human brain circRNAs are found in pig brain, although the overlapping for highly expressed circRNAs could reach to 15% [53]. The similar circRNAs observed in different species suggest that circRNAs may regulate common functions among different eukaryotic cells [54].

The genomic origins of circRNAs are overlapped with coding sequences (CDS), 5′-untranslated region (UTR), 3′-UTR, and ncRNA. Most circRNAs are derived from CDS[21, 49, 55]. However, not

all genes have circRNA counterparts. Multiple studies have also shown that circRNAs have different gene coverage in the human brain, fibroblast-like cells, leukocytes, and heart tissues, with the percentage of 20%, 14%, 10%, and 9%, respectively[21, 22, 48, 49]. In addition, increasing numbers of circRNA NGS datasets indicate that highly proliferative cells such as cancer cells contain less circRNAs than fully differentiated cells such as neuronal cells and aging cells[24, 49]. This may be due to circRNA levels being largely impacted and diluted when cell division takes place, thus suggesting a negative correlation between circRNA levels and cell division rates[18, 44, 56].

Moreover, the majority of circRNAs are expressed at the level of 5-10% compared with the expression level of their linear counterparts due to the low back-splicing efficiency [57]. A small number of circRNAs show a higher level expression level than their linear counterparts in diseased tissue samples as indicated by the circular-to-linear ratio [57]. Although it is largely unknown how some circRNAs can achieve a higher expression than their parental transcripts, CDR1as, a well-known circRNA enriched in the brain, expresses much higher than its counterparts due to the undetectable linear transcript in the NGS dataset.

Biogenesis of circRNAs

Back-splicing is the essential step of circRNA formation, occurs at the co- and post-transcriptional level[47]. As an atypical alternative splicing event, back-splicing of exons is coupled with Pol II-mediated transcription and regulated by spliceosome machinery, evidenced by a study identifying a mutual competition between splicing factor muscleblind (MBL) and circMbl that is derived from MBL linear transcripts[58, 59]. Recent studies have also revealed that

polyadenylation signal is not required for circRNA formation, and a number of nascent circRNAs can be detected only after their corresponding linear pre-mRNA transcription is completed, suggesting that circRNA formation may occur post-transcriptionally[51, 60]. Even though the back-splicing behaves differently with canonical splicing, circRNA formation may require canonical spliceosome machinery and the presence of canonical splicing sites. Indeed, spliceosome inhibitor isoginkgetin blocks circRNA biogenesis[59]. On the other hand, RNAi targeting core spliceosome and transcription termination factors in Drosophila cells, which partially eliminates spliceosomal complexes by U2 small nuclear ribonucleoproteins (snRNP), leads to an increased ratio of circRNA to linear RNA, indicating that RNA production can be directed to alternative splicing pathway, such as back-splicing when traditional splicing is impaired[61, 62]. Unlike canonical linear pre-mRNA splicing in which introns are removed and exons are joined by spliceosomal complex, circRNA back-splicing requires that a donor splice site of exon skips the joining with downstream acceptor splice site but connecting with upstream acceptor splice site[50]. During this process, the downstream splice donor site and upstream acceptor site are bringing into close proximity, forming a closed-loop RNA molecule. The underlying mechanisms of circRNA biogenesis with three well-recognized models are presented in Figure 2.1.

Intronic complementary sequence (ICS)-driven circularization

In circRNA formation, ICSs are often presented as *cis*-acting elements located in the flanking intronic area of exons involved in the back-splicing event, such as nonrepetitive complementary sequence, long interspersed nuclear elements (LINEs), and Alu elements which are known as transposable elements[21, 29, 63]. These ICSs undergo direct base-pairing, bringing two distal splice

sites into proximity. Several studies have observed that ICSs exist on the flanking region of circularized exons, and deletion of ICSs eliminates circRNA production[21, 29, 64]. By shortening two Alu elements flanking exon2 and exon3 of ZKSCAN1 pre-mRNA to 30-40 nucleotides, Liang et al. found that the circularization still occurs as long as the complementary pattern is maintained[64]. However, if multiple ICSs, such as Alu elements, are presented in pre-mRNA intron regions, canonical splicing may compete with back-splicing, leading to a reduction of circRNA production while boosting the linear RNA formation[29, 58]. Likewise, the presence of multiple ICSs may also cause different pairing sites, leading to the diverse formation of circRNAs[65].

RNA binding protein (RBP)-driven circularization

RBPs act as *trans*-regulatory elements that modulate the biogenesis of circRNA[36, 51, 61, 63, 64]. The dimerization or interaction of RBPs bridges distal splice sites and initiates the back-splicing. For example, a study in fruit fly showed that RBP Mbl translated from *Mbl* mRNA promotes the production of circRNA *MBL* from its own pre-mRNA[58]. Another study in fly revealed that a combination of heterogeneous nuclear ribonucleoprotein (hnRNP) and serine-arginine proteins (SR) controls a bunch of circRNA expression[60]. In human cells, during the epithelial-mesenchymal transition, elevated quaking (QKI) level enhances the formation of circRNAs via forming a QKI dimer joining distal splice sites flanking circularized exons[66]. In murine embryonic stem cell-derived motor neurons, knockdown of RBP FUS significantly inhibits circRNA formation but does not affect linear mRNAs[67]. Apart from forming dimers to put two distal splice sites together, RPBs also bind to ICSs to promote back-splicing events, thus increase circRNA production. These RBPs usually contain double-stranded RNA binding domains

(dsRBDs), such as interleukin enhancer-binding factor 3 (ILF3) encoded proteins nuclear factor 90 (NF90) and NF110. Both NF90 and NF110 have strong binding ability with Alu elements. Upon viral infection, a large portion of NF90 and NF110 are retained in the cytoplasm and participate in antiviral immune response while genome-wide nascent circRNA number are significantly decreased, indicating that both NF90 and NF110 are essential for circRNA formation[68]. On the other hand, certain RBPs suppress circRNA biogenesis by sabotaging *cis*-elements base-pairing. One example is adenosine deaminase acting on RNA 1 (ADAR1), which functions via deaminating adenosine to inosines (A-to-I editing) and is involved in multiple disease progression[69]. Upon ADAR1 binding to a pair of Alu elements that flanking the circularized exons, A to I editing destabilizes base-pairing of Alu elements and thus dampens the back-splicing efficiency and decreases circRNA production[63, 70]. ADAR(p150) has been shown to work with DExH-Box helicase 9 (DHX9), an RBP that acts as a resolvase of double-stranded RNAs (dsRNAs). Depletion of DHX9 causes global dsRNA accumulation and upregulation of circRNA level[71].

Lariat-driven circularization

Lariat is a byproduct of pre-mRNA splicing during intron removal or exon skipping, having the 5' end attached to a branch point close to 3' end with a 3' tail[72]. The lariat is further processed to ciRNA by trimming off its 3' tail. The intronic lariats usually are degraded rapidly by debranching enzymes and exonucleases. Zhang et al. discovered the first ciRNA and proposed that spliceosome-mediated intron excision from pre-mRNA produces lariat RNA molecules that can escape from debranching[37]. Subsequent studies found that most stable ciRNAs carry a non-adenosine branch point (mainly cytosine), indicating that debranching enzymes are unable to

cause degradation at these sites[73-75]. In addition, intronic lariats often contain a GU-rich motif near the 5' splice site and C-rich motif at the branch point, which also protects the lariats from debranching, [37].

CircRNA functions, translocation, and degradation

Due to the relatively low abundance of circRNAs, circRNAs initially were thought to be the byproduct of splicing or "junk transcripts"[76]. However, recent blooming studies of circRNAs have completely reshaped the perspective and suggested that circRNAs not only feature unique characteristics but also play potent roles in regulating physiological processes[36, 44, 77].

CircRNAs regulate Pol II-mediated transcription

Once being produced, circRNAs are present in both the nucleus and cytoplasm. The majority of circRNAs that regulate transcription are localized in the nucleus. A Pol II immunoprecipitation study in human cells has identified a vast number of Pol II-interacting circRNAs. Two EIciRNAs, EIciEIF3J and EIciPAIP2, are found to bind with the U1 snRNP and promoter region of the linear cognates and regulate the expression of themselves and their host genes through positive feedback mechanisms [38](Figure 2.2A). In *Arabidopsis thaliana,* circSEP3, a circRNA with a single exon structure, forms an RNA-DNA hybrid with the exon where circSEP3 originated on the host pre-mRNA and cause a transcriptional skip of that exon, leading to a new alternative spliced mRNA[78]. CiRNAs are observed mainly in the nucleus in human cells, functioning *in cis* to regulate Pol II-mediated transcription. Zhang et al. reported that ci-ankrd52

coupling with Pol II elongation complex in human cell nucleus boosts the expression of its host gene counterparts. Depletion of ci-ankrd52 suppresses its host gene expression[37].

CircRNAs sequester miRNAs

Most circRNAs are exported to the cytoplasm, especially exonic circRNAs[79, 80]. Once being exported, circRNAs can act as competing endogenous RNAs (ceRNAs) or miRNA sponges to suppress free miRNAs abundance and consequently prevent target gene from degradation[77] (Figure 2.2B). The most classic example is cerebellar degeneration-related protein 1 antisense RNA (CDR1as, also known as ciRS-7), which is highly enriched in the mammalian brain. Human CDR1as contains 74 binding sites for miR-7 and multiple binding sites for miR-671. In the presence of Argonaute-2 (Ago2), CDR1as can sponge miR-7 to suppressed the inhibitory effect of miR-7 on its target genes[26, 81]. However, CDR1as can be degraded by miR-671, primarily because miR-671 is almost perfectly complementary to CDR1as[82, 83]. Since CDR1as is derived from an antisense RNA nearly undetectable in NGS data, Piwecka et al. generated CDR1as knockout mice by depleting CDR1as host gene using the CRISPR-Cas9 system. Mice with CDR1as depletion show neuropsychiatric disorders with dysfunction of excitatory synaptic transmission, suggesting that brain-enriched CDR1as is critical for maintaining normal brain function[84]. So far, many circRNA candidates have been found to act as miRNAs sponge. However, due to the inequivalent abundance between circRNAs and miRNAs, sponging miRNA with circRNAs is not as common as with linear mRNAs. Therefore, this function may be considered as non-essential or less ubiquitous[25, 44, 85].

CircRNAs act as protein scaffolds and sponge

Similar to other types of ncRNAs, circRNA can also scaffold or sequester proteins to achieve multiple biological purposes (Figure 2.2C)[86]. ccircFoxo3 retards cancer cell cycle progression by harboring cyclin-dependent kinase 2 (CDK2) and cyclin-dependent kinase inhibitor 1 (p21) to form a ternary complex and thus interrupt the interaction between CDK2 and other cyclins[87]. In cardiac tissues, circFoxo3 promotes cardiac-cell senescence via binding with inhibitor of DNA binding 1 (ID-1), E2F transcription factor 1 (E2F1), focal adhesion kinase (FAK), and hypoxia-inducible factor 1α (HIF1α) in the cytoplasm. Mechanistically, the scaffolding of circFoxo3 inhibits FAK transportation to mitochondria and retains HIF1α in the cytoplasm[88]. Another study in mouse cardiomyocytes found that circNfix, promoted by transcription factor Meis1, interacts with Y-box binding protein 1 (Ybx1) and an E3 ubiquitin ligase-Nedd4l to induce Ybx1 degradation through ubiquitination, which further represses cyclin A2 and cyclin B1 expression, leading to arrest of cardiomyocyte proliferation[89]. CircACC1, a circRNA found in a human colon cancer cell line, is upregulated by serum starvation and functions as a scaffold binding with AMP-activated protein kinase (AMPK) holoenzyme β and γ subunits[90].

Aside from acting as protein scaffolds, circRNAs can also serve as a protein sponge. circANRIL exerts an atheroprotective role by manipulating ribosomal RNA (rRNA) maturation via binding with 60S-preribosomal assembly factor pescadillo homologue 1 (PES1), thus activating p53 and nucleolar stress to regulate the survival of vascular smooth muscle cells (VSMCs) and macrophages[91]. Additionally, circPABPN preserves RBP ELAVL1 in the cytoplasm by sponging, which prevents ELAVL1 from translocating to nucleus and binding to its host linear transcript, leading to reduction of Poly(A) binding protein nuclear 1 (PABPN) translation[92].

CircRNAs translate proteins

Owning to the lack of 5' and 3' ends, circRNA can only undergo cap-independent translation, i.e., internal ribosome entry site (IRES)-driven translation or N6-methyladenosine (m^6A)-driven translation (Figure 2.2D). By using a synthetic circRNA containing IRES sequence of encephalomyocarditis virus (EMCV), Chen et al. successfully observed the first protein encoded by circRNA in 1995 [93]. Recent studies have identified a considerable number of translatable circRNAs (more than 200), including those expressed from vectors and endogenous circRNAs[94]. For example, circZNF609, circMbl3, circβ-catenin, and circ-SHPRH are found to have IRES and encode novel proteins or peptides[95-98]. Another set of translatable circRNAs are characterized by undergoing m^6A-driven translation. m^6A reader YTH N6-methyladenosine RNA binding protein 3 (YTHDF3) binds to m^6A site on circRNA and recruits translational initiation factors eIF4G2 and eIF3A, resulting in translation initiation[99]. Moreover, a study screening genome-wide m^6A-methylated circRNAs in human embryonic stem cells has identified thousands of circRNAs containing m^6A sites, indicating that this translation mechanism may be utilized extensively in circRNAs, [100] and circRNA translation may occur much more than we have expected. Indeed, a study using mass spectrometry to screen circRNA candidates with IRES-like sequence have found that nearly 50% of these circRNAs encode proteins [101]. However, the nature of circRNA translation and the mechanisms controlling how circRNAs are translated remain largely unknown.

CircRNAs serve as biomarkers

More than 2,400 circRNAs have been detected in human blood samples [102]. Also, circRNAs can be transported out of cells by exosomes, indicating circRNAs may serve as biomarkers (Figure

2.2E). NGS has detected a number of exosome-enriched circRNAs. The concentration of exosomal circRNA is far greater than that of cellular circRNAs (more than two folds)[103, 104]. For example, circPDE8A, a tumor-released exosomal circRNA, is found in liver-metastatic pancreatic ductal adenocarcinoma (PDAC) cells. High level of circPDE8A in plasma is considered as an independent risk for overall survival[105]. Likewise, prometastatic circPTGR1 is highly expressed in serum exosomes of hepatocellular carcinoma (HCC) patients and is correlated with clinical stage and prognosis, indicating that it may serve as a potential therapeutic target and/or biomarker in HCC[106]. CircRNAs fulfill many requirements for a biomarker. And importantly, as aforementioned, circRNAs have other unique characteristics such as long half-life (stability) and tissue- and disease-specific expression patterns (specificity), which make exosomal circRNAs promising biomarkers for cancer diagnosis and beyond.

The translocation of circRNAs

Certain types of RNA molecules can execute their proper functions only after being exported to the cytoplasm, such as tRNAs and rRNAs[107]. For circRNAs, even though some ciRNAs and ElciRNAs have to be retained in the nucleus, most circRNAs are accumulated in the cytoplasm. Thus far, little is known about the translocation mechanism of circRNAs from the nucleus to the cytoplasm (Figure 2.2F). Recent studies in Drosophila DL1 and human cells have provided some clues. In order to identify factors controlling circRNAs exportation, RNAi screening was used to knock down 26 RNA export-related proteins. Depletion of Drosophila DExH/D box helicase Hel25E only causes accumulation of long circRNAs (more than 800 nucleotides) but does not affect the short circRNAs (less than 702 nucleotides) in the nuclei of DL1 cells. Depletion of two human orthologues of Drosophila Hel25E (DDX39B/UAP56 and DDX39A/URH49) also causes

nuclear accumulation of long (more than 1200 nucleotides) and short circRNAs (less than 400 nucleotides) in human cells, respectively, suggesting that length (or molecular weight) of the mature circRNAs dictates the export mechanism associated with DDX39B or DDX39A[108, 109].

The degradation of circRNAs

Although circRNAs have higher stability than other RNA molecules due to the closed-loop structure, they can still be degraded. However, the understanding of circRNA degradation is currently limited[110]. So far, four pathways of circRNA decay have been proposed (Figure 2.2G). Although circRNAs are resistant to exonuclease digestion, a broadly expressed endoribonuclease RNase L has been determined to initiate global circRNA decay. Upon viral infection, RNase L is activated by the presence of viral dsRNAs in the cellular cytoplasm, thereby triggering global circRNA derogation, especially for those circRNAs containing imperfect dsRNA structures (usually 16-26 base pairs)[111]. A study with circRNAs containing m^6A sites discovered another circRNA decay pathway. m^6A reader YTH N6-Methyladenosine RNA Binding Protein 2 (YTHDF2) can first recognize and bind to the m^6A site of circRNA. Then 2-Iminobutanoate/2-Iminopropanoate Deaminase (HRSP12) binds explicitly to the GGUUC motif on circRNAs and bridges an endonuclease complex RNase P/MRP with YTHDF2 to initiate the circRNA degradation[112]. In addition, the above-mentioned circRNA CDR1as can be cleaved by Ago2 with the help of miR-671, which has a nearly perfect match with CDR1as[81]. Lastly, Fischer et al. recently reported that almost one-third of human circRNAs might contain secondary structures, similar to the structures on 3′ untranslated region (3′ UTR) of mRNAs, which often direct mRNAs for decay. UP-Frameshift-1 (UPF1), a factor regulating mRNA decay by unwinding highly structured RNA, can recognize highly structured circRNAs and associate them with

endonuclease Ras GTPase-activating protein-binding protein 1 (G3BP1) to exert the process of circRNA decay[113].

Approaches to study circRNAs

CircRNA detection

Recent advances in NGS technologies and the booming of bioinformatics have given rise to an expansion of circRNA-related studies (Table 2.1). In 2012, the first genome-wide profiling of circRNAs by RNA-Seq was exposed to the public[22]. A year later, a landmark study conducted by Memczak et al[26] not only demonstrated that circRNAs may act as miRNA sponge and associate with certain RBPs but also developed the first computational pipeline-Findcirc, which allow ones to detect a large number of circRNAs from the NGS dataset, providing insights and ideas for RNA community. Unlike linear RNAs, circRNAs have no 5' cap and 3' poly(A) tail. This unique feature causes difficulties in identifying circRNAs when applying the regular NGS procedure. Therefore, poly(A) associated RNA or ribosomal RNAs (rRNAs) usually need to be eliminated prior to RNA-Seq library preparation and profiling, allowing the enrichment of circRNA levels [25-27, 36, 37, 65]. Ribosomal RNA is the most abundant RNA type, occupying about up to 90% of the components present in a total RNA sample. Hence rRNA depletion is critical before RNA-Seq because this permits to focusing the sequencing resources on RNA types of interest[114]. Moreover, rRNA-depletion RNA-Seq not only allows the identification of circRNAs but also detects other RNA types, such as long non-coding RNA, small non-coding RNA, and mRNA. This approach is suitable for studies focusing on RNA-RNA interaction or RNA co-expression. However, rRNA-depletion RNA-Seq needs more depth than other circRNA NGS approaches to

identify the same circRNA numbers. Enrichment of circRNAs is always a priority to researchers due to the limitation of NGS capacity. RNase R is an enzyme that can degrade all linear RNAs through exonuclease activity but leave circRNAs unaffected[21, 115]. Increased reading of circRNA in RNA-Seq can be achieved when using RNase R pre-treated RNA samples[47]. Also, this selection provides additional evidence of circRNAs' circularity[115]. In 2014, Arraystar launched the first commercial circRNA microarray, which provides a convenient and affordable way to profile circRNAs[116]. However, circRNA microarray is based on known circRNA back-splice junction (BSJ) specific probes; thus, no novel circRNAs can be detected using this microarray.

CircRNA validation and characterization

The most commonly used approach for circRNA validation is reverse-transcription (RT) followed by PCR using divergent primers that amplify the BSJ sequence because the divergent primer pair only amplify BSJ segment from RT-derived cDNA product but not the genomic DNA (Table 2.1). The amplified product with the correct size can be further analyzed by Sanger sequencing to confirm the BSJ sequence[26]. RNase R treatment can also validate the authenticity of circRNAs. Nonetheless, certain validated circRNAs can still be RNase R-sensitive, such as CDR1as, MAN1A2, NCX1, and Ank2[21, 24, 25, 29, 117]. Another gold standard method to validate circRNAs is northern blotting. Both radioactive or nonradioactive probes targeting circRNA BSJ can be used on the membrane transferred from denaturing polyacrylamide gel electrophoresis[26, 118]. Northern blotting allows visualizing circRNA size and circRNA isoforms with better sensitivity compared with other assays. Fluorescence in situ hybridization (FISH), along with high-resolution microscopy, is a powerful combination for visualizing circRNAs in fixed cells or tissues and quantifying its expression by analyzing signal strength[119]. DNA probes with chemical

tags, such as biotin and digoxin, are often used to target circRNAs BSJ[120, 121]. However, this method requires high-resolution microscopy, such as confocal microscopy and suitable hybridization temperature, to ensure specificity, thus distinguishing probe signals from background noise, especially for low abundant circRNAs.

CircRNA localization

Identifying subcellular localization of circRNAs is important because circRNAs in different cellular fractions may have different regulatory functions (Table 2.1). For example, in the cytoplasm, circRNAs can act as miRNA sponges[26], RBPs scaffolds[87], or be translated into protein[95], while in the nucleus, circRNAs may recruit transcriptional factors[122] or enhance polymerase II transcription ability[37, 38]. To identify circRNA localization, researchers often use FISH[38, 123]. Furthermore, cytoplasmic and nuclear fraction separation allow investigations of components in each fraction, providing further evidence of circRNA localization and expression[55]. Moreover, Since circRNAs feature translatable capacity[95, 96], ribosome profiling and polysomal fractionation may capture circRNA footprints associated with actively translating ribosomes[124, 125].

CircRNA interaction

The functions of circRNAs as miRNA sponges[26], RBPs scaffolds[87], or to be translated[95] require the interaction of circRNAs with other components, such as miRNAs, RBPs, or rRNAs. RNA Immunoprecipitation (RIP) assay is a reliable strategy to identify, specifically, circRNA-protein interaction (Table 2.1). In this assay, putative circRNA binding proteins are immunoprecipitated, followed by RNA-Sequencing[84], analysis of associated RNA[68], or blotting of circRNA-

scaffolded proteins[87, 126]. On the other hand, circRNAs can be pulled down by RNA-pulldown assay. Chemically modified DNA probes (such as biotin and digoxin conjugation) specifically targeting circRNA BSJ sites can be used for the pulldown procedure. The pulldown components can be analyzed using diverse methods, including immunoblotting, mass spectrometry of circRNA binding proteins,[87] or RT-PCR analyses of associated RNAs[127]. The specificity could be affected by less specific antibodies or DNA probes. Thus, negative controls need to be included for all circRNA interaction-related assays.

Loss and gain of function of circRNA

Loss of function and gain of function achieved by multiple different techniques are widely used to elucidate gene functions. While most of these techniques are routine for mRNA studies, it is challenge to use them for studying circRNA due to their unique structure (Table 2.1). Nevertheless, knockdown, knockout, and overexpression strategies for circRNA have shown promising outcomes. CircRNA knockdown achieved by siRNA or shRNA is the most efficient loss of function technique in large numbers of studies [38, 128-131]. RNAi-mediated knockdown of circRNA driven by siRNA targeting circRNA BSJ site can reach 75% to 90% knockdown efficiency both in vitro and in vivo[95, 132] although the off-target effects owing to siRNA sequence overlapping with linear mRNA need to be addressed. Strategies for circRNA knockout are challenge. In 2017, Piwecka et al. generated the first circRNA CDR1as knockout mouse model by using CRISPR/Cas system to remove the entire CDR1as-producing genomic region. They designed gRNA pair targeting two ends of CDR1as on the mouse genomic loci. However, this CRISPR/Cas-mediated knockout is an exception because CDR1as locus on genome is mosaiced within a long non-coding RNA. The depletion of this locus has less to no effect on its host

mRNA expression but may have an impact on neighbor genes[36, 133, 134]. Another knockout strategy for circRNA is CRISPR/Cas-mediated intronic complementary sequence depletion[51]. circRNAs can also be overexpressed in cells by cloning circRNA-producing exons into circRNA overexpression vectors[64]. These vectors allow the exon to be expressed and then mimic the circRNA formation process by joining the two ends of the RNA derived from inserted exon together to generate a circRNA. It is noteworthy that some plasmids may incorporate enzyme-cutting residues into circRNA after expression. Furthermore, if the plasmid is compatible with the adenoviral delivery system, adenovirus can be generated to elevate circRNA transfection efficiency[135].

CircRNA databases and online resources

Database and online resources proffer opportunities to get access to large-scale datasets and valuable analysis tools . Currently, there are more than 20 mammalian circRNA online database portals. Most of these databases store circRNA information from numerous NGS datasets based on literature, and others provide practical analysis pipelines to process NGS data (Table 2.2). Since the number of circRNA databases is still growing, the content and quality need to be updated or improved frequently[136].

CircBase[26, 137], first launched in 2013, is the earliest comprehensive circRNA online database that hosts thousands of circRNA information from multiple eukaryotic tissue samples or cell lines. Other than only providing search, browse, and downloadable contents in circBase, several circRNA databases offer functional analysis and additional useful tools. For example, CircAtlas[138] stores circRNAs from six mammalian species, and allows miRNA binding, RBP

binding, ORF, IRES prediction, and circRNA conversation across multiple species. CircInteractome[139], a database based on circBase, provides miRNA and RBP binding prediction, helps design divergent primers and siRNAs for experimental purposes. Alternatively, CIRCpedia[34] contains not only circRNA annotation and expression profiles from six species but also customizable heatmap and point plot generators based on cell lines and species. ENCORI[137], the third version of starBase, is a comprehensive database designed for decoding interaction networks of multiple types of ncRNAs from CLIP-Seq. In this database, users can retrieve circRNA-miRNA and circRNA-RBP interaction evidence. Notably, some databases feature human circRNA modification prediction, such as circRNADb[140], TRCirc[141], and Circbank[142]. Besides the databases containing circRNA information from diverse cell lines and tissue samples, Several other databases feature sample- or disease-specific circRNA annotation. In BBBomics[143], users can browse circRNA information specifically from blood-brain barrier (BBB) samples. Moreover, exoRBase[144] provides data of circRNA, miRNA, and mRNA from blood exosomes. Voineagu Lab developed a genome browser that allows users to visualize circRNA interactions and expression data from multiple human brain NGS datasets[145]. In addition, CSCD[146] is a cancer-specific circRNA database allowing users to search and view circRNA alternative splicing patterns. TSCD[147] is constructed to provide human and mouse tissue-specific circRNAs mainly involved in organogenesis and developmental diseases. Also, there is a downloadable circRNA visualization tool called CircView[148] that enables users to view circRNA regulatory elements. It is noteworthy that manually curated databases are also available online. CircR2Disease[149], circRNADisease[150], circad[151], and CircFunBase[152] contain high-quality disease-related functional circRNA resources, including experimentally validated evidence and corresponding literatures. Recently, an interesting and comprehensive database called riboCIRC

has been released online. It is a repository of computationally predicted ribosome-associated circRNAs (Ribo-circRNAs) and experimentally verified translated circRNAs. Moreover, it provides the evaluation of conservation of translatable circRNAs, and systematic *de novo* annotation of putative circRNA encoded peptides[94]. Lastly, circlncRNAnet[153], an integrated online resource, allows user-defined NGS data frame upload and provides different circRNA and lncRNA functional analyses, including multiple plots generation, pathway enrichment, and interactomics analysis.

CircRNA in the cardiovascular system

CircRNAs in heart diseases

Myocardial infarction: Among different types of cardiovascular diseases, myocardial infarction (MI) is the leading cause of mortality and disability[154]. MI is characterized by cardiac damage and remodeling on account of acute occlusion of the coronary artery, followed by prolonged myocardial ischemia that leads to myocardial cell death, cardiomyocyte loss, cardiac dysfunction, and ultimately heart failure[155]. circRNAs play important roles in MI and post-MI recovery (Table 2.3). Cdr1as is a key regulator for the progression of many diseases, such as cancers, diabetes, neuropsychiatric disorders, pulmonary fibrosis, and heart disease[156]. Cdr1as is a master sponge of miR-7, a protective component in cardiac myocyte injury progression post-MI[157]. miR-7 and Cdr1as are both upregulated in heart after mouse MI surgery and hypoxia-treated cardiomyocytes in culture. Overexpression of Cdar1as aggravates cardiac infarction, myocardial apoptosis and promotes the expression of SP1 and PARP, the downstream targets of

miR-7. Overexpression of miR-7 rescues Cdr1as-induced changes, suggesting that Cdr1as sponges miR-7in MI [158]. Another circRNA MFACR derived from Smyd4 able to sponge miR-652-3p, which targets MTP18, a protein that regulates cardiomyocyte mitochondrial fission. Knockdown of MFACR attenuates the ischemia/reperfusion (I/R) injury-induced upregulation of mitochondrial fission, apoptosis, and MI size[159]. I/R injury-induced cardiomyocyte apoptosis can also be attenuated by knockdown of circNCX1. circNCX1 induces cardiomyocyte apoptosis via binding to miR-133-3p hence elevating the expression of pro-apoptotic protein CDIP1[160].

In addition to regulating cardiomyocytes apoptosis, circRNA can also regulate cardiomyocyte proliferation. Gain- and loss-of-function studies have shown that CircCDYL promotes the proliferation of cardiomyocytes through miR-4793-5p/APP pathway[161]. Besides, a recent study showed that circNfix is involved in the regulation of cardiomyocyte proliferation and angiogenesis, which affect the prognosis of MI. Mechanistically, circNfix induces Y-box binding protein 1 (Ybx1) ubiquitination and degradation by scaffolded Ybx1 and Nedd4l, decreasing the expression of cyclin A2 and B1. Additionally, circNfix sponges miR-214 to increase the expression of glycogen synthase kinase 3 β (Gsk3β) and repress VEGF activity. It has also been reported that circTtc3, one of the most abundant circRNA in heart, is markedly upregulated in the ischemic myocardium and the cardiomyocytes with hypoxic insult. circTtc3 plays a protective role in cardiac dysfunction after MI by sponging endogenous miR-15b, leading to downstream Arl2 expression[162]. CircRNA microarray profiling showed that circFndc3b is significantly downregulated in the post-MI mouse hearts. Overexpression of circFndc3b alleviates cardiomyocyte apoptosis and fibrosis and improves endothelial cell function, neovascularization, and left ventricular functions. circFndc3b appears to interact with RNA binding protein FUS to regulate VEGF expression and signaling[163]. Lastly, CircHipk3, a

powerful regulator in multiple diseases[121, 164-166]. is induced by transcription factor Gata4 and acts as a Notch1 scaffold and miR-133a sponge at the same time after MI. Overexpression of circHipk3 efficiently promotes coronary vessel endothelial cell proliferation, migration, and tube-forming capacity and subsequent angiogenesis, and consequently, attenuates cardiac dysfunction and fibrosis due to MI [166].

Cardiac Fibrosis: Cardiac fibroblasts (CFs) are the key cell type to maintain the integrity and homeostasis of the cardiac extracellular matrix (ECM). However, upon injury, CFs transform into a myofibroblast phenotype and contribute to cardiac fibrosis, resulting in chamber dilation, cardiomyocyte hypertrophy and apoptosis, and eventually, the progression to heart failure[167]. Cardiac fibrosis is observed almost in all heart diseases. Studies in circRNA functions offer new strategies for treating cardiac fibrosis (Table 2.3)[168]. circNFIB induces proliferation of fibroblast NIH/3T3 cells by releasing pro-fibrotic miR-433 to reduce the expression of downstream genes AZIN1 and JNK1[169]. In angiotensin II (Ang II)-induced cardiac fibrosis, circHIPK3 is significantly upregulated. circHIPK3 promotes CF proliferation, migration and cardiac fibrosis by sponging miR-29b-3p and upregulates a-SMA, COL1A1 and COL3A1 expression[170]. A microarray profiling of the myocardium of diabetic db/db mice has identified circRNA_010567 to be significantly upregulated in Ang II-treated myocardium and cardiac fibroblasts. Knockdown of circRNA_010567 suppresses TGF-β1 expression through sponging miR-141 and hence inhibits the expression of fibrosis-associated proteins Col I, Col III and α-SMA [171]. Likewise, circRNA_000203 binds miR-26b-5p to target Col1a2 and CTGF expression[172].

Cardiomyopathy: Cardiomyopathy is often caused by functional impairment of cardiac muscle. There are two major types of primary cardiomyopathy, Hypertrophic cardiomyopathy (HCM) and dilated cardiomyopathy (DCM). HCM is characterized by left ventricular hypertrophy, which is the major cause of sudden death and heart failure, especially in the young population. DCM is characterized by dilated ventricular cavity with systolic dysfunction, with the symptom of heart failure and sudden death (Table 2.3)[173]. A recent comprehensive study using whole transcriptome sequencing for HCM and DCM patients found that a master host gene titin (TTN), the origin of 80 different circRNA isoforms, is regulated by a splicing factor RBM20. Five circRNAs derived from TTN (cTTN1-5) and one circRNA derived from CAMK2D (cCAMK2D) are significantly downregulated in DCM groups while only cCAMK2D is significantly suppressed in HCM[174]. Another candidate, circAmotl1, is preferentially expressed in neonatal cardiac tissues. Overexpression of circAmotl1 in mice treated with doxorubicin to induce cardiomyopathy alleviates the enlargement of the left ventricle, fibrotic remodeling, and cell apoptosis. Mechanistically, circAmotl1 facilitates the nuclear translocation of pAKT through binding to PDK1 and AKT1[175]. In addition, ectopic expression of circFoxo3 induces cardiac senescence and exacerbates doxorubicin-induced cardiomyopathy. CircFoxo3 retains the anti-senescence ID1 and E2F1 and anti-stress FAK and HIF1α proteins in cellular cytoplasm to prevent nuclear translocation of these transcription factors. Conversely, Knockdown of circFoxo3 represses senescence and attenuates cardiomyopathy [88].

Cardiac hypertrophy: Cardiac hypertrophy is closely associated with heart failure, which is an adaptive response to myocardial stress, mutations of sarcomeric proteins, or loss of contractile mass from prior infarction (Table 2.3)[176]. To elucidate the roles of circRNAs in cardiac

hypertrophy, Wang et al. have traced upstream circRNAs of a pro-hypertrophic microRNA miR-223 and identified a heart-related circRNA (HRCR) capable of providing up to six miR-233 binding sites. Forced expression of HRCR shows a cardiac-protective function and attenuates the development of cardiac hypertrophy through miR-233/ARC axis[135]. Although circSlc8a1 is the single most highly abundant cardiomyocyte circRNA in both human and mouse hearts, it had no change during the myocardial stress response. However, circSlc8a1 has the potential to regulate pro-hypertrophic miR-133a. CircSlc8a1 RNA pulldown assay has verified the interaction between circSlc8a1 and miR-133a and also found a significant enrichment of miR-133a. Overexpression of circSlc8a1 via AAV vector deteriorates while knockdown of circSlc8a1 attenuates pressure overload-induced hypertrophy[177]. Interestingly, an artificial circRNA-circmiRs that specifically target cardiac pro-hypertrophic miR-132 and miR-212 successfully attenuated left ventricular hypertrophy. Additionally, the efficacy is better with circRNA-circmiRs than with the equimolar pharmacological antagomiRs, suggesting a more efficient therapeutic application[178].

CircRNAs in vascular diseases

Diabetic Retinopathy (DR): Diabetes mellitus (DM) is connected with various microvascular complications, including DR, one of the major causes of visual impairment and blindness. Mouse circRNA expression profiling for nondiabetic retinas and diabetic retinas has identified a circRNA-cPWWP2A significantly upregulated in diabetic retinas and db/db mouse samples. Retinal cPWWP2A can be brought down when db/db mice are treated with insulin, indicating that cPWWP2A is a potential regulator of diabetic retinopathy. Silencing of cPWWP2A in

pericytes leads to the aggravation of high glucose-induced apoptosis, reduction of pericyte marker expression, decrease of perictye-EC crosstalk. Mechanistically, cPWWP2A sponges miR-579 and further impacts the expression of angiopoietin 1, Occludin, SIRT1, which ultimately regulates retinal vascular dysfunction both in vivo and in vitro [179]. Another circRNA called circDNMT3B causes DR via interaction with miR-20b-5p/BAMBI axis[180]. Moreover, circHIPK3 silencing in vivo alleviates retinal vascular dysfunction through releasing free miR-30a-3p to target downstream VEGF-C, FZD4, and WNT2 [181]. CircZNF609, a circRNA shared by both humans and rats, is significantly upregulated in human vascular endothelial cells (HUVEC) treated with high glucose and in rat episcleral vein ligation model of glaucoma. circZNF609 also functions as miRNA sponge, thus harboring miR-615-5p in both HUVEC and rat glaucoma to regulate diabetic retinopathy and retinal neurodegeneration, respectively [182, 183]. These circRNAs may become potential therapeutic targets for developing therapeutics to treat DR (Table 2.4).

Atherosclerosis: Atherosclerosis is a chronic inflammatory disease characterized by the formation of fibrofatty plaque in the artery wall due to the accumulation of fatty and/or fibrous material in the intima, resulting in the narrowing of the lumen of the artery[184, 185]. The causes of atherosclerosis are diverse, including endothelial dysfunction, vascular smooth muscle cell (VSMC) phenotypic modulation, LDL/HDL particles deposition, and inflammation, etc. [185, 186]. Accumulating evidence indicates that circRNAs have potential to become therapeutic targets in atherosclerosis (Table 2.4). NGS profiling using non-atherosclerotic and atherosclerotic rabbit samples has generated a dysregulated circRNA-related ceRNA network and identified seven circRNAs that are related to atherosclerosis[187]. In addition, numerous studies have reported that non-coding RNAs (ncRNAs), including long ncRNAs, small ncRNAs and miRNAs, have

emerged as key effectors of intimal thickening and potential circulating biomarkers for cardiovascular disease[4, 188, 189]. Among them, miR-221 and miR-222 are required to prevent atherosclerotic plaque rupture[190]. Interestingly, the ratio of circulating circR-284 to miR-221 is significantly upregulated in patients with carotid endarterectomy (CEA) and suffering an acute carotid-related ischemic event, suggesting that circR-284:miR-221 ratio may be an excellent biomarker for the advanced atherosclerosis[191, 192].

Moreover, coronary atherosclerosis NGS study has illustrated that atherosclerosis is of strong association with chromosome 9p21.3 which contains SNPs across more than 100 kilobases[193]. CDKN2A and CDKN2B are two genes derived from the chromosome 9p21.3, and one long ncRNA (ANRIL) derived from CDKN2B antisense has the ability to form a circRNAs-circANRIL. CircANRIL interacts with PES1 to impact exonuclease-mediated processing and maturation of ribosomal RNA in human vascular tissue, leading to activation of p53. CircANRIL is atheroprotective and thus may be a potential therapeutic target for the treatment of atherosclerosis[91]. Circ_0003204 was discovered from microarray analysis and mediated vascular endothelial phenotype through targeting miR-370-3p/TGFβR2/phosph-SMAD3 pathway. Inhibition of circ_0003204 alleviates aberrant EC phenotype in atherosclerosis [194]. Vascular remodeling due to VSMC phenotypic modulation is also considered as a major step in coronary artery disease progression[195]. Only a couple of VSMC circRNAs have been found to regulate the development of atherosclerosis. CircCHFR, expressed aberrantly in the ox-LDL-induced VSMCs, regulates VSMC proliferation and migration via sponging miR-370[196]. Additionally, circNRG-1 is capable of influencing its own host gene NRG-1 through binding with miR-193b-5p in Ang II-blocked VSMC apoptosis [197]. Moreover, circ_Lrp6 acts as a natural master sponge for miR-145, a miRNA that regulates the phenotypic switch from proliferation to differentiation.

However, although they found that miR-145 is reduced in atherosclerotic vessels along with the reduction of Lrp6, the level of circ_Lrp6 is not significantly regulated[198].

Abdominal aortic aneurysm (AAA): AAA refers to an irreversible chronic dilation (exceeding the normal vessel diameter by 50%) of the aortic wall[199]. AAA is often asymptomatic until rupture occurs, which eventually leads to death with a mortality rate of 85 to 90%[200]. VSMCs provide a source of elastin, maintaining the elasticity of the aortic wall. Senescence and apoptosis of VSMCs result in the deficiency of elastin, which eventually leads to AAA wall remodeling[201]. Up to now, only a few studies have linked circRNAs to AAA, and most of them mainly focus on VSMCs apoptosis-related circRNAs (Table 2.4). CircRNA expression profiling AAA patient samples using circRNA microarray has identified 13,295 circRNAs, and 411 circRNAs are differentially expressed. Two candidates, hsa_circ_0005360 and hsa_circ_0002168, are found to be significantly lower in AAA samples[202]. Another study using tissues from AAA patients and hypoxic aortic SMCs revealed that hsa-circ-000595 is not only highly expressed in AAA, but also capable of modulating miR-19a expression to induce aortic SMC apoptosis[203]. CircCCDC66 is another circRNA that is highly expressed in AAA and functionally promotes VSMCs apoptosis while impacting VSMC proliferation. CircCCDC66 exhibits an expression pattern opposite to its host gene CCDC66. It appears that circCCDC66 modulates CCDC66 level via sponging miR-342-3p[204]. Finally, circCBFB, a circRNA derived from CBFB in VSMCs of AAA tissue interacts with pro-AAA miR-28-5p, which targets anti-apoptotic genes, GRIA4 and LYPD3. Overexpression of circCBFB alleviates AAA progression[205].

Neointimal hyperplasia: Neointimal hyperplasia (NH), often caused by percutaneous coronary intervention, such as balloon angioplasty, stent-graft implantation, bypass, and venous arterialization, is the proliferation and migration of VSMCs from the media layer of vascular wall into the tunica intima, leads to neointimal thickening, restenosis, and eventually vessel occlusion[206]. As the key regulator of vessel tone, VSMCs in the media layer undergo dedifferentiation in pathological conditions. VSMC dedifferentiation is a hallmark of NH, atherosclerosis, and AAA[207]. circRNAs play pivotal roles in NH progression (Table 2.4). CircACTA2 is found to modulate SMC marker gene α-SMA expression. CircACTA2 formation is induced by neuregulin-1 ICD (NRG-1-ICD):Ikzf1 complex through binding with the first intron of the Acta2 gene in TGF-β1-treated VSMCs . MiR-548f-5p, the upstream inhibitor of α-SMA, has a direct binding with circACTA2. The axis of NRG-1-ICD/circActa2/miR-548f regulates VSMC contraction via fine-tuning α-SMA expression, providing a novel therapeutic approach to limit vascular disease progression[208, 209]. In addition to circACTA2, circSirt1 is also pro-contractile and highly expressed in the normal artery but reduced in injury-induced neointimal VSMCs. CircSirt1 is found to inhibit TNF-α-induced VSMC phenotypic switching and interact with NF-κB p65 to inhibit NF-κB p65 nuclear translocation. Moreover, circSirt1 decreases TNF-α-induced NF-κB p65 acetylation and transcription via sponging miR-132/212, which further promotes SIRT1 expression. In injured arteries, adenoviral delivery of circSirt1 reduces the intima to media ratio compared to controls[210]. A recent study has identified circMAP3K5 to be another pro-contractile circRNA, important for SMC differentiation. circMAP3K5 is downregulated in PDGF-BB-treated human coronary arterial SMCs and human coronary arteries of patients with dilated cardiomyopathy or coronary heart disease. Forced expression of circMAP3K5 in human SMCs inhibits SMC proliferation and attenuates NH in

mouse wire-injury model, suggesting that circMap3k5 has an antiproliferative effect in SMCs. Mechanistically, CircMAP3K5 sequesters miR-22-3p, an upstream regulator of ten-eleven translocation-2 (TET2). Importantly, loss of Tet2 abolishes the circMap3k5-mediated antiproliferative effect[211].

In addition to pro-contractile circRNAs, there are a few pro-synthetic circRNAs in SMCs. CircDiaph3 is pro-synthetic and promotes VSMC proliferation and migration via sponging miR-148a-5p and further elevating Igf1r level[212]. Similarly, circDcbld1 is also pro-synthetic circRNA highly expressed in balloon-injury rat carotid arteries and promotes intima hyperplasia by targeting miR-145-3p/neuropilin-1. In vivo, suppression of circDcbld1 alleviates injury-induced intimal hyperplasia[213]. Additionally, circ_Lrp6 regulates integrin-β8 (ITGβ8), fascin actin-bundling protein 1 (FASCIN), Kruppel-like factor 4 (KLF4), YES proto-oncogene 1 (Yes1), and lysyl oxidase (Lox) via sponging miR-145. Knock of circ_Lrp6 prevents NH in mouse carotids[198].

Summary and perspective

Once regarded as scramble byproduct of splicing with no biological functions, circRNAs have become the research hotspot in recent years. Even though exciting progress has been achieved, the biological functions of the majority of circRNAs remain unclear. The exact mechanisms controlling circRNA biogenesis are also elusive. Since back-splicing is very different from canonical splicing, there must be novel factors specifically modulating back-splicing. Since strategies for dissecting the spliceosomes on pre-mRNA have been well developed, it is possible to also conduct structural analyses to decode the spliceosomal machinery for circRNAs. In

addition, numerous RBPs have been verified to regulate mRNA at multiples levels, but only a few RBPs have been validated for circRNA biogenesis. More research is needed in this area. Moreover, to properly execute their regulatory functions, circRNAs have to maintain fine-tuned cellular homeostasis by balancing their biogenesis and degradation rates. However, study about the mechanism of circRNA decay is still in its infancy. Elucidation of circRNA decay mechanisms may help researchers link the pathological condition with circRNA turnover. Also, studies investigating the translation of circRNA are mainly conducted by applying synthetic circRNA expression vectors or engineered plasmids. However, endogenously expressed circRNA-encoded proteins are barely discovered. Owing to their covalently closed-loop structures, endogenous circRNAs theoretically undergo infinite loop translation in the cytoplasm. Investigating this infinite loop translation may uncover new mechanisms controlling circRNA translation and novel translational products with biological functions.

As mentioned earlier in the approach section, multiple technical challenges need to be solved. The major challenge for circRNA study is how to increase the targeting specificity on circRNAs. In the siRNA/shRNA knockdown experiment, the off-target effects may be high because siRNA/shRNA is designed based on the BSJ sequence, which highly overlaps with linear mRNAs. Also, the poorly designed probe against BSJ of circRNA may cause highly nonspecific activity. Moreover, overexpression of circRNA heavily relies on the plasmid expression. Sanger sequencing of BSJ of the product after the overexpression is recommended to ensure no nucleotide residue from the backbone is incorporated into the synthetically-overexpressed circRNA. It is challenging to generate knockout animal model for circRNA study because circRNAs are primarily derived from a protein-coding gene. Even for CDR1as whose linear counterpart has no expression, removing its linear counterpart on the genome may cause aberrant

neighbor gene expression. Another knockout strategy is to remove the ICSs regulating circRNA biogenesis on the genome. However, the reliability of this strategy needs to be tested and requires detailed knowledge of circRNA biogenesis as a prerequisite. Surprisingly, limited research is conducted to validate circRNAs as biomarkers although circRNAs are qualified to be promising biomarkers. It is worthwhile to explore if circRNAs can serve as reliable biomarkers that may be used to improve the risk prediction of CVDs, monitor disease progression, or serve as a clinical sign before the appearance of symptoms.

Reference

1. Consortium, E.P. The ENCODE (ENCyclopedia Of DNA Elements) Project. *Science* **306**, 636-640 (2004).

2. Mehler, M.F. & Mattick, J.S. Noncoding RNAs and RNA editing in brain development, functional diversification, and neurological disease. *Physiol Rev* **87**, 799-823 (2007).

3. Amaral, P.P. & Mattick, J.S. Noncoding RNA in development. *Mamm Genome* **19**, 454-492 (2008).

4. Uchida, S. & Dimmeler, S. Long noncoding RNAs in cardiovascular diseases. *Circ Res* **116**, 737-750 (2015).

5. Mattick, J.S. & Rinn, J.L. Discovery and annotation of long noncoding RNAs. *Nat Struct Mol Biol* **22**, 5-7 (2015).

6. Wu, G.C. *et al.* Emerging role of long noncoding RNAs in autoimmune diseases. *Autoimmun Rev* **14**, 798-805 (2015).

7. Tang, R., Zhang, G., Wang, Y.C., Mei, X. & Chen, S.Y. The long non-coding RNA GAS5 regulates transforming growth factor beta (TGF-beta)-induced smooth muscle cell differentiation via RNA Smad-binding elements. *J Biol Chem* **292**, 14270-14278 (2017).

8. Tang, R. *et al.* LncRNA GAS5 regulates vascular smooth muscle cell cycle arrest and apoptosis via p53 pathway. *Biochim Biophys Acta Mol Basis Dis* **1865**, 2516-2525 (2019).

9. Tang, R. *et al.* LncRNA GAS5 attenuates fibroblast activation through inhibiting Smad3 signaling. *Am J Physiol Cell Physiol* **319**, C105-C115 (2020).

10. Li, Y., Baptista, R.P. & Kissinger, J.C. Noncoding RNAs in Apicomplexan Parasites: An Update. *Trends Parasitol* **36**, 835-849 (2020).

11. Esteller, M. Non-coding RNAs in human disease. *Nat Rev Genet* **12**, 861-874 (2011).

12. Sanger, H.L., Klotz, G., Riesner, D., Gross, H.J. & Kleinschmidt, A.K. Viroids are single-stranded covalently closed circular RNA molecules existing as highly base-paired rod-like structures. *Proc Natl Acad Sci U S A* **73**, 3852-3856 (1976).

13. Hsu, M.T. & Coca-Prados, M. Electron microscopic evidence for the circular form of RNA in the cytoplasm of eukaryotic cells. *Nature* **280**, 339-340 (1979).

14. Nigro, J.M. *et al.* Scrambled exons. *Cell* **64**, 607-613 (1991).

15. Cocquerelle, C., Daubersies, P., Majerus, M.A., Kerckaert, J.P. & Bailleul, B. Splicing with inverted order of exons occurs proximal to large introns. *EMBO J* **11**, 1095-1098 (1992).

16. Capel, B. *et al.* Circular transcripts of the testis-determining gene Sry in adult mouse testis. *Cell* **73**, 1019-1030 (1993).

17. Zaphiropoulos, P.G. Circular RNAs from transcripts of the rat cytochrome P450 2C24 gene: correlation with exon skipping. *Proc Natl Acad Sci U S A* **93**, 6536-6541 (1996).

18. Patop, I.L., Wust, S. & Kadener, S. Past, present, and future of circRNAs. *EMBO J* **38**, e100836 (2019).

19. Mardis, E.R. Next-generation DNA sequencing methods. *Annu Rev Genomics Hum Genet* **9**, 387-402 (2008).

20. Yang, L., Duff, M.O., Graveley, B.R., Carmichael, G.G. & Chen, L.L. Genomewide characterization of non-polyadenylated RNAs. *Genome Biol* **12**, R16 (2011).

21. Jeck, W.R. *et al.* Circular RNAs are abundant, conserved, and associated with ALU repeats. *RNA* **19**, 141-157 (2013).

22. Salzman, J., Gawad, C., Wang, P.L., Lacayo, N. & Brown, P.O. Circular RNAs are the predominant transcript isoform from hundreds of human genes in diverse cell types. *PLoS One* **7**, e30733 (2012).

23. Shen, Y., Guo, X. & Wang, W. Identification and characterization of circular RNAs in zebrafish. *FEBS Lett* **591**, 213-220 (2017).

24. Westholm, J.O. *et al.* Genome-wide analysis of drosophila circular RNAs reveals their structural and sequence properties and age-dependent neural accumulation. *Cell Rep* **9**, 1966-1980 (2014).

25. Guo, J.U., Agarwal, V., Guo, H. & Bartel, D.P. Expanded identification and characterization of mammalian circular RNAs. *Genome Biol* **15**, 409 (2014).

26. Memczak, S. *et al.* Circular RNAs are a large class of animal RNAs with regulatory potency. *Nature* **495**, 333-338 (2013).

27. Fan, X. *et al.* Single-cell RNA-seq transcriptome analysis of linear and circular RNAs in mouse preimplantation embryos. *Genome Biol* **16**, 148 (2015).

28. Dong, R., Ma, X.K., Chen, L.L. & Yang, L. Increased complexity of circRNA expression during species evolution. *RNA Biol* **14**, 1064-1074 (2017).

29. Zhang, X.O. *et al.* Complementary sequence-mediated exon circularization. *Cell* **159**, 134-147 (2014).

30. Barrett, S.P., Wang, P.L. & Salzman, J. Circular RNA biogenesis can proceed through an exon-containing lariat precursor. *Elife* **4**, e07540 (2015).

31. Broadbent, K.M. *et al.* Strand-specific RNA sequencing in Plasmodium falciparum malaria identifies developmentally regulated long non-coding RNA and circular RNA. *BMC Genomics* **16**, 454 (2015).

32. Lu, T. *et al.* Transcriptome-wide investigation of circular RNAs in rice. *RNA* **21**, 2076-2087 (2015).

33. Luo, J. *et al.* [Progress in circular RNAs of plants]. *Yi Chuan* **40**, 467-477 (2018).

34. Dong, R., Ma, X.K., Li, G.W. & Yang, L. CIRCpedia v2: An Updated Database for Comprehensive Circular RNA Annotation and Expression Comparison. *Genomics Proteomics Bioinformatics* **16**, 226-233 (2018).

35. Black, D.L. Mechanisms of alternative pre-messenger RNA splicing. *Annu Rev Biochem* **72**, 291-336 (2003).

36. Li, X., Yang, L. & Chen, L.L. The Biogenesis, Functions, and Challenges of Circular RNAs. *Mol Cell* **71**, 428-442 (2018).

37. Zhang, Y. *et al.* Circular intronic long noncoding RNAs. *Mol Cell* **51**, 792-806 (2013).

38. Li, Z. *et al.* Exon-intron circular RNAs regulate transcription in the nucleus. *Nat Struct Mol Biol* **22**, 256-264 (2015).

39. Geng, Y., Jiang, J. & Wu, C. Function and clinical significance of circRNAs in solid tumors. *J Hematol Oncol* **11**, 98 (2018).

40. Szabo, L. & Salzman, J. Detecting circular RNAs: bioinformatic and experimental challenges. *Nat Rev Genet* **17**, 679-692 (2016).

41. Enuka, Y. *et al.* Circular RNAs are long-lived and display only minimal early alterations in response to a growth factor. *Nucleic Acids Res* **44**, 1370-1383 (2016).

42. Schwanhausser, B. *et al.* Global quantification of mammalian gene expression control. *Nature* **473**, 337-342 (2011).

43. Shang, Q., Yang, Z., Jia, R. & Ge, S. The novel roles of circRNAs in human cancer. *Mol Cancer* **18**, 6 (2019).

44. Aufiero, S., Reckman, Y.J., Pinto, Y.M. & Creemers, E.E. Circular RNAs open a new chapter in cardiovascular biology. *Nat Rev Cardiol* **16**, 503-514 (2019).

45. Kumar, L., Shamsuzzama, Haque, R., Baghel, T. & Nazir, A. Circular RNAs: the Emerging Class of Non-coding RNAs and Their Potential Role in Human Neurodegenerative Diseases. *Mol Neurobiol* **54**, 7224-7234 (2017).

46. Chen, Q. *et al.* Circular RNA circSnx5 Controls Immunogenicity of Dendritic Cells through the miR-544/SOCS1 Axis and PU.1 Activity Regulation. *Mol Ther* (2020).

47. Zhang, Y., Yang, L. & Chen, L.L. Characterization of Circular RNAs. *Methods Mol Biol* **1402**, 215-227 (2016).

48. Aufiero, S. *et al.* Cardiac circRNAs arise mainly from constitutive exons rather than alternatively spliced exons. *RNA* **24**, 815-827 (2018).

49. Rybak-Wolf, A. *et al.* Circular RNAs in the Mammalian Brain Are Highly Abundant, Conserved, and Dynamically Expressed. *Mol Cell* **58**, 870-885 (2015).

50. Li, X. *et al.* A unified mechanism for intron and exon definition and back-splicing. *Nature* **573**, 375-380 (2019).

51. Zhang, Y. *et al.* The Biogenesis of Nascent Circular RNAs. *Cell Rep* **15**, 611-624 (2016).

52. Dietrich, W.F. *et al.* A comprehensive genetic map of the mouse genome. *Nature* **380**, 149-152 (1996).

53. Veno, M.T. *et al.* Spatio-temporal regulation of circular RNA expression during porcine embryonic brain development. *Genome Biol* **16**, 245 (2015).

54. Wang, P.L. *et al.* Circular RNA is expressed across the eukaryotic tree of life. *PLoS One* **9**, e90859 (2014).

55. Okholm, T.L.H. *et al.* Circular RNA expression is abundant and correlated to aggressiveness in early-stage bladder cancer. *NPJ Genom Med* **2**, 36 (2017).

56. Bachmayr-Heyda, A. *et al.* Correlation of circular RNA abundance with proliferation--exemplified with colorectal and ovarian cancer, idiopathic lung fibrosis, and normal human tissues. *Sci Rep* **5**, 8057 (2015).

57. Salzman, J., Chen, R.E., Olsen, M.N., Wang, P.L. & Brown, P.O. Cell-type specific features of circular RNA expression. *PLoS Genet* **9**, e1003777 (2013).

58. Ashwal-Fluss, R. *et al.* circRNA biogenesis competes with pre-mRNA splicing. *Mol Cell* **56**, 55-66 (2014).

59. Starke, S. *et al.* Exon circularization requires canonical splice signals. *Cell Rep* **10**, 103-111 (2015).

60. Kramer, M.C. *et al.* Combinatorial control of Drosophila circular RNA expression by intronic repeats, hnRNPs, and SR proteins. *Genes Dev* **29**, 2168-2182 (2015).

61. Kristensen, L.S. *et al.* The biogenesis, biology and characterization of circular RNAs. *Nat Rev Genet* **20**, 675-691 (2019).

62. Liang, D. *et al.* The Output of Protein-Coding Genes Shifts to Circular RNAs When the Pre-mRNA Processing Machinery Is Limiting. *Mol Cell* **68**, 940-954 e943 (2017).

63. Ivanov, A. *et al.* Analysis of intron sequences reveals hallmarks of circular RNA biogenesis in animals. *Cell Rep* **10**, 170-177 (2015).

64. Liang, D. & Wilusz, J.E. Short intronic repeat sequences facilitate circular RNA production. *Genes Dev* **28**, 2233-2247 (2014).

65. Zhang, X.O. *et al.* Diverse alternative back-splicing and alternative splicing landscape of circular RNAs. *Genome Res* **26**, 1277-1287 (2016).

66. Conn, S.J. *et al.* The RNA binding protein quaking regulates formation of circRNAs. *Cell* **160**, 1125-1134 (2015).

67. Errichelli, L. *et al.* FUS affects circular RNA expression in murine embryonic stem cell-derived motor neurons. *Nat Commun* **8**, 14741 (2017).

68. Li, X. *et al.* Coordinated circRNA Biogenesis and Function with NF90/NF110 in Viral Infection. *Mol Cell* **67**, 214-227 e217 (2017).

69. Gallo, A., Vukic, D., Michalik, D., O'Connell, M.A. & Keegan, L.P. ADAR RNA editing in human disease; more to it than meets the I. *Hum Genet* **136**, 1265-1278 (2017).

70. Shi, L. *et al.* Circular RNA expression is suppressed by androgen receptor (AR)-regulated adenosine deaminase that acts on RNA (ADAR1) in human hepatocellular carcinoma. *Cell Death Dis* **8**, e3171 (2017).

71. Aktas, T. *et al.* DHX9 suppresses RNA processing defects originating from the Alu invasion of the human genome. *Nature* **544**, 115-119 (2017).

72. Wolf, E., Kastner, B. & Luhrmann, R. Antisense-targeted immuno-EM localization of the pre-mRNA path in the spliceosomal C complex. *RNA* **18**, 1347-1357 (2012).

73. Talhouarne, G.J.S. & Gall, J.G. Lariat intronic RNAs in the cytoplasm of vertebrate cells. *Proc Natl Acad Sci U S A* **115**, E7970-E7977 (2018).

74. Robic, A., Demars, J. & Kuhn, C. In-Depth Analysis Reveals Production of Circular RNAs from Non-Coding Sequences. *Cells* **9** (2020).

75. Talhouarne, G.J. & Gall, J.G. Lariat intronic RNAs in the cytoplasm of Xenopus tropicalis oocytes. *RNA* **20**, 1476-1487 (2014).

76. Liu, J., Liu, T., Wang, X. & He, A. Circles reshaping the RNA world: from waste to treasure. *Mol Cancer* **16**, 58 (2017).

77. Chen, L.L. The expanding regulatory mechanisms and cellular functions of circular RNAs. *Nat Rev Mol Cell Biol* **21**, 475-490 (2020).

78. Conn, V.M. *et al.* A circRNA from SEPALLATA3 regulates splicing of its cognate mRNA through R-loop formation. *Nat Plants* **3**, 17053 (2017).

79. Wilusz, J.E. A 360 degrees view of circular RNAs: From biogenesis to functions. *Wiley Interdiscip Rev RNA* **9**, e1478 (2018).

80. Ragan, C., Goodall, G.J., Shirokikh, N.E. & Preiss, T. Insights into the biogenesis and potential functions of exonic circular RNA. *Sci Rep* **9**, 2048 (2019).

81. Hansen, T.B. *et al.* miRNA-dependent gene silencing involving Ago2-mediated cleavage of a circular antisense RNA. *EMBO J* **30**, 4414-4422 (2011).

82. Hansen, T.B. *et al.* Natural RNA circles function as efficient microRNA sponges. *Nature* **495**, 384-388 (2013).

83. Kleaveland, B., Shi, C.Y., Stefano, J. & Bartel, D.P. A Network of Noncoding Regulatory RNAs Acts in the Mammalian Brain. *Cell* **174**, 350-362 e317 (2018).

84. Piwecka, M. *et al.* Loss of a mammalian circular RNA locus causes miRNA deregulation and affects brain function. *Science* **357** (2017).

85. You, X. *et al.* Neural circular RNAs are derived from synaptic genes and regulated by development and plasticity. *Nat Neurosci* **18**, 603-610 (2015).

86. Spitale, R.C., Tsai, M.C. & Chang, H.Y. RNA templating the epigenome: long noncoding RNAs as molecular scaffolds. *Epigenetics* **6**, 539-543 (2011).

87. Du, W.W. *et al.* Foxo3 circular RNA retards cell cycle progression via forming ternary complexes with p21 and CDK2. *Nucleic Acids Res* **44**, 2846-2858 (2016).

88. Du, W.W. *et al.* Foxo3 circular RNA promotes cardiac senescence by modulating multiple factors associated with stress and senescence responses. *Eur Heart J* **38**, 1402-1412 (2017).

89. Huang, S. *et al.* Loss of Super-Enhancer-Regulated circRNA Nfix Induces Cardiac Regeneration After Myocardial Infarction in Adult Mice. *Circulation* **139**, 2857-2876 (2019).

90. Li, Q. *et al.* CircACC1 Regulates Assembly and Activation of AMPK Complex under Metabolic Stress. *Cell Metab* **30**, 157-173 e157 (2019).

91. Holdt, L.M. *et al.* Circular non-coding RNA ANRIL modulates ribosomal RNA maturation and atherosclerosis in humans. *Nat Commun* **7**, 12429 (2016).

92. Abdelmohsen, K. *et al.* Identification of HuR target circular RNAs uncovers suppression of PABPN1 translation by CircPABPN1. *RNA Biol* **14**, 361-369 (2017).

93. Chen, C.Y. & Sarnow, P. Initiation of protein synthesis by the eukaryotic translational apparatus on circular RNAs. *Science* **268**, 415-417 (1995).

94. Li, H. *et al.* riboCIRC: a comprehensive database of translatable circRNAs. *Genome Biol* **22**, 79 (2021).

95. Legnini, I. *et al.* Circ-ZNF609 Is a Circular RNA that Can Be Translated and Functions in Myogenesis. *Mol Cell* **66**, 22-37 e29 (2017).

96. Pamudurti, N.R. *et al.* Translation of CircRNAs. *Mol Cell* **66**, 9-21 e27 (2017).

97. Zhang, M. *et al.* A novel protein encoded by the circular form of the SHPRH gene suppresses glioma tumorigenesis. *Oncogene* **37**, 1805-1814 (2018).

98. Liang, W.C. *et al.* Translation of the circular RNA circbeta-catenin promotes liver cancer cell growth through activation of the Wnt pathway. *Genome Biol* **20**, 84 (2019).

99. Yang, Y. *et al.* Extensive translation of circular RNAs driven by N(6)-methyladenosine. *Cell Res* **27**, 626-641 (2017).

100. Zhou, C. *et al.* Genome-Wide Maps of m6A circRNAs Identify Widespread and Cell-Type-Specific Methylation Patterns that Are Distinct from mRNAs. *Cell Rep* **20**, 2262-2276 (2017).

101. Xiaojuan Fan, Y.Y., Chuyun Chen, Zefeng Wang Pervasive translation of circular RNAs driven by short IRES-like elements. *bioRxiv* (2020).

102. Memczak, S., Papavasileiou, P., Peters, O. & Rajewsky, N. Identification and Characterization of Circular RNAs As a New Class of Putative Biomarkers in Human Blood. *PLoS One* **10**, e0141214 (2015).

103. Li, Y. *et al.* Circular RNA is enriched and stable in exosomes: a promising biomarker for cancer diagnosis. *Cell Res* **25**, 981-984 (2015).

104. Dou, Y. *et al.* Circular RNAs are down-regulated in KRAS mutant colon cancer cells and can be transferred to exosomes. *Sci Rep* **6**, 37982 (2016).

105. Li, Z. *et al.* Tumor-released exosomal circular RNA PDE8A promotes invasive growth via the miR-338/MACC1/MET pathway in pancreatic cancer. *Cancer Lett* **432**, 237-250 (2018).

106. Wang, G. *et al.* Three isoforms of exosomal circPTGR1 promote hepatocellular carcinoma metastasis via the miR449a-MET pathway. *EBioMedicine* **40**, 432-445 (2019).

107. Okamura, M., Inose, H. & Masuda, S. RNA Export through the NPC in Eukaryotes. *Genes (Basel)* **6**, 124-149 (2015).

108. Huang, C., Liang, D., Tatomer, D.C. & Wilusz, J.E. A length-dependent evolutionarily conserved pathway controls nuclear export of circular RNAs. *Genes Dev* **32**, 639-644 (2018).

109. Li, Z., Kearse, M.G. & Huang, C. The nuclear export of circular RNAs is primarily defined by their length. *RNA Biol* **16**, 1-4 (2019).

110. Guo, Y., Wei, X. & Peng, Y. Structure-Mediated Degradation of CircRNAs. *Trends Cell Biol* **30**, 501-503 (2020).

111. Liu, C.X. *et al.* Structure and Degradation of Circular RNAs Regulate PKR Activation in Innate Immunity. *Cell* **177**, 865-880 e821 (2019).

112. Park, O.H. *et al.* Endoribonucleolytic Cleavage of m(6)A-Containing RNAs by RNase P/MRP Complex. *Mol Cell* **74**, 494-507 e498 (2019).

113. Fischer, J.W., Busa, V.F., Shao, Y. & Leung, A.K.L. Structure-Mediated RNA Decay by UPF1 and G3BP1. *Mol Cell* **78**, 70-84 e76 (2020).

114. O'Neil, D., Glowatz, H. & Schlumpberger, M. Ribosomal RNA depletion for efficient use of RNA-seq capacity. *Curr Protoc Mol Biol* **Chapter 4**, Unit 4 19 (2013).

115. Suzuki, H. *et al.* Characterization of RNase R-digested cellular RNA source that consists of lariat and circular RNAs from pre-mRNA splicing. *Nucleic Acids Res* **34**, e63 (2006).

116. Qu, S. *et al.* Microarray expression profile of circular RNAs in human pancreatic ductal adenocarcinoma. *Genom Data* **5**, 385-387 (2015).

117. Jeck, W.R. & Sharpless, N.E. Detecting and characterizing circular RNAs. *Nat Biotechnol* **32**, 453-461 (2014).

118. Wang, X. & Shan, G. Nonradioactive Northern Blot of circRNAs. *Methods Mol Biol* **1724**, 135-141 (2018).

119. Zirkel, A. & Papantonis, A. Detecting Circular RNAs by RNA Fluorescence In Situ Hybridization. *Methods Mol Biol* **1724**, 69-75 (2018).

120. Liu, T. *et al.* Circular RNA FAM114A2 suppresses progression of bladder cancer via regulating NP63 by sponging miR-762. *Cell Death Dis* **11**, 47 (2020).

121. Zheng, Q. *et al.* Circular RNA profiling reveals an abundant circHIPK3 that regulates cell growth by sponging multiple miRNAs. *Nat Commun* **7**, 11215 (2016).

122. Chen, N. *et al.* A novel FLI1 exonic circular RNA promotes metastasis in breast cancer by coordinately regulating TET1 and DNMT1. *Genome Biol* **19**, 218 (2018).

123. Zeng, K. *et al.* The pro-metastasis effect of circANKS1B in breast cancer. *Mol Cancer* **17**, 160 (2018).

124. Panda, A.C., Martindale, J.L. & Gorospe, M. Polysome Fractionation to Analyze mRNA Distribution Profiles. *Bio Protoc* **7** (2017).

125. Lei, M., Zheng, G., Ning, Q., Zheng, J. & Dong, D. Translation and functional roles of circular RNAs in human cancer. *Mol Cancer* **19**, 30 (2020).

126. Schneider, T. *et al.* CircRNA-protein complexes: IMP3 protein component defines subfamily of circRNPs. *Sci Rep* **6**, 31313 (2016).

127. Panda, A.C. *et al.* Identification of senescence-associated circular RNAs (SAC-RNAs) reveals senescence suppressor CircPVT1. *Nucleic Acids Res* **45**, 4021-4035 (2017).

128. Guarnerio, J. *et al.* Oncogenic Role of Fusion-circRNAs Derived from Cancer-Associated Chromosomal Translocations. *Cell* **166**, 1055-1056 (2016).

129. Guarnerio, J. *et al.* Intragenic antagonistic roles of protein and circRNA in tumorigenesis. *Cell Res* **29**, 628-640 (2019).

130. Li, W. *et al.* Characterization of hsa_circ_0004277 as a New Biomarker for Acute Myeloid Leukemia via Circular RNA Profile and Bioinformatics Analysis. *Int J Mol Sci* **18** (2017).

131. Chen, S. *et al.* Widespread and Functional RNA Circularization in Localized Prostate Cancer. *Cell* **176**, 831-843 e822 (2019).

132. Pamudurti, N.R. *et al.* An in vivo strategy for knockdown of circular RNAs. *Cell Discov* **6**, 52 (2020).

133. Liu, S.J. *et al.* CRISPRi-based genome-scale identification of functional long noncoding RNA loci in human cells. *Science* **355** (2017).

134. Joung, J. *et al.* Genome-scale activation screen identifies a lncRNA locus regulating a gene neighbourhood. *Nature* **548**, 343-346 (2017).

135. Wang, K. *et al.* A circular RNA protects the heart from pathological hypertrophy and heart failure by targeting miR-223. *Eur Heart J* **37**, 2602-2611 (2016).

136. Chen, L. *et al.* The bioinformatics toolbox for circRNA discovery and analysis. *Brief Bioinform* (2020).

137. Glazar, P., Papavasileiou, P. & Rajewsky, N. circBase: a database for circular RNAs. *RNA* **20**, 1666-1670 (2014).

138. Wu, W., Ji, P. & Zhao, F. CircAtlas: an integrated resource of one million highly accurate circular RNAs from 1070 vertebrate transcriptomes. *Genome Biol* **21**, 101 (2020).

139. Dudekula, D.B. *et al.* CircInteractome: A web tool for exploring circular RNAs and their interacting proteins and microRNAs. *RNA Biol* **13**, 34-42 (2016).

140. Chen, X. *et al.* circRNADb: A comprehensive database for human circular RNAs with protein-coding annotations. *Sci Rep* **6**, 34985 (2016).

141. Tang, Z. *et al.* TRCirc: a resource for transcriptional regulation information of circRNAs. *Brief Bioinform* **20**, 2327-2333 (2019).

142. Liu, M., Wang, Q., Shen, J., Yang, B.B. & Ding, X. Circbank: a comprehensive database for circRNA with standard nomenclature. *RNA Biol* **16**, 899-905 (2019).

143. Kalari, K.R. *et al.* BBBomics-Human Blood Brain Barrier Transcriptomics Hub. *Front Neurosci* **10**, 71 (2016).

144. Li, S. *et al.* exoRBase: a database of circRNA, lncRNA and mRNA in human blood exosomes. *Nucleic Acids Res* **46**, D106-D112 (2018).

145. Gokool, A., Anwar, F. & Voineagu, I. The Landscape of Circular RNA Expression in the Human Brain. *Biol Psychiatry* **87**, 294-304 (2020).

146. Xia, S. *et al.* CSCD: a database for cancer-specific circular RNAs. *Nucleic Acids Res* **46**, D925-D929 (2018).

147. Xia, S. *et al.* Comprehensive characterization of tissue-specific circular RNAs in the human and mouse genomes. *Brief Bioinform* **18**, 984-992 (2017).

148. Feng, J. *et al.* CircView: a visualization and exploration tool for circular RNAs. *Brief Bioinform* **19**, 1310-1316 (2018).

149. Fan, C., Lei, X., Fang, Z., Jiang, Q. & Wu, F.X. CircR2Disease: a manually curated database for experimentally supported circular RNAs associated with various diseases. *Database (Oxford)* **2018** (2018).

150. Zhao, Z. *et al.* circRNA disease: a manually curated database of experimentally supported circRNA-disease associations. *Cell Death Dis* **9**, 475 (2018).

151. Rophina, M., Sharma, D., Poojary, M. & Scaria, V. Circad: a comprehensive manually curated resource of circular RNA associated with diseases. *Database (Oxford)* **2020** (2020).

152. Meng, X., Hu, D., Zhang, P., Chen, Q. & Chen, M. CircFunBase: a database for functional circular RNAs. *Database (Oxford)* **2019** (2019).

153. Wu, S.M. *et al.* circlncRNAnet: an integrated web-based resource for mapping functional networks of long or circular forms of noncoding RNAs. *Gigascience* **7**, 1-10 (2018).

154. Hausenloy, D.J. & Yellon, D.M. Myocardial ischemia-reperfusion injury: a neglected therapeutic target. *J Clin Invest* **123**, 92-100 (2013).

155. Yeap, X.Y., Dehn, S., Adelman, J., Lipsitz, J. & Thorp, E.B. Quantitation of acute necrosis after experimental myocardial infarction. *Methods Mol Biol* **1004**, 115-133 (2013).

156. Guo, Z., Cao, Q., Zhao, Z. & Song, C. Biogenesis, Features, Functions, and Disease Relationships of a Specific Circular RNA: CDR1as. *Aging Dis* **11**, 1009-1020 (2020).

157. Li, B. *et al.* MicroRNA-7a/b protects against cardiac myocyte injury in ischemia/reperfusion by targeting poly(ADP-ribose) polymerase. *PLoS One* **9**, e90096 (2014).

158. Geng, H.H. *et al.* The Circular RNA Cdr1as Promotes Myocardial Infarction by Mediating the Regulation of miR-7a on Its Target Genes Expression. *PLoS One* **11**, e0151753 (2016).

159. Wang, K. *et al.* Circular RNA mediates cardiomyocyte death via miRNA-dependent upregulation of MTP18 expression. *Cell Death Differ* **24**, 1111-1120 (2017).

160. Li, M. *et al.* A circular transcript of ncx1 gene mediates ischemic myocardial injury by targeting miR-133a-3p. *Theranostics* **8**, 5855-5869 (2018).

161. Zhang, M. *et al.* Circular RNA (circRNA) CDYL Induces Myocardial Regeneration by ceRNA After Myocardial Infarction. *Med Sci Monit* **26**, e923188 (2020).

162. Cai, L. *et al.* Circular RNA Ttc3 regulates cardiac function after myocardial infarction by sponging miR-15b. *J Mol Cell Cardiol* **130**, 10-22 (2019).

163. Garikipati, V.N.S. *et al.* Circular RNA CircFndc3b modulates cardiac repair after myocardial infarction via FUS/VEGF-A axis. *Nat Commun* **10**, 4317 (2019).

164. Zhu, X., Wang, X., Wang, Y. & Zhao, Y. The regulatory network among CircHIPK3, LncGAS5, and miR-495 promotes Th2 differentiation in allergic rhinitis. *Cell Death Dis* **11**, 216 (2020).

165. Wen, J. *et al.* Circular RNA HIPK3: A Key Circular RNA in a Variety of Human Cancers. *Front Oncol* **10**, 773 (2020).

166. Si, X. *et al.* circRNA Hipk3 Induces Cardiac Regeneration after Myocardial Infarction in Mice by Binding to Notch1 and miR-133a. *Mol Ther Nucleic Acids* **21**, 636-655 (2020).

167. Travers, J.G., Kamal, F.A., Robbins, J., Yutzey, K.E. & Blaxall, B.C. Cardiac Fibrosis: The Fibroblast Awakens. *Circ Res* **118**, 1021-1040 (2016).

168. Zhang, C. *et al.* Rapid Development of Targeting circRNAs in Cardiovascular Diseases. *Mol Ther Nucleic Acids* **21**, 568-576 (2020).

169. Zhu, Y. *et al.* Upregulation of Circular RNA CircNFIB Attenuates Cardiac Fibrosis by Sponging miR-433. *Front Genet* **10**, 564 (2019).

170. Ni, H. *et al.* Inhibition of circHIPK3 prevents angiotensin II-induced cardiac fibrosis by sponging miR-29b-3p. *Int J Cardiol* **292**, 188-196 (2019).

171. Zhou, B. & Yu, J.W. A novel identified circular RNA, circRNA_010567, promotes myocardial fibrosis via suppressing miR-141 by targeting TGF-beta1. *Biochem Biophys Res Commun* **487**, 769-775 (2017).

172. Tang, C.M. *et al.* CircRNA_000203 enhances the expression of fibrosis-associated genes by derepressing targets of miR-26b-5p, Col1a2 and CTGF, in cardiac fibroblasts. *Sci Rep* **7**, 40342 (2017).

173. Kimura, A. Molecular genetics and pathogenesis of cardiomyopathy. *J Hum Genet* **61**, 41-50 (2016).

174. Khan, M.A. *et al.* RBM20 Regulates Circular RNA Production From the Titin Gene. *Circ Res* **119**, 996-1003 (2016).

175. Zeng, Y. *et al.* A Circular RNA Binds To and Activates AKT Phosphorylation and Nuclear Localization Reducing Apoptosis and Enhancing Cardiac Repair. *Theranostics* **7**, 3842-3855 (2017).

176. Frey, N., Katus, H.A., Olson, E.N. & Hill, J.A. Hypertrophy of the heart: a new therapeutic target? *Circulation* **109**, 1580-1589 (2004).

177. Lim, T.B. *et al.* Targeting the highly abundant circular RNA circSlc8a1 in cardiomyocytes attenuates pressure overload induced hypertrophy. *Cardiovasc Res* **115**, 1998-2007 (2019).

178. Lavenniah, A. *et al.* Engineered Circular RNA Sponges Act as miRNA Inhibitors to Attenuate Pressure Overload-Induced Cardiac Hypertrophy. *Mol Ther* **28**, 1506-1517 (2020).

179. Liu, C. *et al.* Targeting pericyte-endothelial cell crosstalk by circular RNA-cPWWP2A inhibition aggravates diabetes-induced microvascular dysfunction. *Proc Natl Acad Sci U S A* **116**, 7455-7464 (2019).

180. Zhu, K. *et al.* Downregulation of circRNA DMNT3B contributes to diabetic retinal vascular dysfunction through targeting miR-20b-5p and BAMBI. *EBioMedicine* **49**, 341-353 (2019).

181. Shan, K. *et al.* Circular Noncoding RNA HIPK3 Mediates Retinal Vascular Dysfunction in Diabetes Mellitus. *Circulation* **136**, 1629-1642 (2017).

182. Liu, C. *et al.* Silencing Of Circular RNA-ZNF609 Ameliorates Vascular Endothelial Dysfunction. *Theranostics* **7**, 2863-2877 (2017).

183. Wang, J.J. *et al.* Circular RNA-ZNF609 regulates retinal neurodegeneration by acting as miR-615 sponge. *Theranostics* **8**, 3408-3415 (2018).

184. Libby, P. *et al.* Atherosclerosis. *Nat Rev Dis Primers* **5**, 56 (2019).

185. Rader, D.J. & Daugherty, A. Translating molecular discoveries into new therapies for atherosclerosis. *Nature* **451**, 904-913 (2008).

186. Gomez, D. & Owens, G.K. Smooth muscle cell phenotypic switching in atherosclerosis. *Cardiovasc Res* **95**, 156-164 (2012).

187. Zhang, F. *et al.* Comprehensive analysis of circRNA expression pattern and circRNA-miRNA-mRNA network in the pathogenesis of atherosclerosis in rabbits. *Aging (Albany NY)* **10**, 2266-2283 (2018).

188. Small, E.M. & Olson, E.N. Pervasive roles of microRNAs in cardiovascular biology. *Nature* **469**, 336-342 (2011).

189. Poller, W. *et al.* Non-coding RNAs in cardiovascular diseases: diagnostic and therapeutic perspectives. *Eur Heart J* **39**, 2704-2716 (2018).

190. Bazan, H.A. *et al.* Acute Loss of miR-221 and miR-222 in the Atherosclerotic Plaque Shoulder Accompanies Plaque Rupture. *Stroke* **46**, 3285-3287 (2015).

191. Bazan, H.A. *et al.* Carotid Plaque Rupture Is Accompanied by an Increase in the Ratio of Serum circR-284 to miR-221 Levels. *Circ Cardiovasc Genet* **10** (2017).

192. Paloschi, V. & Maegdefessel, L. Towards Point-of-Care Measurements Using Noncoding RNAs: A Novel Tool to Monitor Aggravation of Advanced Atherosclerotic Lesions. *Circ Cardiovasc Genet* **10** (2017).

193. Wellcome Trust Case Control, C. Genome-wide association study of 14,000 cases of seven common diseases and 3,000 shared controls. *Nature* **447**, 661-678 (2007).

194. Zhang, S. *et al.* Circular RNA circ_0003204 inhibits proliferation, migration and tube formation of endothelial cell in atherosclerosis via miR-370-3p/TGFbetaR2/phosph-SMAD3 axis. *J Biomed Sci* **27**, 11 (2020).

195. Shi, N., Mei, X. & Chen, S.Y. Smooth Muscle Cells in Vascular Remodeling. *Arterioscler Thromb Vasc Biol* **39**, e247-e252 (2019).

196. Yang, L., Yang, F., Zhao, H., Wang, M. & Zhang, Y. Circular RNA circCHFR Facilitates the Proliferation and Migration of Vascular Smooth Muscle via miR-370/FOXO1/Cyclin D1 Pathway. *Mol Ther Nucleic Acids* **16**, 434-441 (2019).

197. Sun, Y. *et al.* Angiotensin II inhibits apoptosis of mouse aortic smooth muscle cells through regulating the circNRG-1/miR-193b-5p/NRG-1 axis. *Cell Death Dis* **10**, 362 (2019).

198. Hall, I.F. *et al.* Circ_Lrp6, a Circular RNA Enriched in Vascular Smooth Muscle Cells, Acts as a Sponge Regulating miRNA-145 Function. *Circ Res* **124**, 498-510 (2019).

199. Kent, K.C. Clinical practice. Abdominal aortic aneurysms. *N Engl J Med* **371**, 2101-2108 (2014).

200. Powell, J.T. & Greenhalgh, R.M. Clinical practice. Small abdominal aortic aneurysms. *N Engl J Med* **348**, 1895-1901 (2003).

201. Petsophonsakul, P. *et al.* Role of Vascular Smooth Muscle Cell Phenotypic Switching and Calcification in Aortic Aneurysm Formation. *Arterioscler Thromb Vasc Biol* **39**, 1351-1368 (2019).

202. Zhou, M. *et al.* Circular RNA expression profile and its potential regulative role in human abdominal aortic aneurysm. *BMC Cardiovasc Disord* **20**, 70 (2020).

203. Zheng, C. *et al.* Cyclic RNA hsacirc000595 regulates apoptosis of aortic smooth muscle cells. *Mol Med Rep* **12**, 6656-6662 (2015).

204. Yang, R., Wang, Z., Meng, G. & Hua, L. Circular RNA CCDC66 facilitates abdominal aortic aneurysm through the overexpression of CCDC66. *Cell Biochem Funct* **38**, 830-838 (2020).

205. Yue, J. *et al.* CircCBFB-mediated miR-28-5p facilitates abdominal aortic aneurysm via LYPD3 and GRIA4. *Life Sci* **253**, 117533 (2020).

206. Mitra, A.K. & Agrawal, D.K. In stent restenosis: bane of the stent era. *J Clin Pathol* **59**, 232-239 (2006).

207. Alexander, M.R. & Owens, G.K. Epigenetic control of smooth muscle cell differentiation and phenotypic switching in vascular development and disease. *Annu Rev Physiol* **74**, 13-40 (2012).

208. Weiser-Evans, M.C.M. Smooth Muscle Differentiation Control Comes Full Circle: The Circular Noncoding RNA, circActa2, Functions as a miRNA Sponge to Fine-Tune alpha-SMA Expression. *Circ Res* **121**, 591-593 (2017).

209. Sun, Y. *et al.* A Novel Regulatory Mechanism of Smooth Muscle alpha-Actin Expression by NRG-1/circACTA2/miR-548f-5p Axis. *Circ Res* **121**, 628-635 (2017).

210. Kong, P. *et al.* circ-Sirt1 controls NF-kappaB activation via sequence-specific interaction and enhancement of SIRT1 expression by binding to miR-132/212 in vascular smooth muscle cells. *Nucleic Acids Res* **47**, 3580-3593 (2019).

211. Zeng, Z. *et al.* Circular RNA CircMAP3K5 Acts as a MicroRNA-22-3p Sponge to Promote Resolution of Intimal Hyperplasia Via TET2-Mediated Smooth Muscle Cell Differentiation. *Circulation* **143**, 354-371 (2021).

212. Xu, J.Y. *et al.* circDiaph3 regulates rat vascular smooth muscle cell differentiation, proliferation, and migration. *FASEB J* **33**, 2659-2668 (2019).

213. Rong, Z.H. *et al.* Suppression of circDcbld1 Alleviates Intimal Hyperplasia in Rat Carotid Artery by Targeting miR-145-3p/Neuropilin-1. *Mol Ther Nucleic Acids* **18**, 999-1008 (2019).

Figure Legends

Figure 2.1. Biogenesis of circRNAs.

Figure 2.2. Biological functions, transportation and degradation of circRNAs.

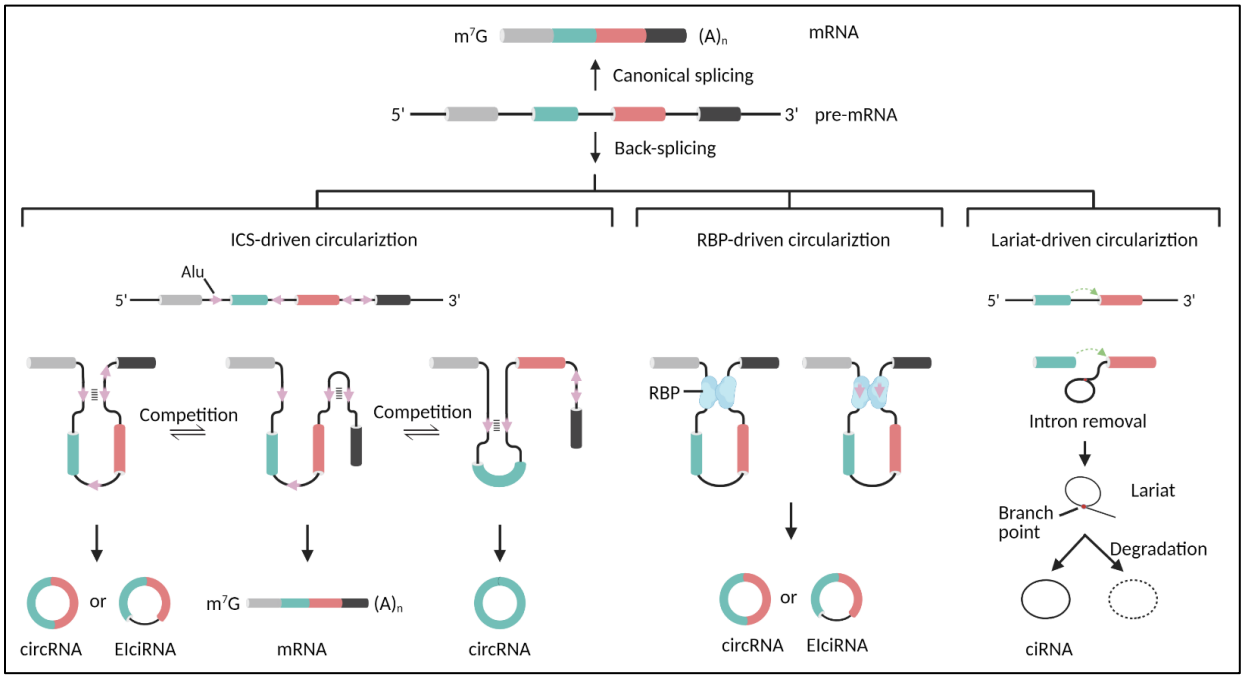

Figure 2.1. Biogenesis of circRNAs.

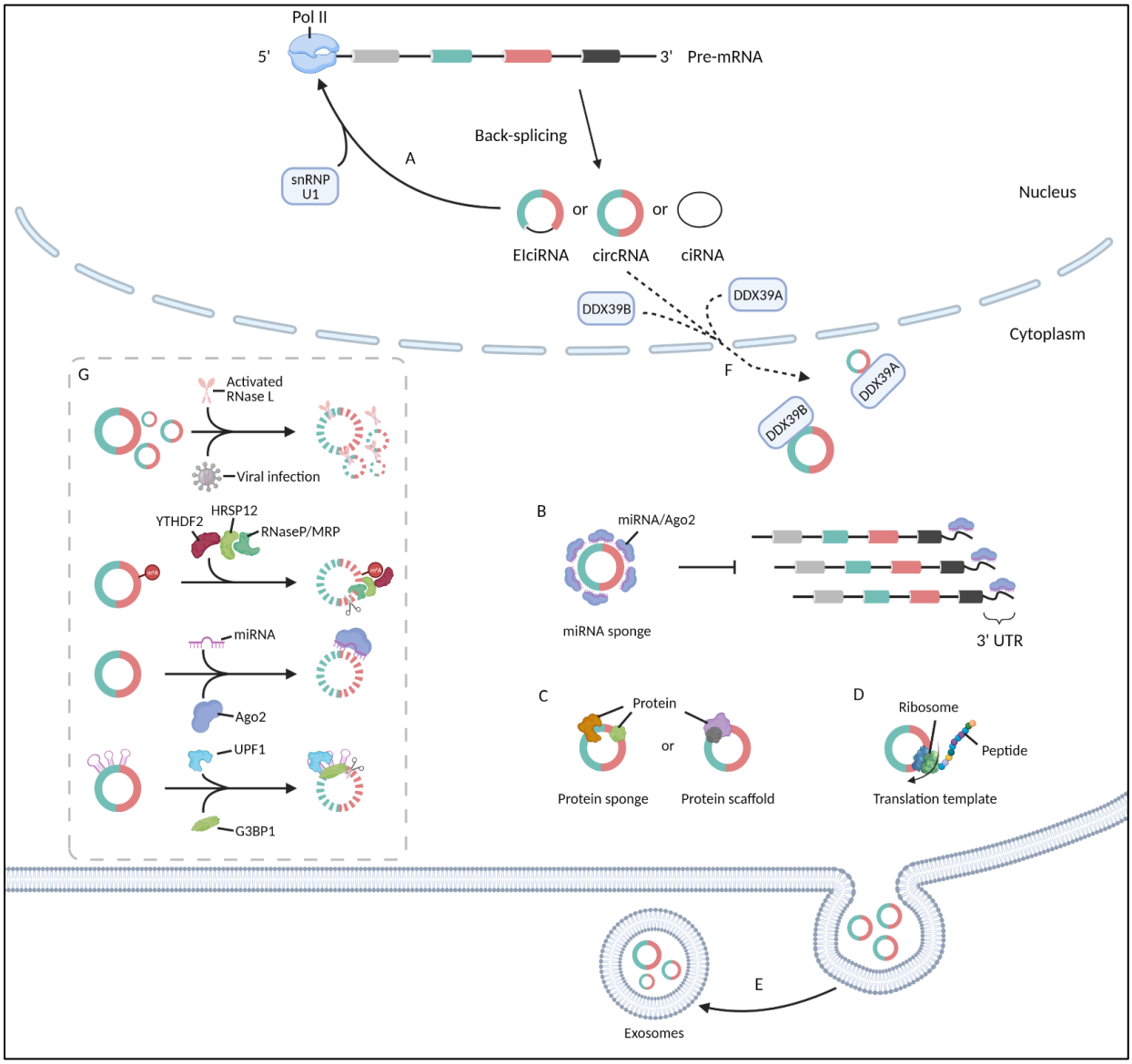

Figure 2.2. Biological functions, transportation, and degradation of circRNAs.

Table 2.1: Approaches to study circRNAs

Purposes	Methods	Technique details	Diagrams
circRNA detection	Ribosomal RNA depletion RNA sequencing	RNA samples are pre-treated to remove ribosomal RNAs and followed by NGS.	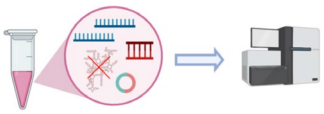
	RNase R treatment RNA sequencing	RNA samples are treated with RNase R to digest the majority of linear RNAs to enrich the circRNAs and followed by NGS.	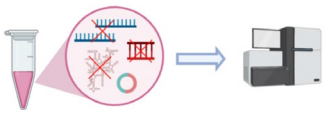
	circRNA microarray assay	RNA samples with either ribosomal RNA removal or RNase R treatment are loaded to microarray chip contains circRNA-specific probes.	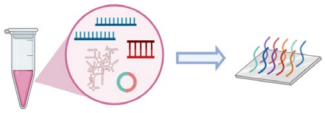
circRNA validation and characterization	RT-PCR	Divergent primers are used to amplify the BSJ part of circRNAs. PCR products are run on the agarose gel.	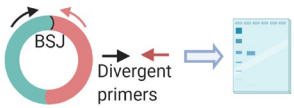
	RNase R treatment	RNase R digests linear RNAs while leaving the circRNAs unaffected.	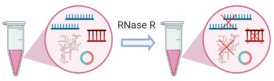
	Sanger sequencing	Bands after size selection are eluted and sent to Sanger sequencing to confirm the BSJ sequence.	
	Northern blot	RNA is run in denaturing polyacrylamide gel and followed by hybridization of radioactive or nonradioactive probe targets circRNA BSJ.	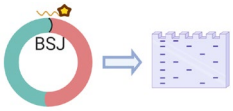
	Fluorescence *in situ* hybridization	Digoxigenin or biotin-labeled probes target circRNA BSJ part. Visualization or quantification of circRNAs in cells or tissue.	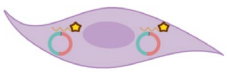
circRNA localization	Nuclear/cytoplasm fraction analysis	Cellular nuclear and cytoplasm are separated and followed by circRNA analysis.	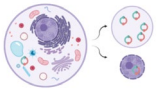
	Fluorescence in situ hybridization	Digoxigenin or biotin-labeled probes target circRNA BSJ part. Visualization of circRNAs localization in cells.	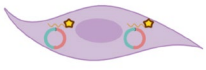

	Ribosome profiling	Cells are pre-treated and fixed and followed by polysome gradient fractions for circRNA translation analysis.	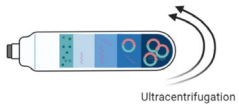
circRNA interaction	RNA Immunoprecipitation	Anti-circRNA-related RBP antibody is used to co-immunoprecipitate circRNAs and RBP for downstream analysis.	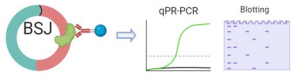
	RNA pulldown assay	Digoxigenin or biotin-labeled probes target circRNA BSJ are used to pull down circRNA for downstream analysis.	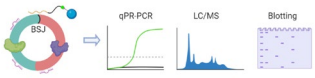
Loss and gain of function of circRNA	siRNA/shRNA mediated knockdown	siRNA or shRNA targets circRNA BSJ part is used to knockdown the circRNA expression level.	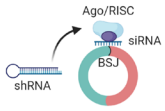
	CRISPR/Cas9 mediated circRNA knockout – intronic deletion	gRNA targets intronic complementary Alu elements to disrupt circRNA formation to knockout circRNA expression by CRISPR/Cas system.	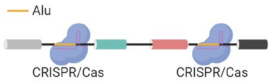
	CRISPR/Cas9 mediated circRNA knockout – exonic deletion	Two gRNAs are designed to target both junction parts of exon's two ends to remove the exon on genome by CRISPR/Cas system.	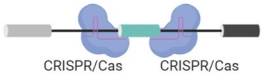
	Plasmid overexpression	The circRNA-related sequence is cloned into circRNA overexpression plasmid.	
	Adenovirus overexpression	The overexpression plasmid can be packaged into adenovirus.	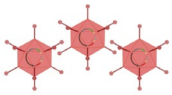

Table 2.2: CircRNA databases and online resources

Database	Species	Tissue/Type	Function	Website	Cardiovascular-related data
BBBomics	H.sapiens	BBB specific	browse	http://bioinformaticstools.mayo.edu/bbbomics/	Human cerebral microvascular endothelial cell line (hCMEC/D3)
exoRBase	H.sapiens	blood exosomes	search/browse	http://www.exorbase.org/	Coronary heart disease
voineagulab-circRNA data browser	H.sapiens	brain	genome browser display	http://www.voineagulab.ums w.edu.au/circrna-data-browser	NA
CSCD	H.sapiens	Cancer specific	search/miRNA target /ORF prediction/alternative splicing visualisation	http://gb.whu.edu.cn/CSCD/	NA
CircR2Disease	H.sapiens/M.musculus/R.norvegicus	Disease specific	search/browse/experimental evidence	http://bioinfo.snnu.edu.cn/CircR2Disease/	Multiple cardiovascular diseases
circRNADisease	H.sapiens/M.musculus	Disease specific	search/browse/experimental evidence	http://cgga.org.cn:9091/circRNADisease/	Multiple cardiovascular diseases
circad	H.sapiens/M.musculus/R.norvegicus/ S.scrofa/G.gallus	Disease specific	search/browse/experimental evidence	http://clingen.igib.res.in/circad/	Multiple cardiovascular diseases
CIRCpedia	H.sapiens/M.musculus/C.elegans/ R.norvegicus/D.melanogaster /D.rerio	multiple cell lines	search/browse/plot generation	https://www.picb.ac.cn/rnomics/circpedia/	Heart/HUVEC
circBase	H.sapiens/M.musculus/C.elegans/ D.melanogaster/L.chalumnae/ L.menadoensis	multiple cell lines and tissues	search/browse/blat	http://circrna.org/	Multiple cardiovascular related cell lines and tissues
ENCORI (starBase)	H.sapiens/M.musculus/C.elegans	multiple cell lines and tissues	miRNA binding/RBP binding	http://starbase.sysu.edu.cn/starbase2/index.php	NA
CircAtlas	H.sapiens/M.musculus/M.mulatta/ R.norvegicus/S.scrofa/G.gallus	multiple cell lines and tissues	search/browse/miRNA binding/ORF prediction/IRES prediction/RBP binding/circRNAs conservation/network annotation	http://circatlas.biols.ac.cn/	Multiple cardiovascular diseases
CircInteractome	H.sapiens	multiple cell lines and tissues	search/RBP binding /miRNA target /Divergent primer design/siRNA design	https://circinteractome.nia.nih.gov/	NA
circRNADb	H.sapiens	multiple cell lines and tissues	search/browse/IRES prediction/ORF prediction/modification prediction/half-life prediction	http://reprod.njmu.edu.cn/cgi-bin/circrnadb/circRNADb.php	NA
TRCirc	H.sapiens	multiple cell lines and tissues	search/browse/methylation search/enhancer search	http://www.licpathway.net/TRCirc/view/index	HUVEC
CircFunBase	H.sapiens/M.musculus/M.mulatta/ R.norvegicus/S.scrofa/G.gallus/ B.taurus/O.cuniculus/Plants	NA	search/browse/blast	http://bis.zju.edu.cn/CircFunBase/	Multiple cardiovascular diseases
Circbank	H.sapiens	NA	search/miRNA-circRNA interaction/protein coding potential /modification prediction	http://www.circbank.cn/	Multiple cardiovascular related cell lines and tissues
circlncRNAnet	customizable	NA	upload of expression matrix data/plot generation(PCA, circos, heatmap,etc.)/pathway enrichment/interactiomic analysis	http://120.126.1.61/circlnc/index.php	Customizable
CircView	customizable	NA	circRNA visualization	http://gb.whu.edu.cn/CircView/	Customizable
TSCD	H.sapiens/M.musculus	tissue specific	search/miRNA target /RBP binding	http://gb.whu.edu.cn/TSCD/	Blood vessel/Heart
riboCIRC	H.sapiens/M.musculus/R.norvegicus/ C.elegans/D.melanogaster/D.rerio	multiple cell lines and tissues	search/browse ribosome-associated circRNAs and translatable circRNAs products/experimental evidence	http://www.ribocirc.com/	NA

Table 2.3: CircRNA in hearts

Heart diseases							
CircRNA	**Diseases**	**Host gene**	**Expression pattern**	**Roles**	**Mechanism**	**Target**	**Types of experiments**	**Refs**
Cdr1as	MI	Cdr1	upregulated	Cdr1as increases cardiac infarct size	miRNA sponge	miR-7a/PARP, SP1	*in vitro/in vivo*	**158**
MFACR		Smyd4	upregulated	MFACR promotes mitochondrial fission and apoptosis	miRNA sponge	miR-652-3p/MTP18	*in vitro/in vivo*	**159**
circNCX1		NCX1	upregulated	circNCX1 induces cardiomyocyte apoptosis and promotes cardiac ischemia-reperfusion injury	miRNA sponge	miR-133a-3p/CDIP1	*in vitro/in vivo*	**160**
CircCDYL		CDYL	downregulated	Induces cardiomyocytes proliferation and myocardial regeneration	miRNA sponge	miR-4793-5p/APP	*in vitro/in vivo*	**161**
circNfix		Nfix	upregulated	circNfix suppresses cardiac regenerative repair and functional recovery after myocardial infarction	Protein binding/miRNA sponge	Ybx1,Nedd4l/cyclinA2, cyclinB1&miR-214/Gsk3β	*in vitro/in vivo*	**89**
circTtc3		Ttc3	upregulated	circTtc3 protects cardiomyocytes from hypoxia-induced ATP depletion and apoptotic death	miRNA sponge	miR-15b-5p/Arl2	*in vitro/in vivo*	**162**
circFndc3b		Fndc3b	downregulated	circFndc3b reduces cardiomyocyte apoptosis, promotes neovascularization, limits infarct size, and preserves post-MI cardiac function	Protein binding	FUS1/VEGF	*in vitro/in vivo*	**163**
circHipk3		Hipk3	downregulated	circHipk3 induces cardiac regeneration and angiogenesis and reduces the infarct size after MI	miRNA sponge/Protein binding	miR-133a /CTGF,NOTCH1/Ccnd1	*in vitro/in vivo*	**166**
CircNFIB	Cardiac Fibrosis	NFIB	downregulated	circNFIB decreases cell proliferation in both NIH/3T3 cells and primary adult fibroblasts	miRNA sponge	miR-433/AZIN1,JNK1	*in vitro*	**169**
circHIPK3		HIPK3	upregulated	circHIPK3 promotes angiotensin II-induced cardiac fibrosis and hypertrophy	miRNA sponge	miR-29b-3p/COL1A1,COL3A1,a-SMA	*in vitro/in vivo*	**170**
circRNA_010567		ZSWIM6	upregulated	circRNA_010567 induces fibrosis-associated protein resection in cardiac fibrosis	miRNA sponge	miR-141 /TGF-b1	*in vitro*	**171**
CircRNA_000203		MYO9A	upregulated	circRNA_000203 increases the expressions of fibrosis-associated proteins in mouse cardiac fibroblasts	miRNA sponge	miR-26b-5p/Col1a2,CTGF	*in vitro*	**172**
cCAMK2D	Cardiomyopathy	CAMK2D	downregulated	Authenticity validated; Significant downregulation in HCM and DCM samples compared with control	NA	NA	*in vitro*	**174**
cTTN1-5		TTN	downregulated in DCM samples	Authenticity validated; Significant downregulation in DCM samples compared with control	NA	NA	*in vitro*	**174**
circAmotl1		Amotl1	downregulated	circ-Amotl1 promotes Dox-induced cardiomyopathy	Protein binding	PDK1,AKT1	*in vitro/in vivo*	**175**
circFoxo3		Foxo3	upregulated	circFoxo3 induces cardiac senescence and promotes Dox-induced cardiomyopathy	Protein binding	ID1,E2F1, FAK,HIF1	*in vitro/in vivo*	**88**
HRCR	Cardiac hypertrophy	PWWP2A	downregulated	HRCR suppresses cardiac hypertrophy	miRNA sponge	miR-223/ARC	*in vitro/in vivo*	**135**
circSlc8a1		Slc8a1	no change	circSlc8a1 promotes cardiac hypertrophy and heart failure	miRNA sponge	miR-133a/pathological hypertrophy stress-genes	*in vitro/in vivo*	**177**
circmiRs		artificially engineered	NA	*In vivo* delivery of circmiRs attenuates left ventricular hypertrophy	miRNA sponge	miR-132&miR-212	*in vitro/in vivo*	**178**

Table 2.4: CircRNA in the cardiovascular system

Vascular diseases								
CircRNA	**Diseases**	**host gene**	**Expression pattern**	**Roles**	**Mechanism**	**Target**	**Types of experiments**	**Refs**
cPWWP2A	Diabetic Retinopathy	PWWP2A	upregulated	cPWWP2A protects pericytes against high glucose-induced injury and suppresses diabetes mellitus-induced microvascular dysfunction	miRNA sponge/Protein binding	miR-579/Angiopoietin 1, Occludin, SIRT1&PWWP2A	*in vitro/in vivo*	**179**
circDNMT3B		DNMT3B	upregulated	circDMNT3B suppresses the angiogenic function of vascular endothelial cells	miRNA sponge	miR-20b-5p/BAMBI	*in vitro/in vivo*	**180**
circHIPK3		HIPK3	upregulated	circHIPK3 promotes retinal vascular dysfunction	miRNA sponge	miR-30a-3p/VEGF-C,FZD4, WNT2	*in vitro/in vivo*	**181**
circZNF609		ZNF609(hsa)	upregulated	circZNF609 retinal vessel loss and pathological angiogenesis	miRNA sponge	miR-615/MEF2A	*in vitro/in vivo*	**182**
		ZNF609(rno)	upregulated	circZNF609 promotes retinal reactive gliosis and glial cell activation	miRNA sponge	miR-615/METRN	*in vitro/in vivo*	**183**
ocu-cirRNAs	Atherosclerosis	mutiple	mixed	seven circRNAs are related to atherosclerosis	NA	mutiple	*in silico*	**187**
CircR-284		HIPK3	circR-284 to miR-221 ratio upregulated	Plasmatic miR-221:circR-284 ratio for biomarker purposes in advanced atherosclerosis	miRNA sponge	miR-221&miR-222	*in vitro/in vivo*	**191,192**
circANRIL		ANRIL (CDKN2B-AS1)	downregulated	circANRIL prevents pre-rRNA binding and exonuclease-mediated rRNA maturation	Protein binding	PES1	*in vitro/in vivo*	**91**
Circ_0003204		USP36	upregulated	circ_0003204 promotes EC aberrant phenotype in atherosclerosis pathology	miRNA sponge	miR-370/TGFbR2/p-SMAD3	*in vitro*	**194**
circCHFR		CHFR	upregulated	circCHFR promotes the proliferation and migration ability of VSMCs	miRNA sponge	miR-370/FOXO1/Cyclin D1	*in vitro*	**196**
circNRG-1		NRG-1	downregulated	circNRG-1 promotes NRG-1 expression and apoptosis of MASMCs	miRNA sponge	miR-193b-5p/NRG-1	*in vitro*	**197**
circ_Lrp6		Lrp6	no change	The level of circ_Lrp6 was not significantly modulated	NA	NA	*in vitro/in vivo*	**198**
circ-000595	Aortic aneurysm	BTBD7	upregulated	hsa-circ-000595 promotes apoptotic rate of HASMCs	miRNA sponge	miR-19a	*in vitro*	**203**
circCCDC66		CCDC66	upregulated	circCCDC66 suppresses proliferation and promotes apoptosis in VSMCs	miRNA sponge	miR-342-3p/CCDC66	*in vitro*	**204**
circCBFB		CBFB	NA	circCBFB suppresses apoptosis of VSMCs	miRNA sponge	miR-28-5p/GRIA4, LYPD3	*in vitro*	**205**
circACTA2	Neointimal hyperplasia	ACTA2	downregulated	circACTA2 promotes α-SMA protein level in mouse SMC	miRNA sponge	NRG-1-ICD/circACTA2/miR-548f-5p	*in vitro/in vivo*	**209**
circDiaph3		Diaph3	upregulated	circDiaph3 suppresses the level of Diaph3 and inhibits the differentiation of VSMCs to contractile type.	miRNA sponge	miR-148a-5p/Igf1r	*in vitro/in vivo*	**212**
circDcbld1		Dcbld1	upregulated	circDcbld1 suppresses expression of contractile smooth muscle cell markers in rat VSMCs	miRNA sponge	miR-145-3p/Nrp1	*in vitro/in vivo*	**213**
circ-Sirt1		SIRT1	downregulated	Circ-Sirt1 inhibits the nuclear translocation of NF-κB and decreases TNF-α-induced NF-κB p65 acetylation and transcriptional activity	miRNA sponge/Protein binding	miR-132/212/SIRT&NF-κB p65	*in vitro/in vivo*	**210**
circ_Lrp6		Lrp6	upregulated	circ_Lrp6 promotes mice wire injury induced neointimal hyperplasia	miRNA sponge	miR-145/fascin, Lox, ITGβ8, KLF4, Yes1	*in vitro/in vivo*	**198**
CircMAP3K5		MAP3K5	downregulated	circMap3k5 promote SMC differentiation and suppresses neointima formation	miRNA sponge	miR-22-3p/TET2	*in vitro/in vivo*	**211**

CHAPTER 3

CIRCSOD2, A NOVEL REGULATOR FOR SMOOTH MUSCLE PROLIFERATION AND VASCULAR REMODELING

Mei X, Cui XB, Li Y and Chen SY.

Submitted to Arterioscler Thromb Vasc Biol. February 24, 2021.

Abstract

Objective— Vascular smooth muscle cell (SMC) proliferation contributes to neointima formation following vascular injury. Circular RNA (circRNA), a novel type of non-coding RNA with closed-loop structure, exhibits cell- and tissue-specific expression patterns. However, the role of circRNA in SMC proliferation and neointima formation is largely unknown. The objective of this study is to investigate the role and mechanism of circSOD2 in SMC proliferation and neointima formation.

Approach and Results— CircRNA profiling of human aortic SMCs revealed that platelet-derived growth factor (PDGF)-BB up- and down-regulated numerous circRNAs. Among them, circSOD2, derived from back-splicing event of superoxide dismutase 2, was significantly enriched. Knockdown of circSOD2 by short hairpin RNA (shRNA) blocked PDGF-BB-induced SMC proliferation. Inversely, circSOD2 ectopic expression promoted SMC proliferation. Mechanistically, circSOD2 acted as a sponge for microRNA 206, leading to downregulation of Notch3, which regulates cyclin D1 and CDK4/6 via ERK1/2 signaling. In vivo studies showed that circSOD2 was induced in neointima SMCs in balloon-injured rat carotid arteries. Importantly, knockdown of circSOD2 attenuated injury-induced neointima formation along with decreased neointimal SMC proliferation.

Conclusions— CircSOD2 is a novel regulator mediating SMC proliferation and neointima formation during injury-induced vascular remodeling. Therefore, circSOD2 could be a potential therapeutic target for preventing neointimal formation in proliferative vascular diseases.

Introduction

Vascular remodeling is a fundamental pathological process following vascular injury which often occurs after percutaneous coronary intervention, bypass surgery, or cardiac transplantation, etc. Vascular remodeling or neointimal hyperplasia in proliferative vascular diseases remains a significant issue despite numerous pharmacological and mechanical approaches have been advanced in recent years[1, 2]. Smooth muscle cells (SMCs) within the medial layer of the artery wall usually maintain in a quiescent state until they are activated to a proliferative state in response to vascular injuries, such as mechanical stretch, medical dissection, and endothelial denudation, leading to exposure to circulating growth factors or mitogens[1, 3]. SMC proliferation is considered as a crucial step in the development of neointima formation[1]. Thus, investigation of molecular mechanisms responsible for SMC proliferation is vital for achieving a better understanding of the pathogenesis of proliferative vascular disorders.

Transcriptomic studies have revealed that up to 90% human genome is transcribed, but only 1-2% of transcripts encode proteins. Substantial numbers of transcripts are categorized as non-coding RNAs (ncRNAs). Emerging evidence has shown that ncRNAs are multifunctional regulators associated with many diseases, including developmental, oncological, neurological, cardiovascular, autoimmune, and cutaneous disorders[4-10]. As a novel class of ncRNA, circular RNA (circRNA) has been found to play a potent role in multiple biological processes and exhibit tissue- and disease-specific expression patterns[11-13]. Unlike linear RNA, circRNA undergoes back-splicing, forming a covalently closed loop structure without 3′ and 5′ ends[14]. Owing to the unique feature, circRNA is speculated to have higher stability and longer half-life than linear RNA due to its resistance to exonuclease degradation and thereby execute exclusive cellular

regulatory fuctions[15]. Only a few studies have investigated circRNA roles in vascular diseases. For example, circANRIL[16], circMAP3K5[17], circACTA2[18, 19], circDcbld1[20] and circ_Lrp6[21], which participate in SMC proliferation, migration, and apoptosis, causing atherosclerosis and neointimal hyperplasia. SMC-enriched circ_Lrp6 regulates SMC proliferation and differentiation via mediating miR-145[21]. circMAP3K5 in SMCs appears to be a master regulator for microRNA (miR)-22-3p/TET2 axis in regulating the neointimal hyperplasia[17].

In this study, we first conducted a circRNA profiling via RNA sequencing (RNA-Seq) of transcripts in control and PDGF-BB-treated human aortic SMCs (HASMCs) and then identified a circRNA candidate derived from the host gene superoxide dismutase 2 (SOD2). circSOD2 was significantly upregulated upon PDGF-BB treatment in both in silico and in vitro expression analyses. Knockdown of circSOD2 by shRNA abolished PDGF-BB-induced HASMC proliferation, whereas ectopic expression of circSOD2 promoted HASMC proliferation. Mechanistically, circSOD2 sponged miR-206, which blocked the inhibitory effect of miR-206, leading to an elevated NOTCH3/ERK/cyclinD1/CDK4/6 signaling axis and thus increased HASMC proliferation. Importantly, in vivo study revealed that knockdown of circSOD2 attenuated injury-induced neointimal formation along with the suppression of SMC proliferation, indicating that circSOD2 is a novel regulator for SMC proliferation and vascular remodeling.

Materials and Methods

Animals

Male Sprague-Dawley rats weighing 450-500 g were purchased from Charles River Laboratories. All animals were housed under conventional conditions in the animal care facilities and received humane care in compliance with the Principles of Laboratory Animal Care formulated by the National Society for Medical Research and the Guide for the Care and Use of Laboratory Animals. Animal surgical procedures were approved by the Institutional Animal Care and Use Committee of the University of Missouri. Sex is a critical biological variable in cardiovascular diseases[22]. Since this is the first report investigating circSOD2 function in vascular diseases, only male animals were used in this study. However, we will investigate if there is a sex-specific role of circSOD2 in vascular remodeling by including both male and female animals in our future studies.

Reagents and cell Culture

HASMCs were purchased from Lifeline (FC-0015) on passage 1 and cultured in VascuLife® Basal Medium (Lifeline, LM-0002) containing VascuLife® SMC LifeFactors® Kit (Lifeline, LS-1040) at 37°C in a humidified atmosphere with 5% CO2. HASMCs <6 passages with 80% of confluence were used in this study. PDGF-BB was obtained from R&D Systems (220-BB-050) and used at 20 ng/mL to treat HASMCs.

RNA sequencing

Total RNA of HASMCs was isolated using Trizol Reagent (Invitrogen, 15596026) and treated with DNase I (Thermo Scientific, EN0525) according to the manufacturer's recommendation. RNA was cleaned by RNA Clean & Concentrator (Zymo, R1017). Ribosomal RNA was

eliminated by RiboMinus™ Eukaryote Kit (Invitrogen, A1083708) according to the manufacturer's Instruction. RNA quality was analyzed by Bioanalyzer 2100 prior to the construction of the RNA-seq libraries. RNA-seq libraries were constructed with 1 ug of RNA using the KAPA Stranded RNA-Seq Kit (Roche, 07962142001). Pair-end sequence reads (150 bp in length) were generated on an HiSeq 4000 Systems (Illumina, San Diego, CA).

circRNA identification and quantification

The RNA-seq raw reads were cleaned and trimmed by Trimmomatic version 0.36. Reads quality was analyzed by FastQC (https://qubeshub.org/resources/fastqc) version 0.11.9. CircRNA candidates were detected by CIRCexplorer2 pipeline version 2.3.0[23]. Briefly, cleaned reads were aligned onto hg19 genome (http://genome.ucsc.edu/) using Tophat2 version 2.1.1[24, 25]. Bam files from alignment were then parsed by CIRCexplorer2 parse module to generate bed files that contained reads information supporting back-splicing junction. Then circRNA annotation was conducted by CIRCexplorer2 annotation module based on annotation files of hg19 genome fetched from the UCSC annotation database. Data merge and processing were performed in R. To avoid infinity values, a pseudo-count of 1 was added to each circRNA read number. The relative expression level of each circRNA was calculated using the formula: SRPBM (Spliced Reads per Billion Mapped Reads) = total number of back-spliced junction reads/the total number of mapped reads*1,000,000,000 [26]. Differential expression of circRNAs was estimated using the Limma Linear Models[27]. In pairwise comparisons, circRNAs with $P < 0.01$ and absolute fold change value greater than 2 were considered to be significantly differentially expressed.

RNase R treatment

1 μg of RNA was incubated with 20 U of RNase R (Lucigen, RNR07250) at 37°C for 10 min. RNA was then cleaned by RNA Clean & Concentrator (Zymo, R1017). The treated RNA was then subjected to RT-qPCR.

Construction of adenoviral vector expressing circSOD2 shRNA

Short hairpin RNAs (shcircSOD2) specifically targeting the back-splicing junctions (BSJ) of human and rat circSOD2 were inserted into pRNAT-H1.1/Adeno vector (Genscript) between MluI and HindIII site. Adenoviral vectors of shcircSOD2 (Ad-shcircSOD2) were constructed using AdEasy system. Adenoviruses were purified by gradient density ultracentrifugation of cesium chloride followed by dialyzing in dialysis buffer (135 mmol/L NaCl, 1mmol/L MgCl2, 10 mmol/L Tris-HCl, pH 7.5, 10% glycerol). Primers for construction of the human and rat circSOD2 shRNA were listed in the Supplemental Table S3.1.

Plasmid construction

For circSOD2 expression plasmid (pcircSOD2) construction, full length circSOD2 cDNA was amplified from the HASMC mRNA using Phusion High-Fidelity PCR Master Mix (Thermo Scientific, F531S) and was inserted into a pcDNA3.1(+) CircRNA Mini Vector (a gift from Dr. Jeremy Wilusz[28], Addgene plasmid #, 60648) between HindIII and XhoI restriction site by using In-Fusion HD Cloning (Clonetech, 638910). Residual sequences flanking the full length of circSOD2 on plasmid, which could be mistakenly included into circSOD2 after circularization, were removed by QuikChange II XL Site-Directed Mutagenesis Kit (Agilent, 200521). For luciferase reporter assay, the full length circSOD2 was amplified from the human SMC cDNA pool and was inserted downstream of firefly luciferase cassette in a PGL4.23 vector with

minimal promoter at XbaI site. All vectors were verified by sequencing. The primers amplifying circSOD2, used in mutagenesis and infusion cloning were listed in the Supplemental Table S3.2.

Western blot

Western blot was performed as described previously[8]. Cultured HASMCs were washed twice with PBS followed by protein extraction using RIPA buffer [50 mmol/L Tris-HCI (pH 7.4), 1% (v/v) Triton X100, 0.25% (w/v) sodium deoxycholate, 150 mM NaCl, 1 mM EGTA, 0.1% (w/v) SDS] containing 1x protease inhibitors (Thermo Scientific, 78429) and phosphatase inhibitors (Thermo Scientific, 78420). Protein concentration was measured using BCA Protein Assay Reagent (Thermo Scientific, 23225). Lysates were denatured by boiling with SDS solution containing 2-mercaptoethanol. Equal amounts of proteins were resolved on SDS-PAGE gels and then transferred to nitrocellulose membranes (Bio-Rad, 1620115). Nonspecific bindings were blocked with 5% BSA (Sigma-Aldrich, A2153), and then incubated with primary antibodies in blocking buffer at 4°C for 16 hours, followed by incubation with IRDye® Secondary Antibodies (LI-COR) for 1 hour. Detection was performed on Odyssey CLx (LI-COR, Lincoln, Nebraska). Antibodies used for immunoblotting were: Cyclin D1 (CST, #2975), NOTCH3 (CST, #5276), CDK4 (CST, #12790), CDK6 (CST, #3136), Cyclin A2 (CST, #4656), Cyclin B1 (CST, #4135), ERK1/2 (CST, #4695S), Phospho-ERK1/2 (CST, #9101S), PCNA (Santa Cruz, sc-56), α-Tubulin (CST, #2125), P27kip (CST, #3698S), Argonaute-2 (abcam, ab32381) and SOD2 (Santa Cruz, sc-137254).

SiRNA transfection

Two siRNAs and one Non-targeting siRNA (D-001210-01-05) were purchased from Horizon Discovery. SiRNAs were designed based on circSOD2 BSJ sequence. Transfection was performed using Lipofectamie 3000 (Invitrogen, L3000075) following manufacture's protocol.

Cells were harvested after 48 hours of transfection. SiRNA information was listed in Supplemental Table S3.3.

Cell proliferation assay

Equal numbers (5 x 104) of HASMCs were seeded on coverglasses that were placed into 24-well cell culture plates. Cells were firstly starved (VascuLife® complete SMC Medium without FBS) for 24 hours and then applied with EdU reagents (EMD Millipore, 17-10528). HASMCs were then treated with vehicle or PDGF-BB for 48 hours. EdU assay was performed by following the manufacturer's recommendation. EdU-positive cells were counted from 10 different microscopic fields (4x). The proliferation rate was assessed by the following formula: [positive cell number/ total cell number]. Cell proliferation was also evaluated with WST-8 [2-(2-methoxy-4-nitrophenyl)-3-(4-nitrophenyl)-5-(2,4-disulfophenyl)-2H-tetrazolium, monosodium salt] using Cell Counting Kit-8 (CCK8) (Dojindo, CK04). The optical density at 450 nm was measured.

Quantitative real time-PCR (RT-qPCR)

RT-qPCR was performed as described previously[9]. HASMC total RNA was extracted using Trizol Reagent (Invitrogen) according to the manufacturer's protocol. cDNA was synthesized with 1 μg of RNA using iScript cDNA Synthesis kit (Bio-Rad, 1708890). qPCR was performed on AriaMx Real-time PCR System (Agilent, Santa Clara, CA) using All-in-One™ qPCR Mix (GeneCopoeia, QP004). The primer used in this study were listed in the Supplemental Table S3.4.

Cell cycle analysis

1 × 106 cells were harvested and resuspended in 500 μl of reaction buffer containing 1 μl of Nuclear-IDTM Red dye from Nuclear-IDTM Red Cell Cycle Analysis Kit (Enzo Life Sciences,

ENZ-51008-100). After mixing, cells were incubated in the dark for 15 min. Cell cycle analysis was performed on a FACSCalibur™ (Becton Dickinson) and analyzed by the Flowjo™ software.

Cell fractionation

Cell fractionation was performed as described previously[7]. A nuclear extraction kit (EMD Millipore, 2900) was used by following standard procedures. Briefly, HASMCs (1 × 106) were washed with PBS twice. After trypsinization, cells were collected by spinning down at 500 × g for 10 min. Cell pellets were washed with ice-cold PBS and resuspended with ice-cold cytoplasmic lysis buffer containing 40 units/ml RNase inhibitor. The cells were lysed by passing through a syringe with a 27-gauge needle. Cell lysates were then centrifuged at 8000 × g for 20 min. Nuclear fractions were pelleted at the bottom. Both the cytoplasmic and nuclear fractions were used for RNA extraction and RT-qPCR analysis.

RNA pulldown assay

RNA pulldown assay was adapted from RNA Antisense Purification protocol with some modifications[29, 30]. We first synthesized anti-circSOD2 probe targeting circSOD2 BSJ and control probes with 10% biotin-UTP (Roche, 11388908910) using in vitro transcription kit (Promega, P1300). The primers used in probe synthesis were listed in the Supplemental Table S3.5. HASMCs at 80-90% confluence on 15-cm culture dishes were fixed with 2% formaldehyde solution at 37°C for 10 mins before being lysed in 200 μl lysis buffer [20 mM HEPES (pH 7.5), 50 mM KCl, 0.5 mM EDTA, 1.5mM MgCl2, 1% (v/v) NP-40, and 0.4% (w/v) sodium deoxycholate (pH 7.5), 0.1% (w/v) N-lauroylsarcosine] containing 40 units/ml RiboLock RNase Inhibitor (Thermo Scientific, EO0384) and 1x protease inhibitors. After 10 mins of incubation on ice, cell lysate was homogenized by passing through a 27-gauge needle 20 times, and then the supernatant was collected by centrifugation at 13,000xg for 20 mins. Cell lysates

(200 µl) were added with 800 µl hybridization/wash buffer [20 mM Tris-HCl (pH 7.5), 7 mM EDTA, 3 mM EGTA, 150 mM LiCl, 1% (v/v) NP-40, 0.2% (w/v) N-lauroylsarcosine, 0.1% (w/v) sodium deoxycyolate] supplied with RNase and protease inhibitors, and then was pre-cleared by incubation with 50 µl of Streptavidin Magnetic Beads (NEB, S1420S) at 37°C for 20 mins. Meanwhile, probes (1µg for each probe) were denatured in water at 85°C for 1 min and then immediately transferred to ice. The pre-cleared lysates were incubated with the denatured probes (500 µl each probe) at 37°C for 2 hours with rotation, followed by adding 500 µl pre-washed Streptavidin Magnetic Beads and incubating with rotation for 30 mins. After six times washing with hybridization/wash buffer, beads were incubated in Proteinase K Digestion Buffer [20 mM Tris-HCl pH 7.5, 10 mM EDTA, 2% N-lauroylsarcosine] supplied with 20 µg/ml of proteinase K at 42 °C for 1 h to digest protein and reverse formaldehyde crosslinks. RNA was purified by using RNA Clean & Concentrator kit (Zymo, R1017) by following the small RNA purification protocol. Elution from the column was subjected to RT-qPCR analysis. Primers used for miRNA reverse transcription and qPCR were listed in the Supplemental Table S3.6.

Ago2 RIP assay

The RIP assay was performed as described previously[7]. Brefly, HASMCs at 80-90% confluence on 15 cm dishes were fixed with 2% paraformaldehyde (PFA) on ice. Cells were then lysed in FA lysis buffer [50 mM HEPES, 140 mM NaCl, 1 mM EDTA, 1% (v/v) NP-40, and 0.1% (w/v) sodium deoxycholate (pH 7.5)] containing 40 units/ml RiboLock RNase Inhibitor and 1x protease inhibitors. The solution was rotated at 4°C for 2 hours and then was incubated with mouse IgG or Argonaute-2 (Ago2) antibody (1 µg) at 4°C for 6 h. The immunoprecipitates were captured with Protein A/G PLUS-Agarose (50 µl) (Santa Cruz Biotechnology, sc-2003). After washing with FA lysis buffer for six times, the samples were incubated with 20 µg/ml proteinase

K at 42 °C for 1 h to digest the proteins. The immunoprecipitated RNA was purified by using RNA Clean & Concentrator kit (Zymo, R1017). Purified RNA was subjected to RT-qPCR analysis.

Rat carotid artery injury model and adenoviral gene transfer

Rat carotid artery balloon injury was performed as described previously[8]. Briefly, rats were anesthetized by isoflurane (2%) inhalation. A 2F Fogarty arterial embolectomy balloon catheter (Baxter Edwards Healthcare) was introduced through the left external carotid artery and advanced 4 cm toward the thoracic aorta into the common carotid artery. The balloon was inflated with 20 µl saline and then withdrawn back to the carotid bifurcation with constant rotation during denudation of the endothelium. This procedure was repeated for two additional times to ensure complete endothelial denudation. To transduce the injured artery with adenovirus expressing rat shcircSOD2, the injured artery was washed with saline, and incubated with 100 µl saline or adenovirus (5x109 pfu) for 20 minutes, as described previously[7, 8]. 3, 7, or 14 days later, the balloon-injured segment of the artery from the proximal edge of the omohyoid muscle to the carotid bifurcation was perfused with saline and excised. The balloon-injured and/or adenovirus-dwelled segments were fixed with 4% paraformaldehyde (PFA) and embedded in paraffin. Subsequent morphometric analyses were performed in a double-blinded manner.

Histomorphometric Analysis and Immunofluorescent Staining (IF)

Paraffin-embedded carotid arteries were cut by a serial sectioning (5 µm each), and 10 sections evenly distributed in the vessel segment were collected for analyses. The artery sections were stained with modified hematoxylin and eosin (H&E) or Elastica van Gieson stain, and section images were captured using Eclipse 90i Nikon microscope. The circumference of lumen, internal elastic lamina, and external elastic lamina were measured by Image J[31]. For IF, sections were

rehydrated, blocked with 10% goat serum and permeabilized with 0.01% Triton X-100 in PBS, and then incubated with PCNA primary antibody at 4°C overnight followed by incubation with Alexa Fluor 488 secondary antibodies (Invitrogen, A11034).

Fluorescent in situ hybridization (FISH)

Biotin-labeled anti-circSOD2 RNA probes and negative control probes derived from eGFP gene were synthesized as described previously[7]. HASMCs grown on coverglass were firstly washed with cold PBS twice and then fixed with 1% PFA for 30 mins at room temperature, followed by wash with PBS for three times. Permeabilization was performed with 0.5% Triton X-100 in PBS for 10 mins, followed by PBS wash for three times. Endogenous biotin was blocked with 0.05% avidin incubation for 15 mins, followed by 0.005% biotin incubation for 15 mins to block excessive biotin binding pockets on avidin. Free biotins were removed by washing with PBS for three times. The cells were then incubated with pre-denatured probes in hybridization buffer (10% w/v dextran sulfate, 10% formamide, in 2× SSC, 1 mg/ml fragmented salmon testes DNA) in dark and humid environment at 55 °C for 16 h to allow hybridization. After hybridization, cells were washed with wash buffer (10% formamide in 2× SSC) for 3 times. Finally, cells were incubated with streptavidin-conjugated Alexa-fluor 488 (Invitrogen, S11223) in PBS for 1 hour and counterstained with DAPI. For tissue FISH, biotin-labeled rat anti-circSOD2 ssDNA probe was obtained from Integrated DNA Technologies (IDT, Coralville, Iowa). Vessel segments were harvested and fixed in 4% paraformaldehyde at 4°C for 3 h, transferred to 15% sucrose overnight for cryoprotection. Samples were then embedded in Tissue-Tek O.C.T. compound (EMS, Hatfield, PA). Tissue blocks were frozen in liquid nitrogen, stored at −80°C, and 5-μm thick sections were made. The FISH procedure was similar to cellular FISH, except for streptavidin-

conjugated Alexa fluor 594 (Invitrogen, S11227) was used for detection. Probe sequences were listed in the supplemental primer Table S3.5.

Luciferase reporter assay

PGL4.23 or pcircSOD2 firefly luciferase reporter along with miRNA mimics were transfected or co-transfected into HASMCs in 12-well plates using Lipofectamine 3000 (Invitrogen). Luciferase activities were measured using a luciferase assay kit (Promega, E1500) according to the manufacturer's instruction.

Statistical analysis

All statistical analyses were performed using GraphPad Prism software version 8. Data are expressed as means ± SEM. Data were analyzed for normality and equal variance. An unpaired 2-tailed Student t test was used to compare data between 2 groups and one-way ANOVA was used for comparisons among >2 groups with the Sidak post hoc correction. Significance is depicted with asterisks or pound on graphs as follows: *P<0.05; #P<0.05.

Results

Bioinformatic Identification and Profiling of CircRNAs in SMCs

SMC proliferation is a crucial step in neointima formation, and PDGF-BB is a potent stimulator for SMC proliferation[32]. To identify circRNAs involved in human SMC proliferation, we profiled circRNA candidates in vehicle and PDGF-BB-treated HASMCs by sequencing their ribosomal RNA-depleted RNAs (Supplement Figure S3.1A). Raw reads were mapped to human hg19 genome and processed by CIRCexplorer2 to identify circRNA candidate information, including genomic position, host gene name, and the number of junction reads supporting

circRNA candidates (Figure 3.1A). We then used spliced reads per billion mapped reads (SRPBM) to calculate the relative expression of individual circRNAs. RNA sequencing detected 7,713 circRNAs, in which 323 circRNAs were differentially expressed ($p \leq 0.01$ and fold change≥ 2). Besides, 3,192 circRNAs were considered novel circRNAs since they are not included in the most comprehensive circRNA database - circBase (http://www.circbase.org/) (Figure 3.1B and Supplemental Figure S3.1B). Among the 323 differentially expressed circRNAs, 62 were upregulated by PDGF-BB (Figure 3.1C). It appeared that the PDGF-BB-regulated circRNAs are distributed in various different human genomic loci (Figure 3.1D). In order to validate the authenticity of circRNAs identified with CIRCexplorer2, we randomly selected eight circRNA candidates and performed RT-PCR using divergent primers to specifically amplify BSJ of the circRNAs on both human genomic DNA and HASMC cDNA. These amplicons were also sent for Sanger sequencing to verify the BSJ information. As shown in Supplement Figure S3.2, all eight circRNAs were endogenously expressed and matched with the RNA-Seq results, suggesting a high fidelity and reliability of the circRNA identification pipeline.

Characterization of PDGF-BB Enriched CircSOD2

Among the differentially expressed circRNAs, circSOD2, derived from host gene SOD2, was highly upregulated in PDGF-BB-treated cells and thus was selected for further investigation. CircSOD2 contains three exons from SOD2 pre-mRNA with a sequence length of 462 nt (Figure 3.2A). The genomic location of circSOD2 is on the reverse strand of human chromosome 6, starting from 160,103,505 to 160,109,274. By performing the divergent primer amplification and Sanger sequencing of the BSJ amplicon, we confirmed circSOD2 sequence annotated from the

circRNA identification pipeline (Figure 3.2B). To further validate the authenticity of circSOD2, we performed RNase R digestion using RNA isolated from HASMCs. RNase R is a ribonuclease only digesting linear RNAs while leaving the RNAs with loop structure intact. CircSOD2 showed resistance to RNase R digestion, whereas linear host gene SOD2 and housekeeping gene cyclophilin mRNAs were degraded by RNAase R (Figure 3.2C). Cellular fractioning followed by RT-qPCR assay revealed that circSOD2 was largely located in SMC cytoplasm while only a small portion was in the nuclei (Figure 3.2D). Since RNA-Seq showed that circSOD2 was highly induced by PDGF-BB (Figure 3.2E), we treated HASMCs with 20 ng/ml PDGF-BB for 0, 12, 24, and 48 hours to validate circSOD2 expression. As shown in Figure 3.2F, circSOD2 expression was induced by PDGF-BB in a time-dependent manner. RNA-FISH of circSOD2 also verified that circSOD2 was enriched by in PDGF-BB-treated HASMCs and mainly located in cytoplasm (Figure 3.2G).

CircSOD2 Was Required for PDGF-BB-Induced SMC proliferation

To determine whether circSOD2 is involved in HASMC proliferation, we conducted a series of loss and gain-of-function experiments. We first designed two small interfering RNAs (siRNAs) specifically targeting circSOD2 BSJ with different coverages, and the circSOD2 knockdown efficiency was confirmed by RT-qPCR (Supplemental Figure S3.3A). CircSOD2 siRNAs did not alter the expression of its host gene SOD2 (Supplemental Figure S3.3B & C). We then constructed an adenoviral vector expressing circSOD2 short hairpin RNA (shRNA) (shcircSOD2) based on the siRNA1 sequence because it showed a better knockdown efficiency. In order to determine if circSOD2 is important for SMC proliferation, we tested if circSOD2 knockdown alters the expression of genes regulating cell proliferation in PDGF-BB-treated

HASMCs. As shown in Figure 3.3, A-B, circSOD2 shRNA reversed PDGF-BB-upregulated PCNA expression while increased the expression of $P27^{kip}$, a well-known SMC proliferation inhibitor,[33] that was suppressed by PDGF-BB. Conversely, forced expression of circSOD2 increased PCNA while inhibited $P27^{kip}$ expression (Figure 3.3, C-D). EDU and CCK8 assays showed that knockdown of circSOD2 decreased PDGF-BB-induced HASMCs proliferation (Figure 3.3, E-G).

Because cell growth relies on cell cycle progression, we hypothesized that circSOD2 might regulate HASMC cell cycle transition. Indeed, knockdown of circSOD2 attenuated PDGF-BB-promoted G1-to-S transition in HASMCs, and thus arrested HASMCs in the G1 phase (Figure 3.4, A-B). Forced expression of circSOD2 promoted G1-to-S phase transition of HASMCs (Supplemental Figure S3.4A & B). Since G1-to-S phase transition is associated with the cyclin-dependent kinases CDK4 and CDK6, which form complexes with D-type cyclins,[34] we tested if circSOD2 regulates the expression of these kinases. As shown in Figure 3.4, C-D, circSOD2 shRNA inhibited the expression of Cyclin D1, CDK4, and CDK6, but did not affect the expression of Cyclin A and B, suggesting that circSOD2 mediates PDGF-BB-induced SMC cell cycle progression through Cyclin D1, CDK4, and CDK6. These results indicated that circSOD2 is a novel factor regulating SMC proliferation.

CircSOD2 bound miR-206

Since circSOD2 was predominantly expressed in the cytoplasm of HASMCs (Figure 3.2, D & G), we hypothesized that circSOD2 might act as a miRNA sponge to regulate gene expression. As a critical element of RNA-induced silencing complex (RISC), Argonaute RISC Catalytic Component 2 (Ago2) binds with miRNA to form a complex to target mRNAs[35]. RNA

immunoprecipitation (RIP) assays revealed that circSOD2 could bind with Ago2 (Figure 3.5A). circRNA pulldown assay using biotin-labeled circSOD2 BSJ RNA probe followed by RT-qPCR identified three miRNA candidates that potentially bind with circSOD2 (Fig 3.5B), as predicted by miRanda package[36]. Among these miRNAs, miR-206 was highly enriched by circSOD2 probe (Figure 3.5B) and showed tentative site for binding to circSOD2 (Figure 3.5C, upper panel). We thus cloned the circSOD2 linear sequence into PGL4.23 luciferase reporter immediately after the luc2 gene to generate pGL4-circSOD2 reporter vector. Luciferase assays showed that miR-206 mimic significantly decreased the luciferase activity of pGL4-circSOD2 in HASMCs, as compared to the scramble miRNA mimic (Figure 3.5C), demonstrating that circSOD2 physically bound miR-206.

CircSOD2 Regulates SMC Proliferation via circSOD2-miR-206-NOTCH3 Axis

NOTCH signaling is a vital regulator for SMC differentiation and proliferation. NOTCH3 can be activated by PDGF-BB to promote SMC proliferation through ERK1/2 signaling and Cyclin D expression[37, 38]. Knockdown of circSOD2 in HASMCs significantly reduced PDGF-BB-induced NOTCH3 expression and ERK1/2 phosphorylation (Figure 3.6, A-B), suggesting that circSOD2 was essential for NOTCH3 signaling in SMCs. Since miR-206 has been shown to bind NOTCH3 mRNA 3' UTR (Figure 3.6C, upper panel) and down-regulate NOTCH3 expression in SMCs [39], we speculated that circSOD2 might mediate PDGF-BB-activated NOTCH3 signaling by sponging miR206. To test this, we performed a miR-206 mimic rescue assay by co-transfecting scramble or miR-206 mimics with control or circSOD2 overexpression plasmid followed by vehicle or PDGF-BB treatment. As shown in Figure 3.6C (lower panel), circSOD2 upregulated NOTCH3 and PCNA expression, but miR-206 mimics alleviated the effects. These results

indicated that circSOD2 modulated SMC proliferation via sponging miR-206, which reduced the availability of miR-206 and thus its binding to NOTCH3 mRNA 3' UTR, leading to the up-regulation of NOTCH3 expression and further the enhanced SMC proliferation.

Knockdown of CircSOD2 Attenuated Injury-Induced Neointimal Formation

In the normal artery, circSOD2 showed a very low level of expression. However, in a rat carotid balloon injury model, injury significantly induced circSOD2 expression in neointimal SMCs (Figure 3.7A). Quantitative analyses revealed that circSOD2 was significantly induced as early as three days after the injury, and its expression reached the highest level (7.8 folds increase) 7 days and maintained the level until 14 days post-injury (Figure 3.7B). To determine whether circSOD2 is functionally vital for neointimal formation, we incubated endothelium-denuded rat carotid arteries with shcircSOD2 for 20 minutes immediately after the balloon injury in order to transduce circSOD2 shRNA into carotid arterial SMCs. RNA-FISH and RT-qPCR assay confirmed that the shRNA was successfully delivered into neointimal SMCs, and circSOD2 level was reduced by 70% in the shcircSOD2-treated vessels (Supplemental Figure S3.5). Importantly, knockdown of circSOD2 significantly attenuated injury-induced neointimal formation (Figure 3.7, C-D) with significant reductions in neointima area, intima/media ratio, and intima/lumen ratio (Figure 3.6E). To determine if circSOD2 regulates neointimal SMC proliferation in vivo, we detected PCNA expression in injured arteries. Immunofluorescent staining showed that knockdown of circSOD2 decreased the PCNA+ SMC number by 50% in neointima as compared with the injured arteries transduced with scramble shRNA (Figure 3.7, F-G). Taken together, these results indicated that circSOD2 regulated injury-induced vascular remodeling by promoting SMC proliferation.

Discussion

CircRNAs have been found to be important players in the development of multiple diseases[40-42]. Although the expression levels of circRNAs are relatively low compared with mRNAs, the circRNAs have longer average half-life with 24-48 hours[12, 43] compared withthe linear mRNAs whoes average lifetime is only 4 to 9 hours[44]. Therefore, circRNAs are considered to be very promising regulators to modify gene expression patterns via acting as miRNA sponges, RNA binding protein scaffold, nuclear transcriptional regulator, or peptide/protein translation templates [11]. Our study identified circSOD2 as a novel regulator for SMC proliferation and vascular remodeling. Both PDGF-BB treatment and balloon injury increased circSOD2 expression in SMCs. Although it showed a very low level of expression in normal healthy arterial SMCs, circSOD2 was highly upregulated in the proliferative neointimal SMCs in balloon-injured arteries. Notably, circSOD2 maintained a high level of expression for a relatively long time post-injury, which is likely due to the resistance to exonuclease degradation. Functionally, knockdown of circSOD2 repressed while overexpression of circSOD2 promoted SMC proliferation. Most importantly, circSOD2 knockdown attenuated neointima formation while inhibiting SMC proliferation in injured arteries in vivo, demonstrating that circSOD2 promotes vascular remodeling by stimulating SMC proliferation.

Previously our lab has reported that SOD2 is induced by vascular injury and enriched in vascular injury-induced neointima area[45]. In rat carotid balloon injury model, SOD2 played its function via scavenging superoxide anion generated by the injury and enforced overexpression of SOD2 inhibited VSMC proliferation and the neointima formation *in vivo*. The injury of the vascular wall (1 day post-injury) and neointima formation (7-14 days post-injury) maintained high

expression of SOD2 because of the superoxide anion produced from these areas, except for the intermediate period between the initial injury and the starting of neointima formation (1-3 days post-injury). The author suspected that the endogenous level of SOD2 was not sufficient to halt the growth of neointima and other factors were still in play in this progression. Surprisingly, in this study, we found the circSOD2 derived from SOD2 played an opposite role in the process of neointima formation. Although the underlying mechanisms controlling circSOD2 upregulation in response to vascular injury are still not clear, we highly suspecte that circSOD2 level may positively correlate with SOD2 mRNA level since there are two typical intronic complementary sequences (ICSs) flanking the exons on SOD2 mRNA that produces circSOD2 (data not shown). Upon the vascular injury, the upregulated level of SOD2 may cause a higher formation rate of circSOD2, which has a pro-proliferative role in VSMC and may be the reason causing SOD2 failure to halt the neointima formation. Additionally, Wang et al. revealed that SOD2 overexpression inhibited neointima progression. However, the overexpression experiment only ectopically expressed SOD2 mRNA, which could not affect circSOD2 level, indicating only purely overexpress SOD2 may represent a promising therapeutic strategy for the prevention of restenosis. Therefore, the study of circSOD2 provides a reasonable explanation for why the high level of endogenous SOD2 fails to halt neointima formation in response to vascular injury. Moreover, researcher may need to consider more about the by-products from mRNA, such as circRNA, when conducting the loss- and gain- of function experiments.

CircSOD2 regulates SMC proliferation by promoting cell cycle progression. Specifically, circSOD2 appears to be important for G1-to-S phase transition. Knockdown of circSOD2 caused cell cycle arrest at the G1 phase. At the molecular level, circSOD2 inhibits the expression of cyclin-dependent kinase inhibitor $p27^{Kip1}$. In addition, circSOD2 is also essential for PDGF-BB-

induced expression of cyclin D1, CDK4 and CDK6, suggesting that circSOD2 may promote cell cycle progression in SMCs by both inhibiting $p27^{Kip1}$ and promoting CDK4/6 expression/activity. CircSOD2 does not affect the expression of cyclin A and B, indicating that circSOD2 mainly regulates the G1-to-S transition, but not other phases.

CircSOD2 regulates cell cycle progression/SMC proliferation by serving as a miR-206 sponge. MiR-206 level has been shown to be critical for SMC proliferation [46], and miR-206 mimics can override circSOD2 activity and inhibit circSOD2-mediated SMC proliferation. It appears that circSOD2 suppresses miR-206 inhibitory activity on NOTCH3 expression, causing activation of downstream ERK1/2 signaling, which is critical for cyclin D1 expression and G1-to-S transition[47, 48]. NOTCH signaling pathway is highly conserved and important for vascular development and physiology [49]. Among different NOTCH receptors, NOTCH2 and NOTCH3 play important roles in SMC growth, survival, and cell fate determination[50]. NOTCH2 inhibits PDGF-BB-induced SMC proliferation, whereas NOTCH3 promotes SMC proliferation through MEK/ERK1/2 signaling[38]. Our results are consistent with previous study showing that miR-206 is a potent inhibitor for NOTCH3 expression[37], [51].

In summary, this study revealed a novel mechanism underlying SMC proliferation and injury-induced neointima formation. The mechanism involves circSOD2 regulation of miR-206 inhibition to NOTCH3/ERK1/2/CyclinD1/CDK4/6 axis in SMCs (Figure 3.8). Therefore, targeting circSOD2/miR-206/NOTCH3 axis may be a promising strategy to hinder injury-induced vascular remodeling in proliferative vascular diseases.

Reference

1. Marx, S.O., Totary-Jain, H. & Marks, A.R. Vascular smooth muscle cell proliferation in restenosis. *Circ Cardiovasc Interv* **4**, 104-111 (2011).

2. Farooq, V., Gogas, B.D. & Serruys, P.W. Restenosis: delineating the numerous causes of drug-eluting stent restenosis. *Circ Cardiovasc Interv* **4**, 195-205 (2011).

3. Kalavakunta, J.K., Gangula, S. & Gupta, V. In-stent ulceration: an unusual pathology. *Case Rep Cardiol* **2014**, 893143 (2014).

4. Mehler, M.F. & Mattick, J.S. Noncoding RNAs and RNA editing in brain development, functional diversification, and neurological disease. *Physiol Rev* **87**, 799-823 (2007).

5. Amaral, P.P. & Mattick, J.S. Noncoding RNA in development. *Mamm Genome* **19**, 454-492 (2008).

6. Wu, G.C. *et al.* Emerging role of long noncoding RNAs in autoimmune diseases. *Autoimmun Rev* **14**, 798-805 (2015).

7. Tang, R., Zhang, G., Wang, Y.C., Mei, X. & Chen, S.Y. The long non-coding RNA GAS5 regulates transforming growth factor beta (TGF-beta)-induced smooth muscle cell differentiation via RNA Smad-binding elements. *J Biol Chem* **292**, 14270-14278 (2017).

8. Tang, R. *et al.* LncRNA GAS5 regulates vascular smooth muscle cell cycle arrest and apoptosis via p53 pathway. *Biochim Biophys Acta Mol Basis Dis* **1865**, 2516-2525 (2019).

9. Tang, R. *et al.* LncRNA GAS5 attenuates fibroblast activation through inhibiting Smad3 signaling. *Am J Physiol Cell Physiol* **319**, C105-C115 (2020).

10. Esteller, M. Non-coding RNAs in human disease. *Nat Rev Genet* **12**, 861-874 (2011).

11. Li, X., Yang, L. & Chen, L.L. The Biogenesis, Functions, and Challenges of Circular RNAs. *Mol Cell* **71**, 428-442 (2018).

12. Jeck, W.R. *et al.* Circular RNAs are abundant, conserved, and associated with ALU repeats. *RNA* **19**, 141-157 (2013).

13. Patop, I.L., Wust, S. & Kadener, S. Past, present, and future of circRNAs. *EMBO J* **38**, e100836 (2019).

14. Zhang, X.O. *et al.* Complementary sequence-mediated exon circularization. *Cell* **159**, 134-147 (2014).

15. Zhang, Y. *et al.* The Biogenesis of Nascent Circular RNAs. *Cell Rep* **15**, 611-624 (2016).

16. Holdt, L.M. *et al.* Circular non-coding RNA ANRIL modulates ribosomal RNA maturation and atherosclerosis in humans. *Nat Commun* **7**, 12429 (2016).

17. Zeng, Z. *et al.* Circular RNA CircMAP3K5 Acts as a MicroRNA-22-3p Sponge to Promote Resolution of Intimal Hyperplasia via TET2-Mediated SMC Differentiation. *Circulation* (2020).

18. Sun, Y. *et al.* A Novel Regulatory Mechanism of Smooth Muscle alpha-Actin Expression by NRG-1/circACTA2/miR-548f-5p Axis. *Circ Res* **121**, 628-635 (2017).

19. Weiser-Evans, M.C.M. Smooth Muscle Differentiation Control Comes Full Circle: The Circular Noncoding RNA, circActa2, Functions as a miRNA Sponge to Fine-Tune alpha-SMA Expression. *Circ Res* **121**, 591-593 (2017).

20. Rong, Z.H. *et al.* Suppression of circDcbld1 Alleviates Intimal Hyperplasia in Rat Carotid Artery by Targeting miR-145-3p/Neuropilin-1. *Mol Ther Nucleic Acids* **18**, 999-1008 (2019).

21. Hall, I.F. *et al.* Circ_Lrp6, a Circular RNA Enriched in Vascular Smooth Muscle Cells, Acts as a Sponge Regulating miRNA-145 Function. *Circ Res* **124**, 498-510 (2019).

22. Robinet, P. *et al.* Consideration of Sex Differences in Design and Reporting of Experimental Arterial Pathology Studies-Statement From ATVB Council. *Arterioscler Thromb Vasc Biol* **38**, 292-303 (2018).

23. Zhang, X.O. *et al.* Diverse alternative back-splicing and alternative splicing landscape of circular RNAs. *Genome Res* **26**, 1277-1287 (2016).

24. Trapnell, C., Pachter, L. & Salzberg, S.L. TopHat: discovering splice junctions with RNA-Seq. *Bioinformatics* **25**, 1105-1111 (2009).

25. Kim, D. & Salzberg, S.L. TopHat-Fusion: an algorithm for discovery of novel fusion transcripts. *Genome Biol* **12**, R72 (2011).

26. Tan, W.L. *et al.* A landscape of circular RNA expression in the human heart. *Cardiovasc Res* **113**, 298-309 (2017).

27. Ritchie, M.E. *et al.* limma powers differential expression analyses for RNA-sequencing and microarray studies. *Nucleic Acids Res* **43**, e47 (2015).

28. Liang, D. & Wilusz, J.E. Short intronic repeat sequences facilitate circular RNA production. *Genes Dev* **28**, 2233-2247 (2014).

29. Engreitz, J.M. *et al.* RNA-RNA interactions enable specific targeting of noncoding RNAs to nascent Pre-mRNAs and chromatin sites. *Cell* **159**, 188-199 (2014).

30. Engreitz, J.M. *et al.* The Xist lncRNA exploits three-dimensional genome architecture to spread across the X chromosome. *Science* **341**, 1237973 (2013).

31. Schneider, C.A., Rasband, W.S. & Eliceiri, K.W. NIH Image to ImageJ: 25 years of image analysis. *Nat Methods* **9**, 671-675 (2012).

32. George, S.J., Williams, A. & Newby, A.C. An essential role for platelet-derived growth factor in neointima formation in human saphenous vein in vitro. *Atherosclerosis* **120**, 227-240 (1996).

33. Marra, D.E., Simoncini, T. & Liao, J.K. Inhibition of vascular smooth muscle cell proliferation by sodium salicylate mediated by upregulation of p21(Waf1) and p27(Kip1). *Circulation* **102**, 2124-2130 (2000).

34. Topacio, B.R. *et al.* Cyclin D-Cdk4,6 Drives Cell-Cycle Progression via the Retinoblastoma Protein's C-Terminal Helix. *Mol Cell* **74**, 758-770 e754 (2019).

35. Winter, J., Jung, S., Keller, S., Gregory, R.I. & Diederichs, S. Many roads to maturity: microRNA biogenesis pathways and their regulation. *Nat Cell Biol* **11**, 228-234 (2009).

36. Enright, A.J. *et al.* MicroRNA targets in Drosophila. *Genome Biol* **5**, R1 (2003).

37. Morris, H.E., Neves, K.B., Montezano, A.C., MacLean, M.R. & Touyz, R.M. Notch3 signalling and vascular remodelling in pulmonary arterial hypertension. *Clin Sci (Lond)* **133**, 2481-2498 (2019).

38. Baeten, J.T. & Lilly, B. Differential Regulation of NOTCH2 and NOTCH3 Contribute to Their Unique Functions in Vascular Smooth Muscle Cells. *J Biol Chem* **290**, 16226-16237 (2015).

39. Jalali, S. *et al.* Mir-206 regulates pulmonary artery smooth muscle cell proliferation and differentiation. *PLoS One* **7**, e46808 (2012).

40. Kristensen, L.S., Hansen, T.B., Veno, M.T. & Kjems, J. Circular RNAs in cancer: opportunities and challenges in the field. *Oncogene* **37**, 555-565 (2018).

41. Flemming, A. The enigma of circular RNA. *Nat Rev Immunol* **19**, 351 (2019).

42. Carrara, M., Fuschi, P., Ivan, C. & Martelli, F. Circular RNAs: Methodological challenges and perspectives in cardiovascular diseases. *J Cell Mol Med* **22**, 5176-5187 (2018).

43. Enuka, Y. *et al.* Circular RNAs are long-lived and display only minimal early alterations in response to a growth factor. *Nucleic Acids Res* **44**, 1370-1383 (2016).

44. Schwanhausser, B. *et al.* Global quantification of mammalian gene expression control. *Nature* **473**, 337-342 (2011).

45. Wang, J.N., Shi, N. & Chen, S.Y. Manganese superoxide dismutase inhibits neointima formation through attenuation of migration and proliferation of vascular smooth muscle cells. *Free Radic Biol Med* **52**, 173-181 (2012).

46. Xing, T. *et al.* Upregulation of microRNA-206 induces apoptosis of vascular smooth muscle cells and decreases risk of atherosclerosis through modulating FOXP1. *Exp Ther Med* **14**, 4097-4103 (2017).

47. Ravenhall, C., Guida, E., Harris, T., Koutsoubos, V. & Stewart, A. The importance of ERK activity in the regulation of cyclin D1 levels and DNA synthesis in human cultured airway smooth muscle. *Br J Pharmacol* **131**, 17-28 (2000).

48. Meloche, S. & Pouyssegur, J. The ERK1/2 mitogen-activated protein kinase pathway as a master regulator of the G1- to S-phase transition. *Oncogene* **26**, 3227-3239 (2007).

49. Fouillade, C., Monet-Lepretre, M., Baron-Menguy, C. & Joutel, A. Notch signalling in smooth muscle cells during development and disease. *Cardiovasc Res* **95**, 138-146 (2012).

50. Gridley, T. Notch signaling in vascular development and physiology. *Development* **134**, 2709-2718 (2007).

51. Song, G., Zhang, Y. & Wang, L. MicroRNA-206 targets notch3, activates apoptosis, and inhibits tumor cell migration and focus formation. *J Biol Chem* **284**, 31921-31927 (2009).

Figure Legends

Figure 3.1. circRNA expression profile in HASMCs. A, HASMC sample preparation and screening strategy of candidate circRNAs. **B**, Volcano plot of all identified circRNAs. Red and green dots indicate up-regulated and down-regulated circRNAs with statistical significance, respectively. The cutoff is p-value<0.01, and fold changes > 2 (PDGF-BB vs. control (Ctrl) group). **C**, Hierarchical clustering and heatmap visualization of circRNA expression levels. **D**, Circos plot of the distribution of all circRNAs on the human chromosomes.

Figure 3.2. circSOD2 was upregulated in SMCs by PDGF-BB. A, Diagram of circSOD2 formation. CircSOD2 was derived from SOD2 pre-mRNA via back-splicing. The region of back-splicing junction is shown. **B**, Divergent primers only amplified circSOD2 in cDNA, but not the genomic DNA (gDNA) (upper panel). Sanger sequencing confirmed the head-to-tail junction (lower panel). Red solid line shows the back-splicing junction site. **C**, Cyclophilin (CYP) and SOD2 linear RNAs, but not circSOD2, were digested by RNase R, as detected by RT-qPCR. *P<0.05 vs Mock group, n=3; N.S. non-significant. **D,** CircSOD2 was mainly located in cytoplasm of HASMCs. Cytoplasmic and nuclear RNAs of HASMCs were isolated, and CircSOD2 was assessed by RT-qPCR. *P<0.05 vs cytoplasmic portion, n=3. **E,** Spliced reads per billion mapped reads (SRPBM) of circSOD2 from RNAseq data was upregulated by PDGF-BB (20 ng/mL). *P<0.05 vs Ctrl group, n=5. **F,** CircSOD2 was time-dependently induced by PDGF-BB (20 ng/mL) as assessed by RT-qPCR. *P<0.05 vs vehicle group (0 h), n=3. **G**, In situ hybridization for circSOD2 in vehicle- or PDGF-BB-treated HASMCs. circSOD2 was detected by biotin-labeled anti-circSOD2 probe (green). Nuclei stained by DAPI (bule). Random probe served as negative control (NC). Bar: 10 μm.

Figure 3.3. Knockdown of circSOD2 inhibited SMC proliferation. A, ShRNA knockdown of circSOD2 (shcircSOD2) reversed PDGF-BB-altered PCNA and $p27^{kip}$ expression. **B**, Quantification of PCNA and $p27^{kip}$ protein level shown in A by normalizing to α-Tubulin. *P<0.05 vs scramble shRNA (shScramble)-transduced cells; #P<0.05 vs shScramble-transduced cells with PDGF-BB (n=3). **C**, Forced expression of circSOD2 (circSOD2) promoted PCNA while suppressed $p27^{kip}$ expression regulated by PDGF-BB. **D**, Quantification of PCNA and $p27^{kip}$ protein level shown in C by normalizing to α-Tubulin. *P<0.05 vs control vector (circCtrl)-transfected cells; #P<0.05 vs circCtrl-transfected cells with PDGF-BB (n=3). **E**, Knockdown of circSOD2 inhibited HASMC proliferation as measured by EdU assay. Bar: 100 μm. **F**, Quantification of EdU-positive cells shown in E. *P<0.05 vs shScramble-transduced cells; #P<0.05 vs shScramble-transduced cells with PDGF-BB (n=3). **G**, Knockdown of circSOD2 inhibited HASMC proliferation as measured by CCK8 assay. *P<0.05 vs shScramble-transduced cells; #P<0.05 vs shScramble-transduced cells with PDGF-BB (n=9).

Figure 3.4. circSOD2 mediated SMC proliferation via cyclinD1- and CKD4/6-regulated G0/G1 progression. A, Knockdown of circSOD2 (shcircSOD2) caused HASMC cell cycle arrest as assessed by Flow cytometry with propidium iodide (PI) staining. **B,** Cell cycle distribution shown in F. *P<0.05 vs scramble shRNA (shScramble)-transduced cells in G1 group; #P<0.05 vs shScramble-transduced cells in G1 group with PDGF-BB treatment (n=3). **C,** Knockdown of circSOD2 inhibited Cyclin D1 and CKD4/6 protein expression but had no effect on the expression of Cyclin A and Cyclin B. **D,** Quantification of protein expression shown in C by normalizing to α-Tubulin level. *P<0.05 vs shScramble-transduced cells; #P<0.05 vs shScramble-transduced cells with PDGF-BB (n=3). N.S.: Non-siginificant.

Figure 3.5. circSOD2 sponged miRNA-206. A, HASMC cytoplasmic and total cellular protein fractions were isolated and immunoprecipitated (IP) using Ago2 or IgG antibody. circSOD2 was detected by RT-qPCR, *P<0.05 vs IgG IP group (n = 3). **B**, CircSOD2-interacting molecules was pulled down by biotin-labelled anti-circSOD2 probe. Potential circSOD2-binding microRNAs (miRNA) were screened by RT-qPCR. *P<0.05 vs control (Ctrl) probe pull-down group (n=3). **C**, CircSOD2 sponging miRNA-206 as shown by luciferase assay. Putative miR-206 binding sites on circSOD2 transcript was shown on the upper panel. Lower panel: HASMCs were co-transfected pGL4 luciferase plasmid or pGL4-circSOD2 (containing circSOD2 sequence after luc2P gene) with scramble or miR-206 Mimics. Luciferase activity was detected 48 h after the transfection, *P < 0.05 vs cells transfected with pGL4 plasmid with miR-206 mimic (n=3).

Figure 3.6. circSOD2 mediated PDGF-BB-induced SMC proliferation and NOTCH3 expression via sponging miR-206. A, Knockdown of circSOD2 blocked PDGF-BB-induced NOTCH3 protein expression and ERK1/2 phosphorylation. **B**, Quantification of NOTCH3, ERK1/2 and p-ERK1/2 protein level shown in A by normalizing to α-Tubulin. *P<0.05 vs scramble shRNA (shScramble)-transduced cells; #P<0.05 vs shScramble-transduced cells with PDGF-BB treatment (n=3), N.S.: Non-siginificant. **C**, CircSOD2 mediated NOCTH3 expression via inhibiting miR206 activity. Upper panel: putative miR-206 binding sites on the 3'UTR of NOTCH3 mRNA. Lower panel: control circRNA (circCtrl) or circSOD2 overexpression plasmid were co-transfected into HASMCs with scramble (Scrm mimic) or miR-206 Mimics followed by vehicle or PDGF-BB treatment. NOTCH3 and PCNA protein expression were detected by Western blot. **D,** Quantification of NOTCH3 and PCNA levels shown in C by normalizing to α-Tubulin. *P<0.05 vs circSOD2-transduced cells with Scrm mimic; #P<0.05 vs circSOD2-transduced cells with Scrm mimic with PDGF-BB treatment (n=3).

Figure 3.7. Knockdown of circSOD2 attenuated injury-induced neointima formation *in vivo.* **A**, CircSOD2 was induced in injured rat carotid arteries. The control or injured arteries (for 14 days) were stained for circSOD2 by RNA-FISH. M: media; L: lumen; Bar: 100 μm. **B**, CircSOD2 were time-dependently induced by balloon injury. CircSOD2 levels in injured rat carotid arteries were detected by RT-qPCR. *P<0.05 vs uninjured (Ctrl) rat carotid arteries (n=5). **C-D,** Knockdown of circSOD2 by shcircSOD2 blocked injury-induced neointima formation, as shown by H&E (C) and Elastica van Gieson (VG) staining (D). **E**, Quantification of the neointima area, intima/media, and intima/lumen ratio. *P<0.05 vs scramble shRNA (shScramble)-treated arteries, n=5. **F**, Knockdown of circSOD2 reduced PCNA-positive cell numbers in balloon-injured arteries. Bar: 100 μm. **G**, Quantification of the PCNA-positive cells shown in F by calibrating its staining intensity to the mean signal in uninjured arteries, *P<0.05 vs Ctrl; #P<0.05 vs shScramble-treated arteries, n=5. White arrows: internal elastic lamina.

Figure 3.8. Schematic diagram of circSOD2 function in SMC proliferation and neointima formation. Upon vascular injury or PDGF-BB stimulation, circSOD2 is induced and then translocated to the cytoplasm where it acts as a miR-206 sponge and causes a decreased number of free miR-206, which reduces the inhibitory effect of miR-206 on NOTCH3 transcription, thus increases NOTCH3 expression. The enhanced NOTCH3 signaling promotes ERK1/2 phosphorylation and further CDK4/6 and Cyclin De expression, resulting in an increased SMC proliferation and thus neointima formation in injured arteries.

Supplementary Figure S3.1. RNAseq data verification and analysis. A, Principal component analysis (PCA) shows that the gene expression patterns for control or PDGF-BB-treated HASMCs were clustered separately. **B**, Venn diagram shows that 3,192 circRNAs detected from

this study were not found in the most comprehensive circRNA database (circBase), and thus represent novel circRNAs.

Supplementary Figure S3.2. Validation of circRNA candidates. A, Divergent primers amplified circRNAs, but not genomic DNA fragment, as shown by RT-PCR. 100bp DNA ladder was used to mark the amplicon size, and all ladder fragments presented on each gel showing standard DNA size 100bp, 200bp and 300bp. **B**, CircRNA information and Sanger sequencing confirmation of the head-to-tail junction in A.

Supplementary Figure S3.3. CircSOD2 siRNAs knocked down circSOD2, but not SOD2 expression. A, CircSOD2 expression level was knocked down by two siRNAs in a dose-dependent manner in HASMCs. 100 nM siRNA1 showed a better knockdown efficiency. CircSOD2 expression was quantified by RT-qPCR. The expression was normalized to cyclophilin. *P< 0.05 vs Scramble siRNA (Scrm) treated cells (n = 3). **B**, circSOD2 siRNAs did not impact SOD2 protein expression. **C**, Quantification of SOD2 protein expression in B by normalizing to α-Tubulin levels. N.S.: Non-significant.

Supplementary Figure S3.4. Forced expression of circSOD2 promoted HASMC cell cycle transition. A, HASMC cell cycle transition as assessed by Flow cytometry with PI staining. **B,** Cell cycle distribution shown in A. *P<0.05 vs scramble shRNA (shScramble)-transduced cells in G1 group; #P<0.05 vs scramble shRNA (shScramble)-transduced cells in G1 group with PDGF-BB treatment (n=3).

Supplementary Figure S3.5. circSOD2 shRNA knocked down its expression in injured arteries. The tissue sections were from rat carotid arteries injured for 14 days. A, circSOD2 expression in injured rat carotid arteries with control (shScramble) or circSOD shRNA (sh-circSOD2) transduction was detected by RNA-FISH. circSOD2 shRNA effectively reduced

circSOD2 expression in the injured arteries. M: media; L: lumen; Bar: 100 μm. **B**, The knockdown efficiency of shcircSOD2 was confirmed by RT-qPCR using RNA extracted from the injured rat carotid arteries *P<0.05 vs shScramble-transduced arteries (n=5).

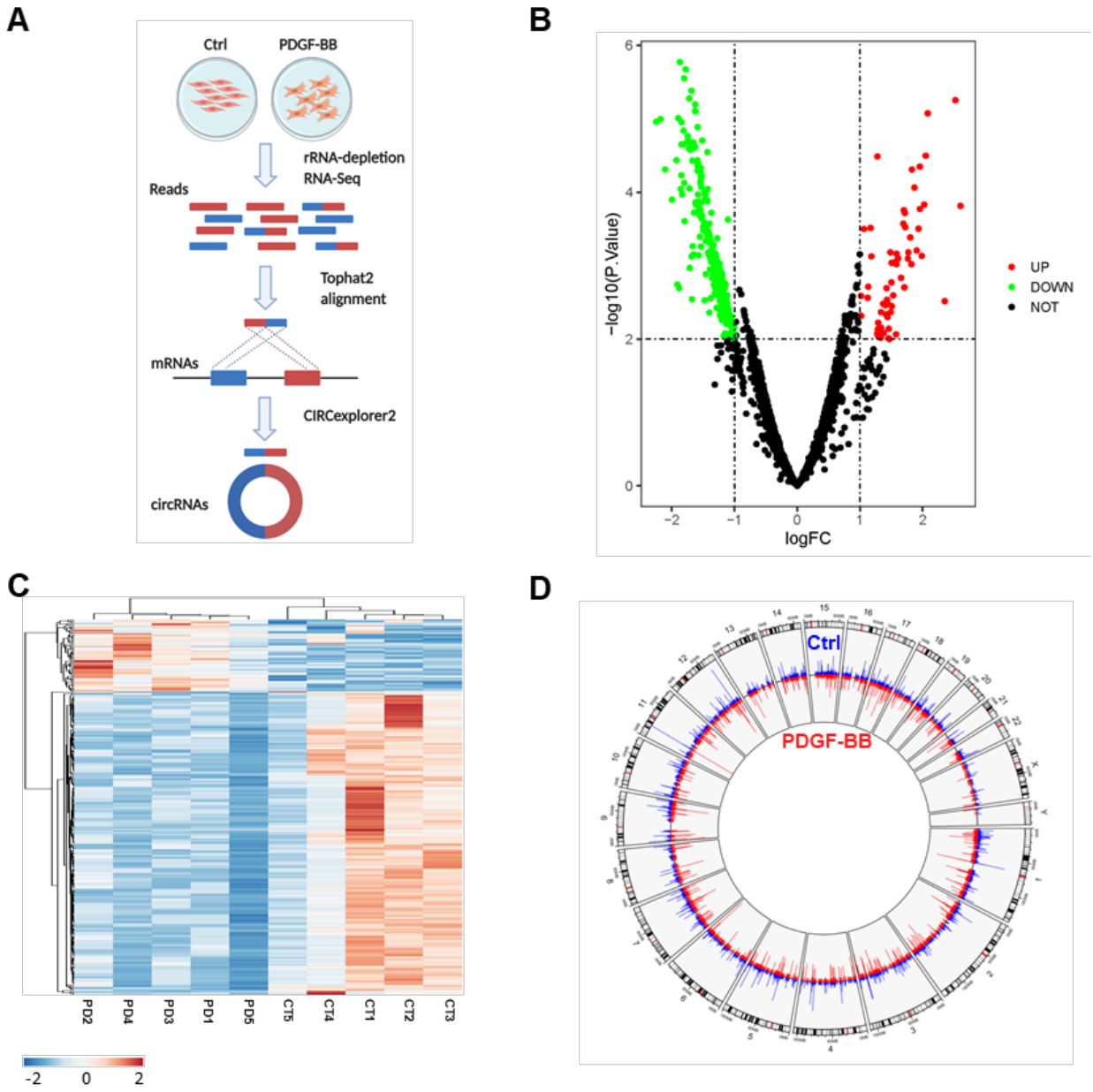

Figure 3.1. circRNA expression profile in HASMCs.

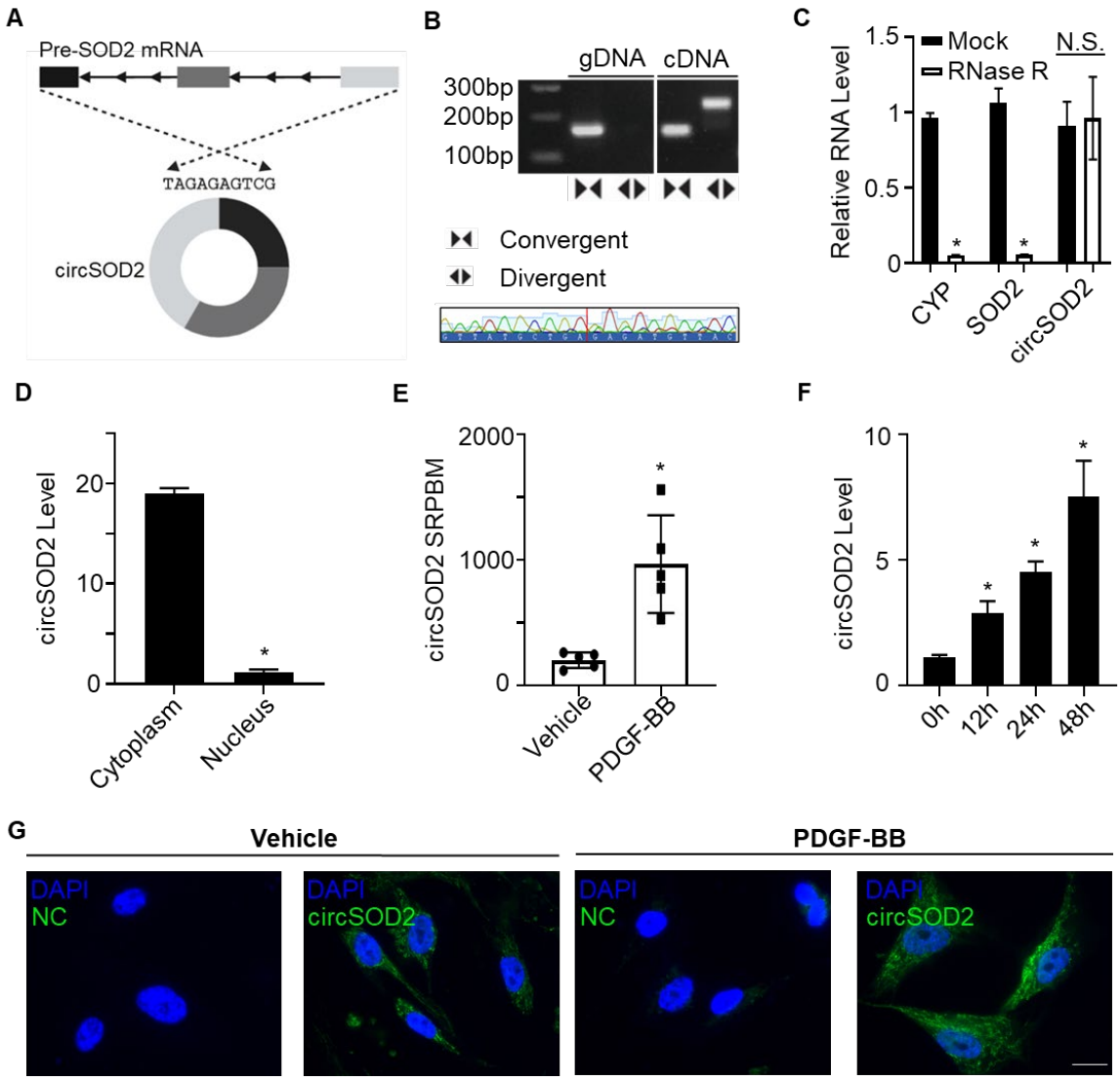

Figure 3.2. circSOD2 was upregulated in SMCs by PDGF-BB.

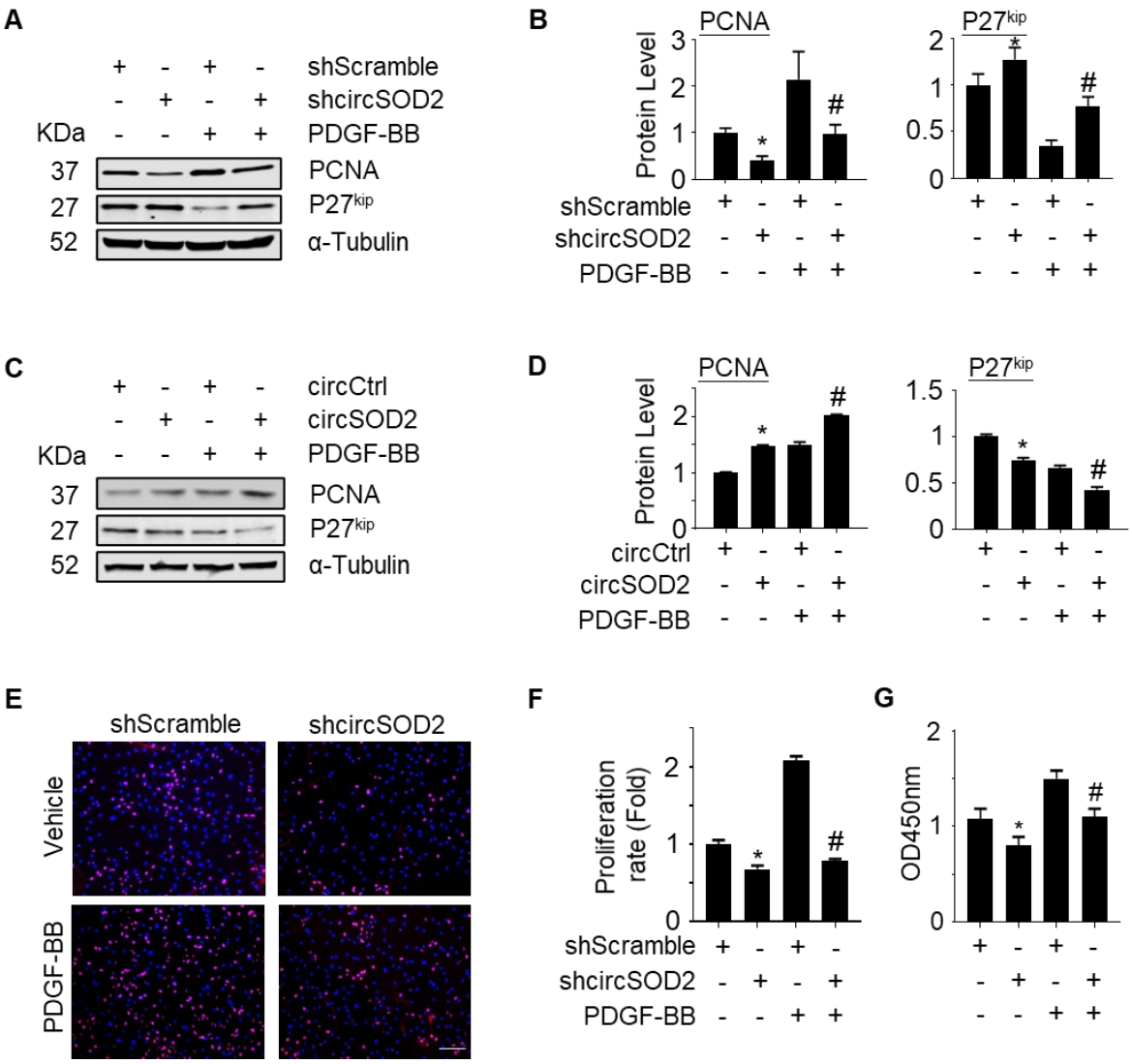

Figure 3.3. Knockdown of circSOD2 inhibited SMC proliferation.

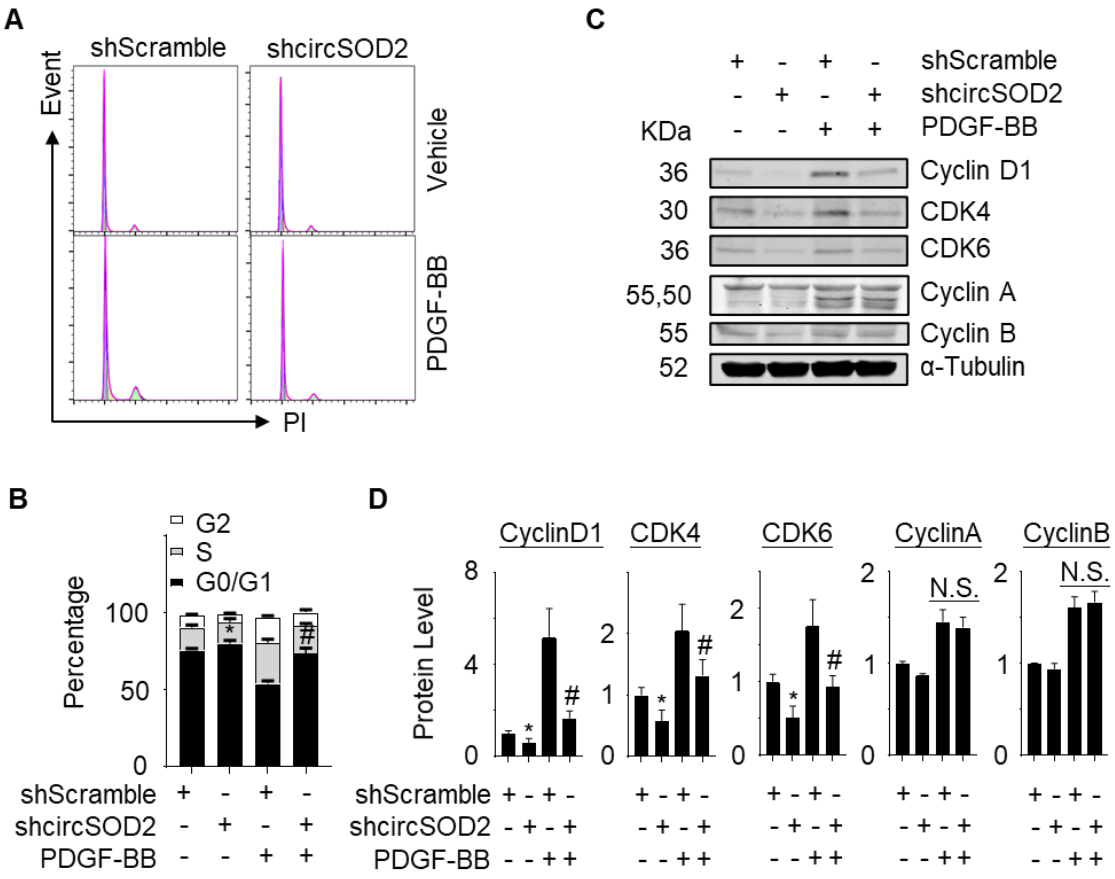

Figure 3.4. circSOD2 mediated SMC proliferation via cyclinD1- and CKD4/6-regulated G0/G1 progression.

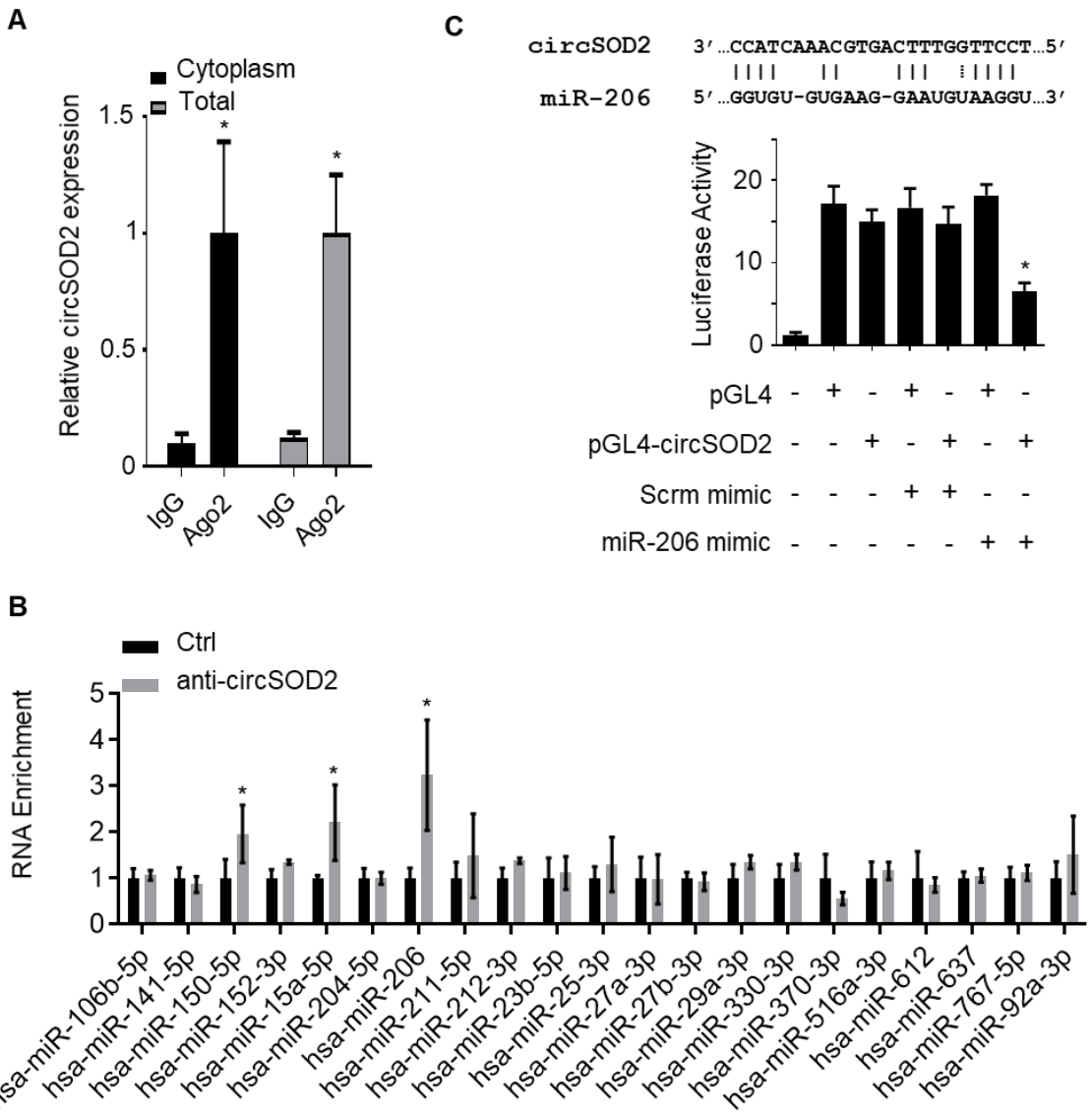

Figure 3.5. circSOD2 sponged miRNA-206.

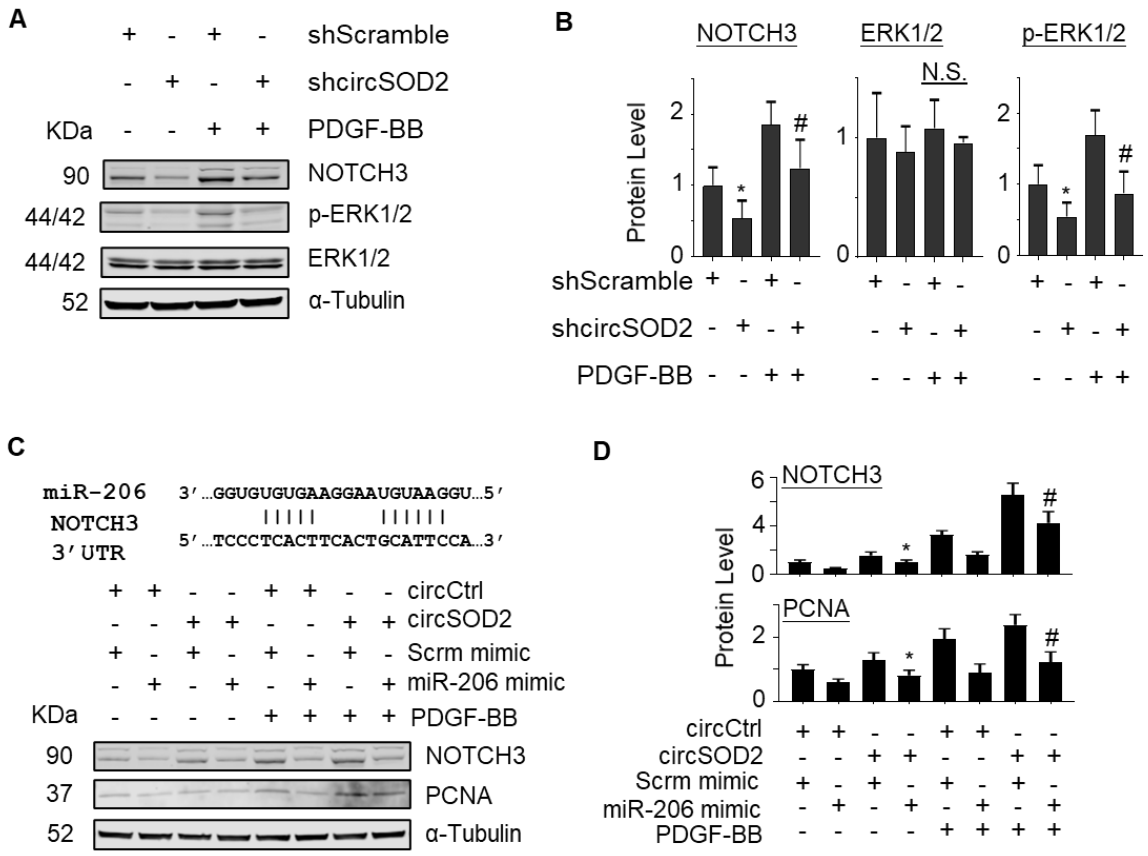

Figure 3.6. circSOD2 mediated PDGF-BB-induced SMC proliferation and NOTCH3 expression via sponging miR-206.

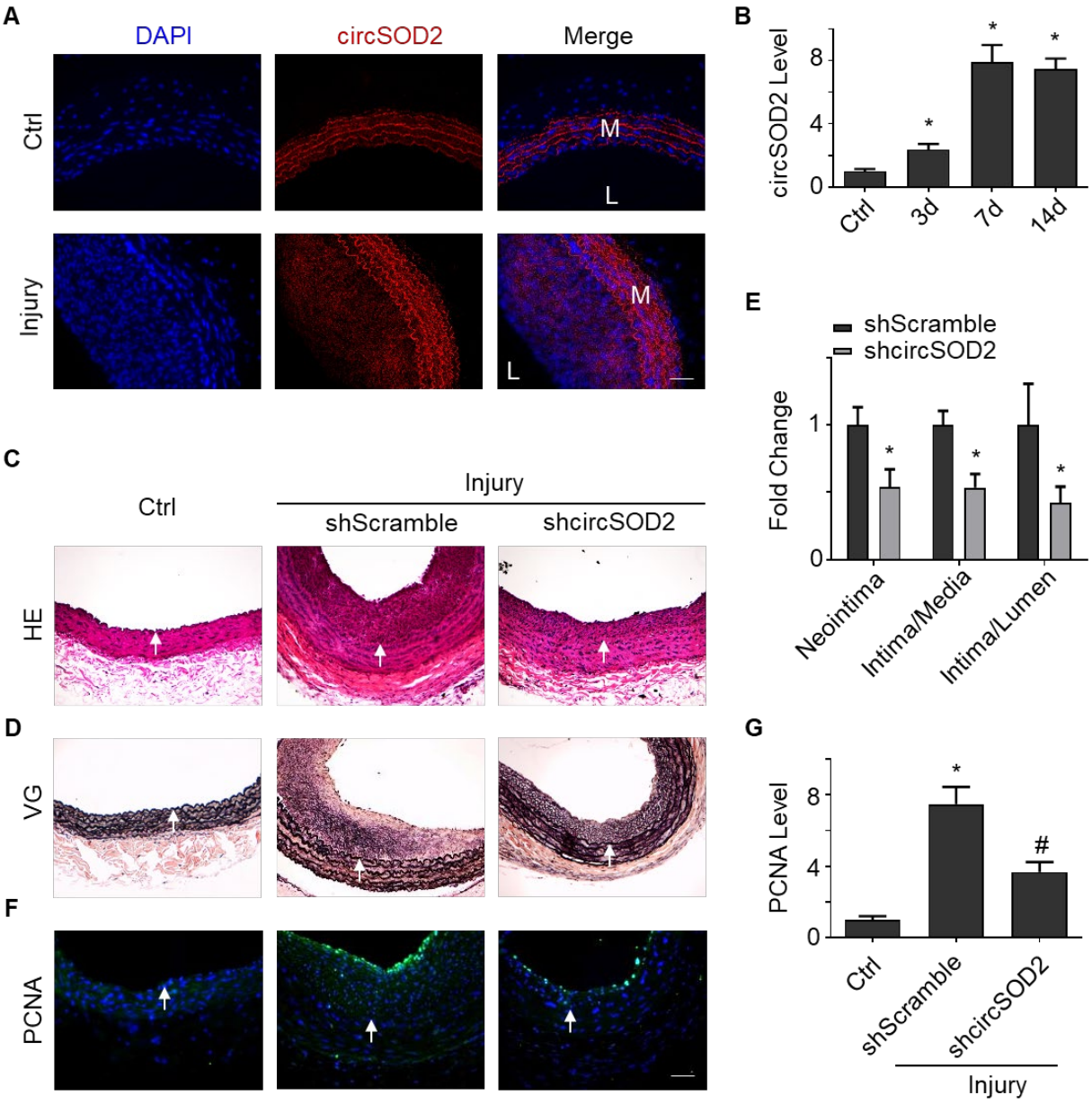

Figure 3.7. Knockdown of circSOD2 attenuated injury-induced neointima formation in vivo.

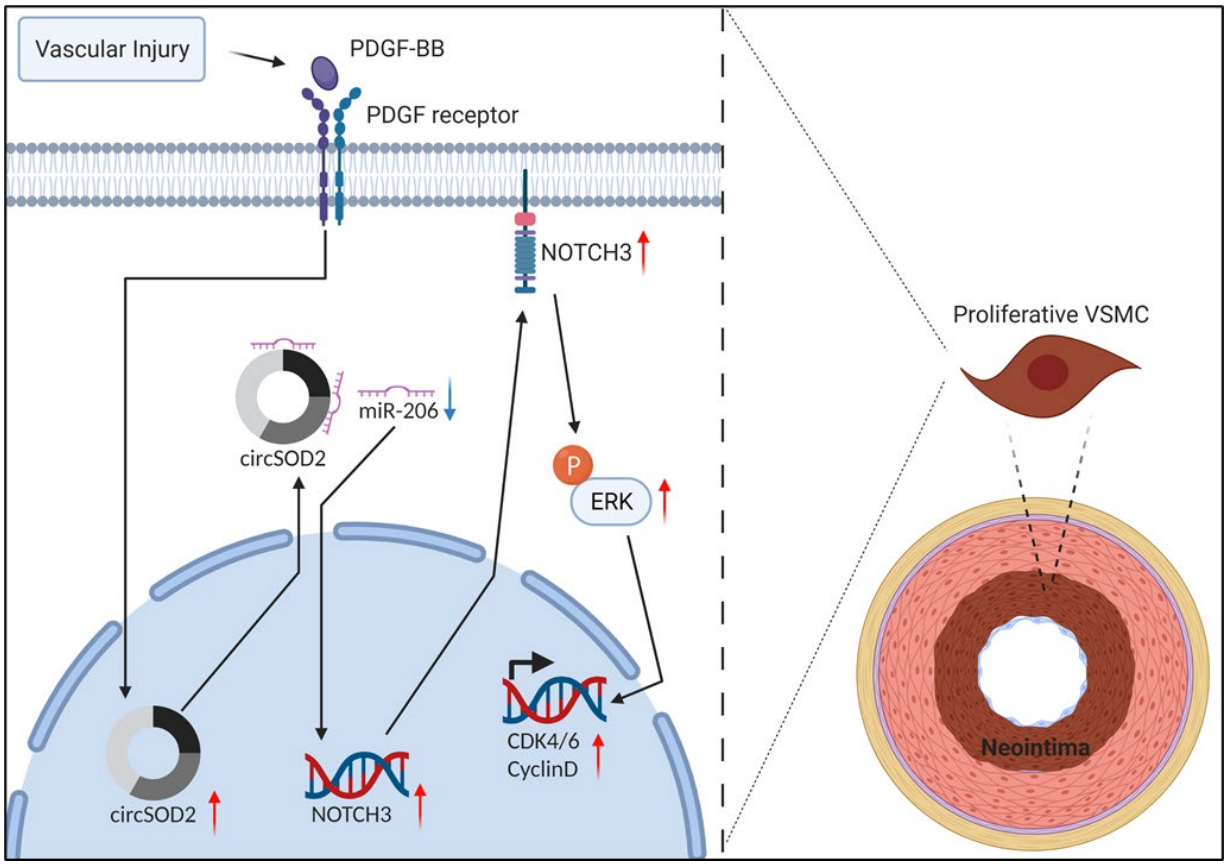

Figure 3.8. Schematic diagram of circSOD2 function in SMC proliferation and neointima formation.

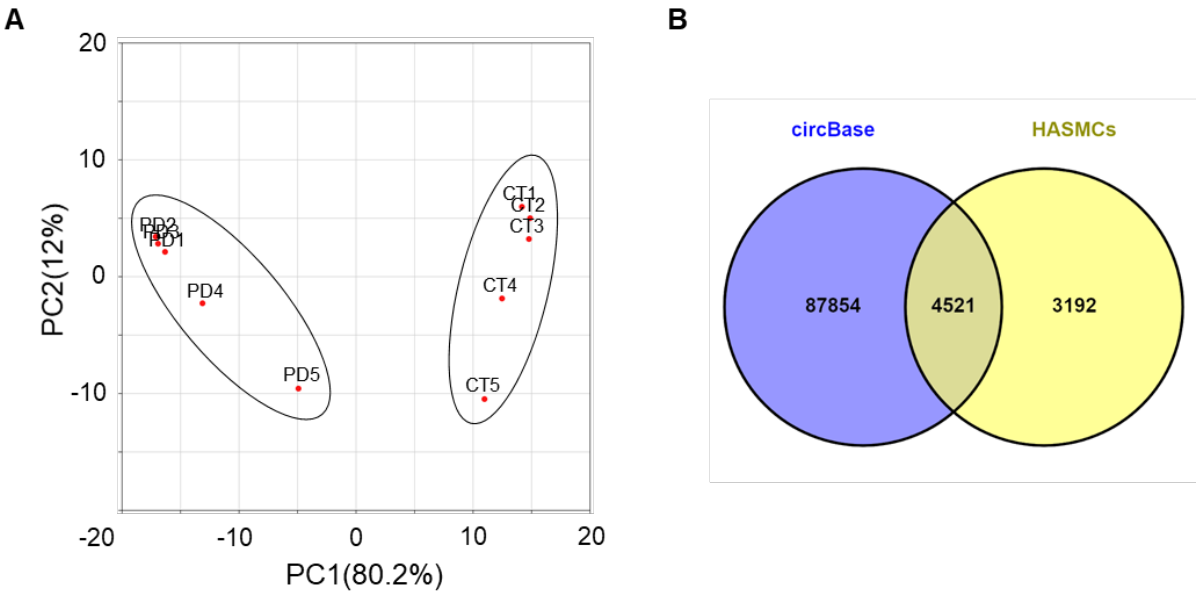

Supplementary Figure S3.1. RNAseq data verification and analysis.

A

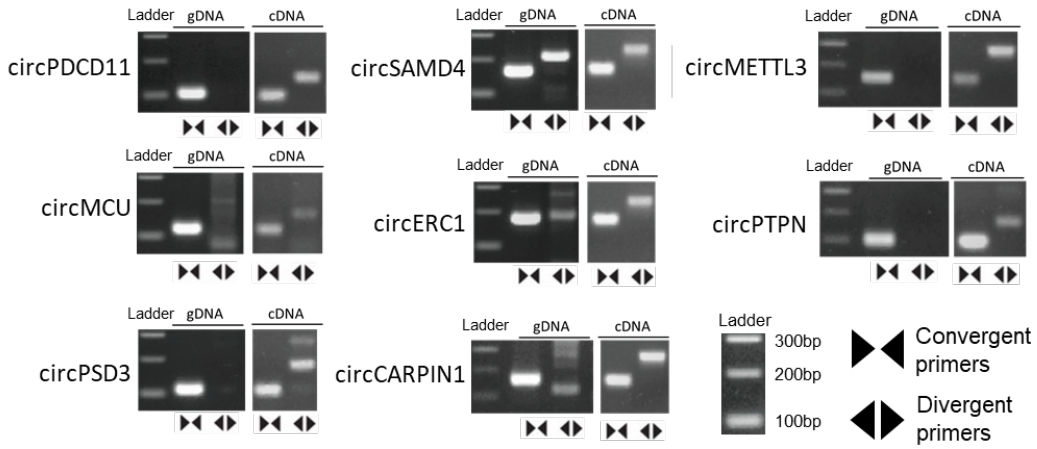

B

circRNA name	Expected size ▶◀	Expected size ◀▶	Sanger sequencing results
circPDCD11	101bp	154bp	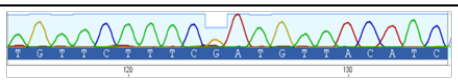
circMCU	117bp	166bp	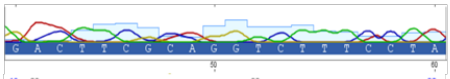
circPSD3	108bp	181bp	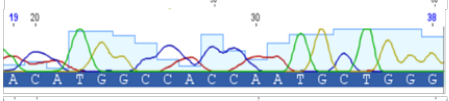
circSAMD4	160bp	210bp	
circERC1	175bp	243bp	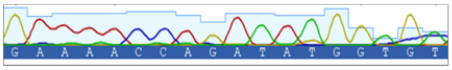
circCARPIN1	156bp	246bp	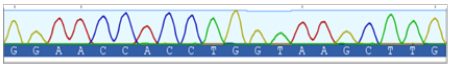
circMETTL3	159bp	243bp	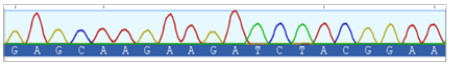
circPTPN	96bp	153bp	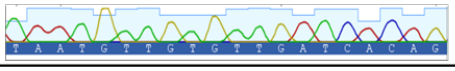

Supplementary Figure S3.2. Validation of circRNA candidates.

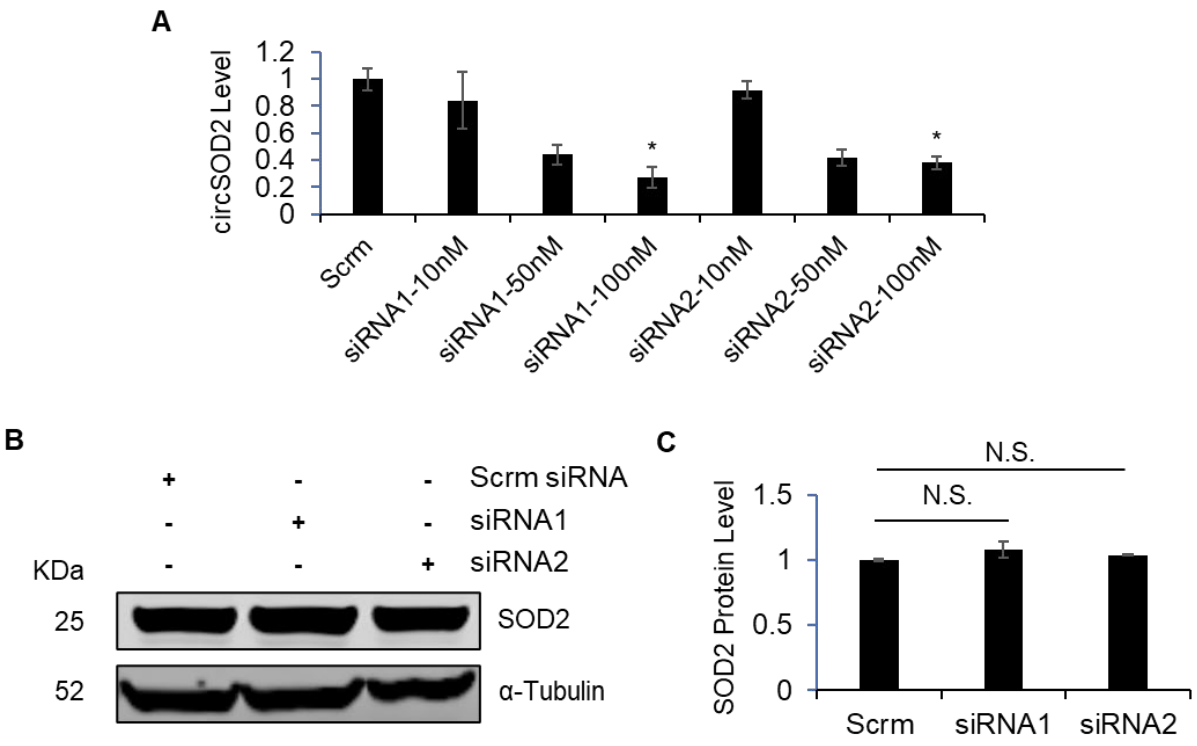

Supplementary Figure S3.3. CircSOD2 siRNAs knocked down circSOD2, but not SOD2 expression.

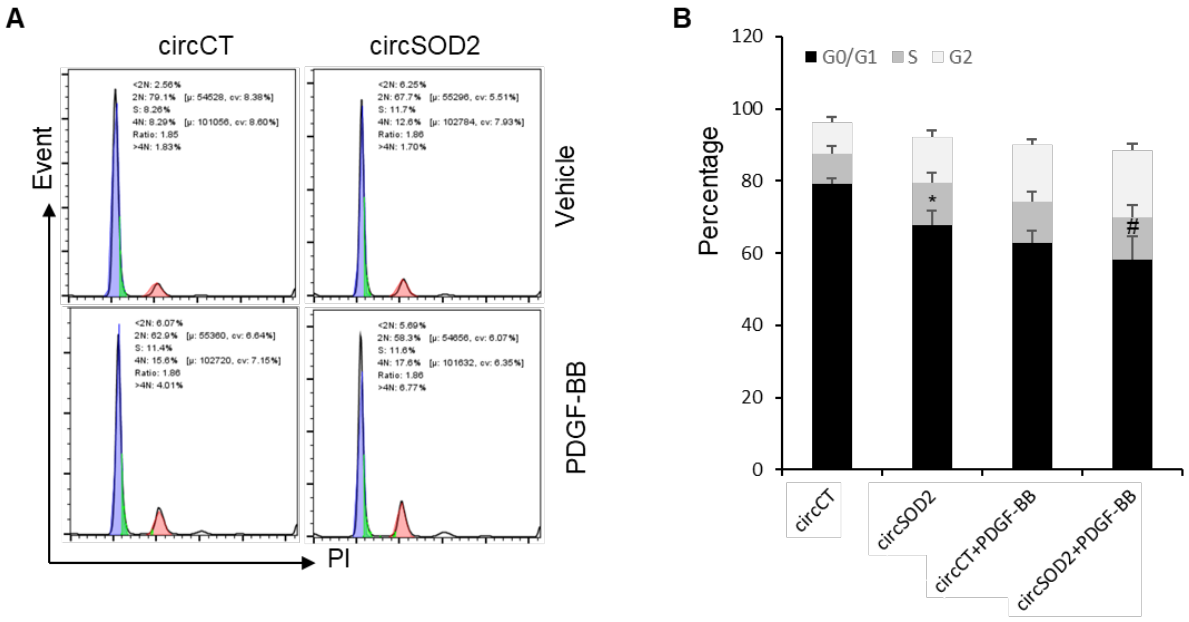

Supplementary Figure S3.4. Forced expression of circSOD2 promoted HASMC cell cycle transition.

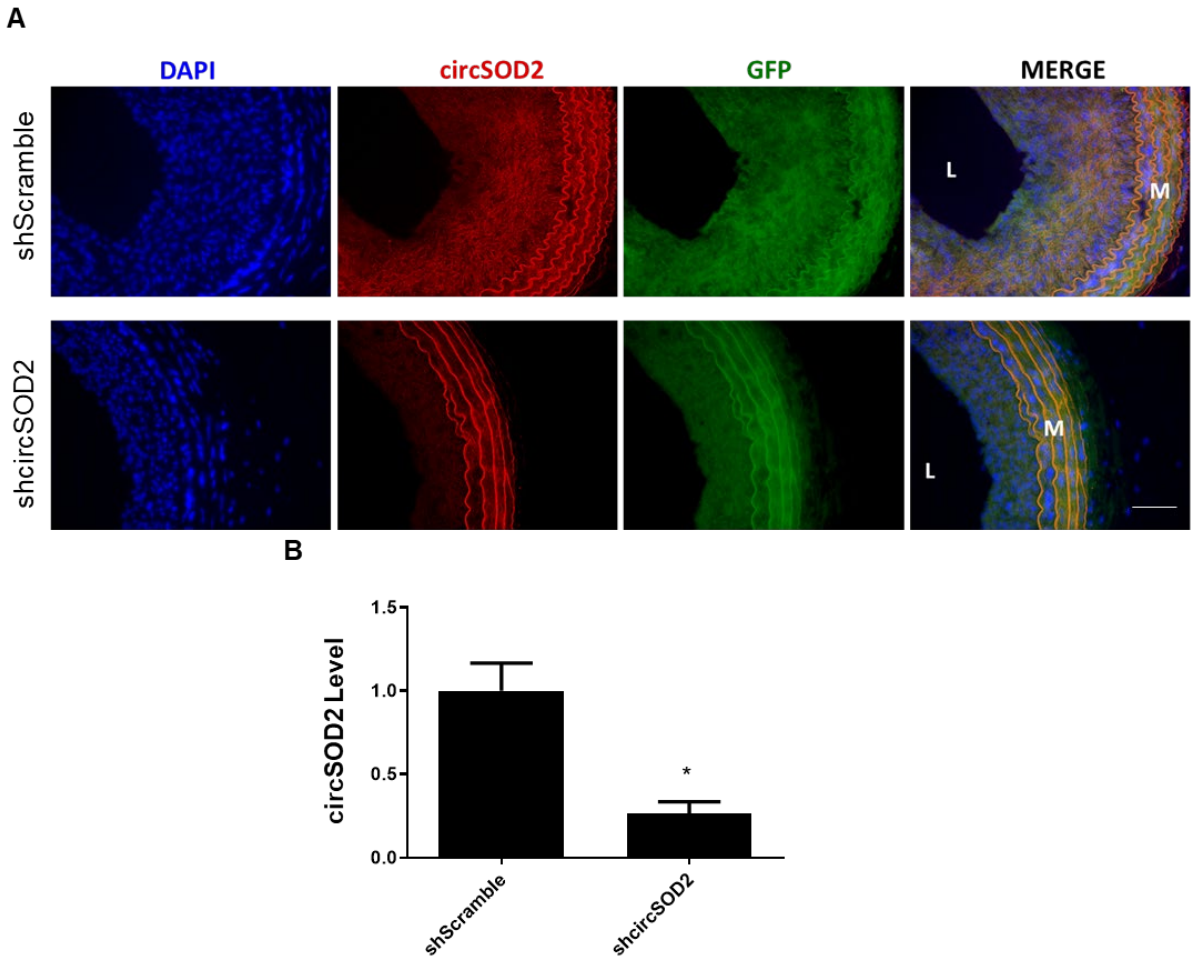

Supplementary Figure S3.5. circSOD2 shRNA knocked down its expression in injured arteries.

Supplementary Table S3.1: Primer sets used in shRNA vector construction.

Primer name	**sequence (5' to 3')**
Rno-shcSOD2-F	CGC GTC GTA GTA GTG TAG AGC ATT GCA GCA AGC ACT TCA AGA GAG TGC TTG CTG CAA TGC TCT ACA CTA CTA CTT TTT TCC AAA
Rno-shcSOD2-R	AGC TTT TGG AAA AAA GTA GTA GTG TAG AGC ATT GCA GCA AGC ACT CTC TTG AAG TGC TTG CTG CAA TGC TCT ACA CTA CTA CGA
Hsa-shCSOD2-F	CGC GTC GTT ATG CTG AGA GAT GTT ACA TTC AAG AGA TGT AAC ATC TCT CAG CAT AAC TTT TTT CCA AA
Hsa-shCSOD2-R	AGC TTT TGG AAA AAA GTT ATG CTG AGA GAT GTT ACA TCT CTT GAA TGT AAC ATC TCT CAG CAT AAC GA

Supplementary Table S3.2: Primer sets used in mutagenesis and infusion cloning.

Primer name	sequence (5' to 3')
Circmini-csod2-infusion-F	TTT ATA CTT CAG GAT GAG ATG TTA CAG CCC AGA TA
Circmini-csod2-infusion-R	TTA CCT CCG CGG GTT TCA GCA TAA CGA TCG TGG TT
Circmini-csod2-mut-5'-F	AAT GAC TTT TTT TTT ATA CTT CAG GAG ATG TTA CAG CCC AGA TAG C
Circmini-csod2-mut-5'-R	GCT ATC TGG GCT GTA ACA TCT CCT GAA GTA TAA AAA AAA AGT CAT T
Circmini-csod2-mut-3'-F	GTA AAC CAC GAT CGT TAT GCT GAG TAA GAA GCA AGG AAA AGA ATT A
Circmini-csod2-mut-3'-R	TAA TTC TTT TCC TTG CTT CTT ACT CAG CAT AAC GAT CGT GGT TTA C
pGL-csod2-infusion-F	GTG TAA TAA TTC TAG GAG ATG TTA CAG CCC AGA TAG CTC
pGL-csod2-infusion-R	CCG CCC CGA CTC TAG TCA GCA TAA CGA TCG TGG TTT AC

Supplementary Table S3.3: siRNAs used in knockdown of circSOD2. *

siRNA name	Sequence
siRNA1	Sense - 5' GUUAUGCUGAGAGAUGUUAdTdT 3’ Antisense -5' UAACAUCUCUCAGCAUAACdTdT 3'
siRNA2	Sense - 5' UCGUUAUGCUGAGAGAUGUdTdT 3’ Antisense - 5' ACAUCUCUCAGCAUAACGAdTdT 3'

* 3’ dTdT hangover was added to each strand to increase nuclease resistance of siRNAs in the cell culture medium and within transfected cells.

Supplementary Table S3.4: Primer sets used in circRNA related RT-qPCR.

Primer name	sequence (5' to 3')
circSOD2-Div-F	GTG TGG GAG CAC GCT TAC TA
circSOD2-Div-R	CGT TAG GGC TGA GGT TTG TC
circSOD2-Con-F	GGA AGC CAT CAA ACG TGA CT
circSOD2-Con-R	TTG CAG TGG ATC CTG ATT TG
circPDCD11-Div-F	AAC AAA CCC GGA GAC GAA A
circPDCD11-Div-R	ACG TTG TCT GCA GTG GAC AG
circPDCD11-Con-F	ACA AAC CCG GAG ACG AAA AG
circPDCD11-Con-R	TGG ATG GAC CCT ACA TAG CC
circMCU -Div-F	GTA TTG GTG ATG TGA CCT GTT CAC GC
circMCU -Div-R	TTG ACT CCC ACA GGC CAG C
circMCU -Con-F	GGT CTT TCA CTA CCA TTC CTA CAG TGA T
circMCU -Con-R	TTG ACT CCC ACA GGC CAG C
circPSD3-Div-F	TGG AGT CCA TTG CCT TAC CT
circPSD3-Div-R	CTT TTG GCT GCT TCC ACA TT
circPSD3-Con-F	GGG TGA AAA CAA CAC GGC TA
circPSD3-Con-R	CTT CCA CAT TGC TGC TGG TA
circSAMD4A-Div-F	AAC TGG CAG GAC AAA AGC AT
circSAMD4A-Div-R	TCT ACT TTC GCG TCG AGG TT
circSAMD4A-Con-F	ACC TCG ACG CGA AAG TAG AA
circSAMD4A-Con-R	AGC CAC ATG GCT AAA GCA CT
circERC1-Div-F	CCA GAG CTG AAG AAG GAA CG
circERC1-Div-R	TCA GGA AAG GTG TGA GCA GA
circERC1-Con-F	TAG CTA GCA GTG GGG TTG CT
circERC1-Con-R	TCC TTC CGC AAG AGA TCA TT
circPTPN12-Div-F	GGG CCA AAA GCA TAT GTA GC
circPTPN12-Div-R	TGC ATT GAT ATA GTC TGA ATC TTG TG
circPTPN12-Con-F	GGC GTC TAT GGG CCA AAA GCA TA
circPTPN12-Con-R	CAC AAC ATT ATA CTC CCA TAT CAT CCT CC
circMETTL3-Div-F	GTA GCT GCC TTT GCC AGT TC
circMETTL3-Div-R	ACC AGA GGT GGG TGC AGT AG
circMETTL3-Con-F	CTA CTG CAC CCA CCT CTG GT
circMETTL3-Con-R	TGG AGA TGG CAA GAC AGA TG
circCAPRIN1-Div-F	AGT AGA CCC TGA ACG GGA CA
circCAPRIN1-Div-R	AGC CTT TCC CCT TTG TTC AT
circCAPRIN1-Con-F	CGG GAG CAG CTT ATG AGA GA
circCAPRIN1-Con-R	TGA CAA CTC CTC TTC GGA CA
human-CYP-F	GAC CCA ACA CAA ATG GTT CC
human-CYP-R	TCG AGT TGT CCA CAG TCA GC

Supplementary Table S3.5: Primer sets and probe used in RNA-FISH.

Primer name	**sequence (5' to 3')**
eGFP-T7	TAA TAC GAC TCA CTA TAG TTC TTC TGC TTG TCG GCC AT
eGFP-T3	AAT TAA CCC TCA CTA AAG GGG CAC AAG CTG GAG TAC AA
hsa-cricSOD2-T7	TAA TAC GAC TCA CTA TAG ACA TGG CTT GCA AAA AGT AA
hsa-cricSOD2-T3	AAT TAA CCC TCA CTA AAG CAG TGC AGG CTG AAG AGC
anti-rnocsod2-bio	/5Biosg/GTGCTTGCTGCAATGCTCTACACT/3Bio/

Supplementary Table S3.6: Primer used in miRNA RT-qPCR.

Primer name	**sequence (5' to 3')**
hsa-miR-106b-5p-RT	CTC AAC TGG TGT CGT GGA GTC GGC AAT TCA GTT GAG ATC TGC AC
hsa-miR-106b-5p-q	ACA CTC CAG CTG GGT AAA GTG CTG ACA GT
hsa-miR-141-5p-RT	CTC AAC TGG TGT CGT GGA GTC GGC AAT TCA GTT GAG TCC AAC AC
hsa-miR-141-5p-q	ACA CTC CAG CTG GGC ATC TTC CAG TAC AGT
hsa-miR-150-5p-RT	CTC AAC TGG TGT CGT GGA GTC GGC AAT TCA GTT GAG CAC TGG TA
hsa-miR-150-5p-q	ACA CTC CAG CTG GGT CTC CCA ACC CTT GTA
hsa-miR-152-3p-RT	CTC AAC TGG TGT CGT GGA GTC GGC AAT TCA GTT GAG CCA AGT TC
hsa-miR-152-3p-q	ACA CTC CAG CTG GGT CAG TGC ATG ACA GA
hsa-miR-15a-5p-RT	CTC AAC TGG TGT CGT GGA GTC GGC AAT TCA GTT GAG CAC AAA CC
hsa-miR-15a-5p-q	ACA CTC CAG CTG GGT AGC AGC ACA TAA TGG
hsa-miR-204-5p-RT	CTC AAC TGG TGT CGT GGA GTC GGC AAT TCA GTT GAG AGG CAT AG
hsa-miR-204-5p-q	ACA CTC CAG CTG GGT TCC CTT TGT CAT CCT
Hsa-mir206-RT	CTC AAC TGG TGT CGT GGA GTC GGC AAT TCA GTT GAG CCA CAC AC
has-mir206-q	ACA CTC CAG CTG GGT GGA ATG TAA GGA AGT
hsa-miR-211-5p-RT	CTC AAC TGG TGT CGT GGA GTC GGC AAT TCA GTT GAG AGG CGA AG
hsa-miR-211-5p-q	ACA CTC CAG CTG GGT TCC CTT TGT CAT CCT
hsa-miR-212-3p-RT	CTC AAC TGG TGT CGT GGA GTC GGC AAT TCA GTT GAG GGC CGT GA
hsa-miR-212-3p-q	ACA CTC CAG CTG GGT AAC AGT CTC CAG TC
hsa-miR-23b-5p-RT	CTC AAC TGG TGT CGT GGA GTC GGC AAT TCA GTT GAG AAA TCA GC
hsa-miR-23b-5p-q	ACA CTC CAG CTG GGT GGG TTC CTG GCA TGC
hsa-miR-25-3p-RT	CTC AAC TGG TGT CGT GGA GTC GGC AAT TCA GTT GAG TCA GAC CG
hsa-miR-25-3p-q	ACA CTC CAG CTG GGC ATT GCA CTT GTC TCG
hsa-miR-27a-3p-RT	CTC AAC TGG TGT CGT GGA GTC GGC AAT TCA GTT GAG GCG GAA CT
hsa-miR-27a-3p-q	ACA CTC CAG CTG GGT TCA CAG TGG CTA AG
hsa-miR-27b-3p-RT	CTC AAC TGG TGT CGT GGA GTC GGC AAT TCA GTT GAG GCA GAA CT
hsa-miR-27b-3p-q	ACA CTC CAG CTG GGT TCA CAG TGG CTA AG
hsa-miR-29a-3p-RT	CTC AAC TGG TGT CGT GGA GTC GGC AAT TCA GTT GAG TAA CCG AT
hsa-miR-29a-3p-q	ACA CTC CAG CTG GGT AGC ACC ATC TGA AAT
hsa-miR-330-3p-RT	CTC AAC TGG TGT CGT GGA GTC GGC AAT TCA GTT GAG TCT CTG CA

hsa-miR-330-3p-q	ACA CTC CAG CTG GGG CAA AGC ACA CGG CCT G
hsa-miR-370-3p-RT	CTC AAC TGG TGT CGT GGA GTC GGC AAT TCA GTT GAG ACC AGG TT
hsa-miR-370-3p-q	ACA CTC CAG CTG GGG CCT GCT GGG GTG GAA
hsa-miR-516a-3p-RT	CTC AAC TGG TGT CGT GGA GTC GGC AAT TCA GTT GAG ACC CTC TG
hsa-miR-516a-3p-q	ACA CTC CAG CTG GGT GCT TCC TTT CA
hsa-miR-612-RT	CTC AAC TGG TGT CGT GGA GTC GGC AAT TCA GTT GAG AAG GAG CT
hsa-miR-612-q	ACA CTC CAG CTG GGG CTG GGC AGG GCT TCT GAG
hsa-miR-637-RT	CTC AAC TGG TGT CGT GGA GTC GGC AAT TCA GTT GAG ACG CAG AG
hsa-miR-637-q	ACA CTC CAG CTG GGA CTG GGG GCT TTC GGG CT
hsa-miR-767-5p-RT	CTC AAC TGG TGT CGT GGA GTC GGC AAT TCA GTT GAG CAT GCT CA
hsa-miR-767-5p-q	ACA CTC CAG CTG GGT GCA CCA TGG TTG TCT G
hsa-miR-92a-3p-RT	CTC AAC TGG TGT CGT GGA GTC GGC AAT TCA GTT GAG ACA GGC CG
hsa-miR-92a-3p-q	ACA CTC CAG CTG GGT ATT GCA CTT GTC CCG
URP	TGG TGT CGT GGA GTC G

CHAPTER 4

CIRCULAR CRIM1, A NOVEL REGULATOR FOR SMOOTH MUSCLE PHENOTYPIC MODULATION AND CAN PERFORM CONTINUOUS LOOP-TRANSLATION VIA N^6-METHYLADENOSINE

Mei X and Chen SY.

To be submitted to Circulation.

Abstract

Objective— Circular RNAs (circRNAs), a novel class of endogenous RNA molecules, are characterized by covalently closed-loop structures without a 5′ cap or a 3′ Poly A tail, exhibits cell- and disease-specific expression patterns. CircRNAs exert their function via sponging microRNAs (miRNA) and being a template of translation. In this study, we investigated whether circular cysteine-rich motor neuron 1 (circCRIM1) regulated SMC phenotypic modulation through sequestering miR-16 and could undergo continuous loop-translation.

Approach and Result— CircCRIM was highly enriched in platelet-derived growth factor-BB (PDGF-BB) treated human aortic smooth muscle cells (HASMCs) and neointima SMCs in balloon-injured rat carotid arteries. Forced expression and knockdown of circCRIM1 in HASMCs promoted and blocked SMC phenotypic modulation. CircCRIM1 pulldown and luciferase assay revealed that circCRIM1 could physically bind with miR-16, and following rescue assay confirmed that circCRIM1 regulated SMC phenotypic modulation via sequestering miR-16. Furthermore, circCRIM1 could undergo continuous loop-translation producing a novel protein detected by Liquid Chromatography-Mass Spectrometer (LC/MS). Mechanistically, N^6-Methyladenosine (m^6A) modifications on circCRIM1 were read by YTH N6-methyladenosine RNA binding protein 3 (YTHDF3), which initiated continuous loop-translation via interacting with translational initiation factors.

Conclusions—CircCRIM1 is a novel regulator mediating SMC phenotypic modulation and neointima formation during injury-induced vascular remodeling. Additionally, circCRIM1 undergoes continuous loop-translation to produce novel protein. Therefore, circCRIM1 can be a

potential therapeutic target for preventing neointimal formation in proliferative vascular diseases and a qualified RNA translation study model.

Introduction

Cardiovascular diseases (CVDs) are the leading causes of morbidity and mortality worldwide and the significant factors to impact the quality of life[1]. Cardiovascular intervention, such as percutaneous coronary intervention (PCI), is a widely used technique for treating obstructive coronary artery disease[2]. However, the procedure of PCI and the application of the intervention device cause a relatively high rate of restenosis, majorly due to vascular smooth muscle cell (VSMC) phenotypic modulation, vascular remodeling, and neointimal hyperplasia[3]. Mature VMSCs have extreme plasticity. Fully differentiated VSMCs in adult mammals, which proliferate at a very low rate and show low synthetic phenotype, are vital for maintaining vessel tone[4, 5]. However, the contractile VSMC phenotype can be switched to synthetic phenotype in response to injury or growth factors, such as platelet-derived growth factor (PDGF), exhibiting decreased expression of SMC marker genes, such as SM alpha-actin (αSMA)[6], SM myosin heavy chain (SMMHC)[7], Calponin 1 (CNN1)[8], Smooth Muscle Protein 22-Alpha (SM22α)[8] and smoothelin[9]. The alteration of VSMCs phenotype will further lead to developmental disorders and various vascular diseases such as atherosclerosis, hypertension, intimal hyperplasia, vein graft stenosis, and restenosis following angioplasty[10-13]. Therefore, insightful investigation of underlying molecular mechanisms responsible for VSMC phenotype switching is crucial for better understanding the pathogenesis of proliferative vascular disorders.

Circular RNA (circRNA) becomes a research hotspot due to its unique structure. Unlike typical linear RNA, circRNA has its 3' and 5' ends brought into close proximity by *cis* or *trans* elements, forming a closed-loop RNA molecule via an alternative splicing event called "back-splicing"[14]. The high-throughput RNA-sequencing (RNAseq) has identified tens of thousands of

circRNAs from multiple cell types and tissues, showing at least 20% of active genes express circRNAs[15]. Owing to the unique circular trait, circRNAs exhibit resistance to RNA exonucleases, making intracellular circRNAs highly stable and abundant[16]. CircRNA is thought to be an essential regulatory factor in multiple biological processes[17]. So far, the several functions of circRNAs have been elucidated, such as acting as miRNA sponges, the scaffold of proteins, alternative splicing regulator, and peptides or proteins template[18]. However, the circRNAs function in VSMC phenotypic modulation is largely unknown.

Our previous study has constructed circRNA profiling via RNAseq of transcripts in control and PDGF-BB-treated human aortic SMCs (HASMCs) and then identified more than 7,000 circRNA candidates. Among all these circRNAs, circCRIM1, derived from the host gene cysteine-rich motor neuron 1 (CRIM1) was significantly upregulated upon PDGF-BB treatment in both *in silico* and *in vitro* expression analyses. Knockdown of circCRIM1 by shRNA abolished PDGF-BB-induced HASMC phenotypic modulation, whereas ectopic expression of circCRIM1 promoted HASMC phenotypic modulation. CircCRIM1 controlled HASMC phenotypic modulation via sponging miR-16. Besides, circCRIM1 could undergo continuous loop-translation producing a novel protein detected by Liquid Chromatography-Mass Spectrometer (LC/MS). This translation was found to be driven by N^6-Methyladenosine (m^6A) modifications which bridge circCRIM1 with YTH N^6-methyladenosine RNA binding protein 3 (YTHDF3), resulting in the initiation of a continuous loop-translation via interacting with translational initiation factors. All data suggests that circCRIM1 is a novel regulator for SMC phenotypic modulation and vascular remodeling.

Materials and Methods

Animals

Male Sprague-Dawley rats weighing 450-500 g and RNU nude rats were purchased from Charles River Laboratories. All animals were housed under conventional conditions in the animal care facilities and received humane care in compliance with the Principles of Laboratory Animal Care formulated by the National Society for Medical Research and the Guide for the Care and Use of Laboratory Animals. Animal surgical procedures were approved by the Institutional Animal Care and Use Committee of the University of Missouri. Sex is a critical biological variable in cardiovascular diseases[19]. Since this is the first report investigating circCRIM1 function in vascular diseases, only male animals were used in this study. However, we will investigate if there is a sex-specific role of circCRIM1 in vascular remodeling by including both male and female animals in our future studies.

Reagents and cell Culture

HASMCs were purchased from Lifeline (FC-0015) on passage 1 and cultured in VascuLife® Basal Medium (Lifeline, LM-0002) containing VascuLife® SMC LifeFactors® Kit (Lifeline, LS-1040) at 37°C in a humidified atmosphere with 5% CO2. HASMCs <6 passages with 80% of confluence were used in this study. PDGF-BB was obtained from R&D Systems (220-BB-050) and used at 20 ng/mL to treat HASMCs.

RNase R treatment

1 µg of RNA was incubated with 20 U of RNase R (Lucigen, RNR07250) at 37°C for 10 min. RNA was then cleaned by RNA Clean & Concentrator (Zymo, R1017). The treated RNA was then subjected to RT-qPCR.

Construction of adenoviral vector expressing circCRIM1 shRNA

Short hairpin RNA (shcircCRIM1) specifically targeting the back-splicing junctions (BSJ) of human circCRIM1 was inserted into pRNAT-H1.1/Adeno vector (Genscript) between MluI and HindIII site. Adenoviral vectors of shcircCRIM1 (Ad-shcircCRIM1) were constructed using AdEasy system[20]. Adenoviruses were purified by gradient density ultracentrifugation of cesium chloride followed by dialyzing in dialysis buffer (135 mmol/L NaCl, 1mmol/L $MgCl_2$, 10 mmol/L Tris-HCl, pH 7.5, 10% glycerol). Primers for construction of the human circCRIM1 shRNA were listed in the Supplemental Table 4.1.

Plasmid construction

For circCRIM1 expression plasmid (circCRIM1) construction, full-length circCRIM1 cDNA was amplified from the HASMC mRNA using Phusion High-Fidelity PCR Master Mix (Thermo Scientific, F531S) and was inserted into a pcDNA3.1(+) CircRNA Mini Vector (a gift from Dr. Jeremy Wilusz[21], Addgene plasmid #, 60648) between HindIII and XhoI restriction site by using In-Fusion HD Cloning (Clonetech, 638910). Residual sequences flanking the full length of circCRIM1 on plasmid, which could be mistakenly included into circCRIM1 after circularization, were removed by QuikChange II XL Site-Directed Mutagenesis Kit (Agilent, 200521). For luciferase reporter assay, the full length circCRIM1 was amplified from the human SMC cDNA pool and was inserted downstream of firefly luciferase cassette in a Myocd vector[22] with myocardin promoter at XbaI site. For circCRIM1 Flag tag expression vector (c-Flag), 1x Flag tag DNA sequence was inserted after ATG on circCRIM1 overexpression vector by QuikChange II XL Site-Directed Mutagenesis Kit (Agilent, 200521). For c-Flag m^6A substitution vectors, A was substituted to T by QuikChange II XL Site-Directed Mutagenesis Kit

(Agilent, 200521). All vectors were verified by sequencing. The primers amplifying circCRIM1, used in mutagenesis and infusion cloning, were listed in the Supplemental Table 4.2.

Western blot

Western blot was performed as described previously[12]. Cultured HASMCs were washed twice with PBS followed by protein extraction using RIPA buffer [50 mmol/L Tris-HCI (pH 7.4), 1% (v/v) Triton X100, 0.25% (w/v) sodium deoxycholate, 150 mM NaCl, 1 mM EGTA, 0.1% (w/v) SDS] containing 1x protease inhibitors (Thermo Scientific, 78429) and phosphatase inhibitors (Thermo Scientific, 78420). Protein concentration was measured using BCA Protein Assay Reagent (Thermo Scientific, 23225). Lysates were denatured by boiling with SDS solution containing 2-mercaptoethanol. Equal amounts of proteins were resolved on SDS-PAGE gels and then transferred to nitrocellulose membranes (Bio-Rad, 1620115). Nonspecific bindings were blocked with 5% BSA (Sigma-Aldrich, A2153), and then incubated with primary antibodies in blocking buffer at 4°C for 16 hours, followed by incubation with IRDye® Secondary Antibodies (LI-COR) for 1 hour. Detection was performed on Odyssey CLx (LI-COR, Lincoln, Nebraska). Antibodies used for immunoblotting were: α-Tubulin (CST, #2125), Calponin 1 (abcam, ab46794), ACTA2 (Sigma-Aldrich, A2547), MYH11 (Biomedical Technologies Inc, BT-562), TAGLN (Abcam, ab10135), FLAG M2 (Sigma-Aldrich, F1804), GAPDH (Sigma-Aldrich, G8795), YTHDF3 (Proteintech, 25537-1-AP), Argonaute-2 (abcam, ab32381) and CRIM1 (Invitrogen, PA5-34410).

SiRNA transfection

Two siRNAs and one Non-targeting siRNA (D-001210-01-05) were purchased from Horizon Discovery. SiRNAs were designed based on circCRIM1 BSJ sequence. Transfection was performed using Lipofectamie 3000 (Invitrogen, L3000075) following manufacture's protocol.

Cells were harvested after 48 hours of transfection. SiRNA information was listed in Supplemental Table 4.3.

Quantitative real time-PCR (RT-qPCR)

RT-qPCR was performed as described previously[13]. HASMC total RNA was extracted using Trizol Reagent (Invitrogen) according to the manufacturer's protocol. cDNA was synthesized with 1 μg of RNA using iScript cDNA Synthesis kit (Bio-Rad, 1708890). qPCR was performed on AriaMx Real-time PCR System (Agilent, Santa Clara, CA) using All-in-One™ qPCR Mix (GeneCopoeia, QP004). The primer used in this study were listed in the Supplemental Table 4.4.

Cell fractionation

Cell fractionation was performed as described previously[23]. A nuclear extraction kit (EMD Millipore, 2900) was used by following standard procedures. Briefly, HASMCs (1×10^6) were washed with PBS twice. After trypsinization, cells were collected by spinning down at 500 × g for 10 min. Cell pellets were washed with ice-cold PBS and resuspended with ice-cold cytoplasmic lysis buffer containing 40 units/ml RNase inhibitor. The cells were lysed by passing through a syringe with a 27-gauge needle. Cell lysates were then centrifuged at 8000 × g for 20 min. Nuclear fractions were pelleted at the bottom. Both the cytoplasmic and nuclear fractions were used for RNA extraction and RT-qPCR analysis.

RNA pulldown assay

RNA pulldown assay was adapted from RNA Antisense Purification protocol with some modifications[24, 25]. We first synthesized anti-circCRIM1 probe targeting circCRIM1 BSJ and control probes with 10% biotin-UTP (Roche, 11388908910) using *in vitro* transcription kit (Promega, P1300). The primers used in probe synthesis were listed in the Supplemental Table 4.6. HASMCs at 80-90% confluence on 15-cm culture dishes were fixed with 2% formaldehyde

solution at 37°C for 10 mins before being lysed in 200 µl lysis buffer [20 mM HEPES (pH 7.5), 50 mM KCl, 0.5 mM EDTA, 1.5mM $MgCl_2$, 1% (v/v) NP-40, and 0.4% (w/v) sodium deoxycholate (pH 7.5), 0.1% (w/v) N-lauroylsarcosine] containing 40 units/ml RiboLock RNase Inhibitor (Thermo Scientific, EO0384) and 1x protease inhibitors. After 10 mins of incubation on ice, cell lysate was homogenized by passing through a 27-gauge needle 20 times, and then the supernatant was collected by centrifugation at 13,000xg for 20 mins. Cell lysates (200 µl) were added with 800 µl hybridization/wash buffer [20 mM Tris-HCl (pH 7.5), 7 mM EDTA, 3 mM EGTA, 150 mM LiCl, 1% (v/v) NP-40, 0.2% (w/v) N-lauroylsarcosine, 0.1% (w/v) sodium deoxycyolate] supplied with RNase and protease inhibitors, and then was pre-cleared by incubation with 50 µl of Streptavidin Magnetic Beads (NEB, S1420S) at 37°C for 20 mins. Meanwhile, probes (1µg for each probe) were denatured in water at 85°C for 1 min and then immediately transferred to ice. The pre-cleared lysates were incubated with the denatured probes (500 µl each probe) at 37°C for 2 hours with rotation, followed by adding 500 µl pre-washed Streptavidin Magnetic Beads and incubating with rotation for 30 mins. After six times washing with hybridization/wash buffer, beads were incubated in Proteinase K Digestion Buffer [20 mM Tris-HCl pH 7.5, 10 mM EDTA, 2% N-lauroylsarcosine] supplied with 20 µg/ml of proteinase K at 42 °C for 1 h to digest protein and reverse formaldehyde crosslinks. RNA was purified by using RNA Clean & Concentrator kit (Zymo, R1017) by following the small RNA purification protocol. Elution from the column was subjected to RT-qPCR analysis. Primers used for miRNA reverse transcription and qPCR were listed in the Supplemental Table 4.5.

Ago2 RIP assay

The RIP assay was performed as described previously[23]. Briefly, HASMCs at 80-90% confluence on 15 cm dishes were fixed with 2% paraformaldehyde (PFA) on ice. Cells were then

lysed in FA lysis buffer [50 mM HEPES, 140 mM NaCl, 1 mM EDTA, 1% (v/v) NP-40, and 0.1% (w/v) sodium deoxycholate (pH 7.5)] containing 40 units/ml RiboLock RNase Inhibitor and 1x protease inhibitors. The solution was rotated at 4°C for 2 hours and then was incubated with mouse IgG or Argonaute-2 (Ago2) antibody (1 μg) at 4°C for 6 h. The immunoprecipitates were captured with Protein A/G PLUS-Agarose (50 μl) (Santa Cruz Biotechnology, sc-2003). After washing with FA lysis buffer for six times, the samples were incubated with 20 μg/ml proteinase K at 42 °C for 1 h to digest the proteins. The immunoprecipitated RNA was purified by using RNA Clean & Concentrator kit (Zymo, R1017). Purified RNA was subjected to RT-qPCR analysis.

Polysome fractioning analysis

Cytoplasmic extract from 293T cells were subjected to sucrose gradient fractionation. Cells were firstly treated with native and 2mM puromycin, which causes the dissociation of the ribosomes on the translating RNAs[26]. Then the cell lysates were loaded on top of 10-50% sucrose gradient. After ultracentrifugation, the gradient was separated equally into 22 fractions from top to bottom manually, and for each fraction, the absorbance of 253nm was measured using the spectrophotometer to make the profiling. Collected fractions were next proceeded to RNA extraction and reverse transcription. RNA expression levels were detected by RT-qPCR amplification. Finally, the percentage of recovered RNA was calculated by ΔCT method[27].

LC/MS sample processing and analytical methods

Five volumes of cold acetone were added to the samples and incubated at -20C for overnight. All samples were washed by 80% cold acetone twice. Then 10ul 6M urea 2M thiourea and 100mM ammonium bicarbonate was added to the pellet. The solubilized protein was reduced by DTT and alkylated by iodoacetamide. After that, trypsin was added for digestion overnight. The

digested peptide was C18 ziptip desalted, lyophilized and resuspended in 10uL 5/0.1 % acetonitrile/formic acid. For LC-MS+MSMS (TimsTOF pro), 1ul suspended peptide was loaded onto a on C18 column (20 cm X 75 μm 1.7 μm) with a step gradient of acetonitrile at 300nL/min. The Bruker nanoElute system is connected to a timsTOF pro mass spectrometer. For LC gradient conditions, the initial conditions were 2%B (A: 0.1% formic acid in water, B: 99.9% acetonitrile, 0.1% formic acid), followed by 17 min ramp to 17%B. 17-25%B over 23min, 25-37%B over 10min, gradient of 37%B to 80%B over 5 min, hold at 80%B for 5 min. Total run time was 60min. MS data was collected over a m/z range of 100 to 1700. During MS/MS data collection, each TIMS cycle included 1 MS + an average of 10 PASEF MS/MS scans. Raw data was searched using PEAKS (version X+) with customized Uniprot Human protein database with target protein sequence. Data were searched with trypsin as enzyme, 2 missed cleavages allowed; carbamidomethyl cysteine as a fixed modification; deamidation of asparagine and glutamine, oxidized methionine, and acetylation on protein N terminus as variable modification. 20ppm mass tolerance on precursor ions, 0.1Da on fragment ions. Search protein and peptide results file were export from PEAKS.

Rat carotid artery injury model

Rat carotid artery balloon injury was performed as described previously[12]. Briefly, rats were anesthetized by isoflurane (2%) inhalation. A 2F Fogarty arterial embolectomy balloon catheter (Baxter Edwards Healthcare) was introduced through the left external carotid artery and advanced 4 cm toward the thoracic aorta into the common carotid artery. The balloon was inflated with 20 μl saline and then withdrawn back to the carotid bifurcation with constant rotation during denudation of the endothelium. This procedure was repeated for two additional times to ensure complete endothelial denudation. 3, 7, or 14 days later, the balloon-injured

segment of the artery from the proximal edge of the omohyoid muscle to the carotid bifurcation was perfused with saline and excised. The balloon-injured segments were fixed with 4% paraformaldehyde (PFA) and embedded in paraffin. Subsequent morphometric analyses were performed in a double-blinded manner.

Fluorescent in situ hybridization (FISH)

Biotin-labeled anti-circCRIM1 RNA probes and negative control probes derived from eGFP gene were synthesized as described previously[23]. HASMCs grown on coverglass were firstly washed with cold PBS twice and then fixed with 1% PFA for 30 mins at room temperature, followed by wash with PBS for three times. Permeabilization was performed with 0.5% Triton X-100 in PBS for 10 mins, followed by PBS wash for three times. Endogenous biotin was blocked with 0.05% avidin incubation for 15 mins, followed by 0.005% biotin incubation for 15 mins to block excessive biotin-binding pockets on avidin. Free biotins were removed by washing with PBS for three times. The cells were then incubated with pre-denatured probes in hybridization buffer (10% w/v dextran sulfate, 10% formamide, in 2× SSC, 1 mg/ml fragmented salmon testes DNA) in dark and humid environment at 55 °C for 16 h to allow hybridization. After hybridization, cells were washed with wash buffer (10% formamide in 2× SSC) for 3 times. Finally, cells were incubated with streptavidin-conjugated Alexa-fluor 488 (Invitrogen, S11223) in PBS for 1 hour and counterstained with DAPI. For tissue FISH, biotin-labeled rat anti-circCRIM1 ssDNA probe was obtained from Integrated DNA Technologies (IDT, Coralville, Iowa). Vessel segments were harvested and fixed in 4% paraformaldehyde at 4°C for 3 h, transferred to 15% sucrose overnight for cryoprotection. Samples were then embedded in Tissue-Tek O.C.T. compound (EMS, Hatfield, PA). Tissue blocks were frozen in liquid nitrogen, stored at −80°C, and 5-μm thick sections were made. The FISH procedure was similar to cellular

FISH, except for streptavidin-conjugated Alexa fluor 594 (Invitrogen, S11227) was used for detection. Probe sequences were listed in the supplemental primer Table 4.6.

Luciferase reporter assay

Myocd or MyocdcCRIM1 firefly luciferase reporter along with miRNA mimics were transfected or co-transfected into HASMCs in 12-well plates using Lipofectamine 3000 (Invitrogen). Luciferase activities were measured using a luciferase assay kit (Promega, E1500) according to the manufacturer's instruction.

Statistical analysis

All statistical analyses were performed using GraphPad Prism software version 8. Data are expressed as means ± SEM. Data were analyzed for normality and equal variance. An unpaired 2-tailed Student *t* test was used to compare data between 2 groups and one-way ANOVA was used for comparisons among >2 groups with the Sidak post hoc correction. Significance is depicted with asterisks or pound on graphs as follows: *P<0.05; #P<0.05.

Results

CircCRIM1 is Expressed in VSMCs and May Play a Role in Vascular Remodeling

Phenotypic modulation of VSMCs plays an essential role in intimal formation, and PDGF-BB is a potent stimulator for VSMC phenotypic modulation[28]. Previous genome-wide profiling of circRNAs in SMC has identified hundreds of circRNAs are differentially expressed in response to PDGF-BB. Among them, circCRIM1, derived from the host gene Cysteine-Rich Motor neuron 1 (CRIM1), was highly upregulated in PDGF-BB-treated HASMCs and thus was selected

for further investigation (Figure 4.1A). CircCRIM1 contains six exons from CRIM1 pre-mRNA with a sequence length of 1041 nucleotides (nt) (Figure 4.1B). The genomic location of circCRIM1 is on the forward strand of human chromosome 2, starting from 36,623,756-36,706,837. PCR amplification using divergent primers flanking the back-splicing junction of circCRIM1 and convergent primers only produced expected amplicon in cDNA but not in genomic DNA of HASMC. Following Sanger sequencing of the amplicon confirmed that circCRIM1 was originated from the exon 2 to 6 of the CRIM1 gene which was consistent with the information identified from our circRNA detection pipeline (Figure 4.1C). RNase R is a ribonuclease only digesting linear RNAs while leaving other types of RNA molecules unimpacted[29]. To further authenticate circCRIM1, we performed RNase R digestion using total RNA isolated from HASMCs. After the digestion of RNase R, circCRIM1 exhibited resistance to the digestion, but linear CRIM1 mRNA was degraded significantly (Figure 4.1D). To reveal the localization of circCRIM1, we performed cellular fractioning followed by RT-qPCR assay. CircCRIM1 was largely located in HASMC cytoplasm while only a small portion was in the nuclei (Figure 4.1E). Since RNA-Seq showed that circCRIM1 was highly induced by PDGF-BB, we treated HASMCs with 20 ng/ml PDGF-BB for 0, 12, 24, and 48 hours to validate circCRIM1 expression. As shown in Figure 4.1F, circCRIM1 expression was induced by PDGF-BB in a time-dependent manner. RNA-FISH of circCRIM1 also verified that circCRIM1 was enriched in PDGF-BB-treated HASMCs and mainly located in cytoplasm (Figure 4.1G). In the normal artery, circCRIM1 level was very low. However, in a rat carotid balloon injury model, injury significantly induced circCRIM1 expression in neointimal SMCs (Figure 4.1H). Quantitative analyses revealed that circCRIM1 was significantly induced as early as three days after the injury, and its expression reached the highest level (8.89 folds increase) 7 days and maintained

the level until 14 days post-injury (Figure 4.1I). additionally, orthologs of circCRIM1 in mice and rats were detected in other NGS datasets[30-32]. Alignment analysis showed circCRIM1 was highly conserved among humans, mice, and rats with 90% pairwise Identity, indicating circCRIM1 may play essential biological functions in these species (Supplemental Figure S4.1 A-C).

CircCRIM1 Regulates HASMC Phenotypic Modulation

To elucidate if circCRIM1 is involved in HASMC phenotypic modulation, we then conducted a series of in vitro loss and gain-of-function experiments. Two small interfering RNAs (siRNAs) specifically targeting the BSJ region of circCRIM1 with different coverages were designed, and the circCRIM1 knockdown efficiency was confirmed by RT-qPCR (Supplemental Figure S4.2A). We then constructed an adenoviral vector expressing circCRIM1 short hairpin RNA (shRNA) (shcircCRIM1) based on the siRNA1 sequence and the knockdown efficiency of shcircCRIM1 in HASMC was also confirmed by RT-qPCR (Figure 4.2A). Additionally, to enforce-express circCRIM1, we constructed circCRIM1 overexpression vector (circCRIM1) by inserting circCRIM1 full length into circmini vector flanking by two intronic complementary sequences (ICSs), and the overexpression efficiency of circCRIM1 in HASMCs was validated by RT-qPCR (Figure 4.2B). Furthermore, overexpression and knockdown of circCRIM1 had no effect on CRIM1 expression (Supplemental Figure S4.2 B&C). Next, we tested if knockdown of circCRIM1 in HASMCs regulates HASMC phenotypic modulation. As shown in Figure 4.2 C&D, knockdown of circCRIM1 inhibited PDGF-BB–induced VSMC dedifferentiation, evidenced by significantly increased expression level of SMC markers, including Myosin Heavy Chain 11 (MYH11), Actin Alpha 2 (αSMA), Calponin 1 (CNN1), and Smooth Muscle Protein 22-Alpha (SM22α) in PDGF-BB treatment group. Conversely, forced expression of circCRIM1

further inhibited PDGF-BB suppressed SMC makers expression (Figure 4.2 E&F). These data suggest that circCRIM1 may be involved in PDGF-BB–mediated SMC phenotype modulation.

CircCRIM1 Regulates SMC Phenotypic Modulation via Sponging miR-16

As above-mentioned, RNA-FISH and cellular fractioning assay revealed that circCRIM1 was predominantly expressed in the cytoplasm of HASMCs (Figure 4.1D and 4.1G). We hypothesized that circCRIM1 might sequester miRNA to regulate gene expression. Generally, miRNA exerts function via binding with Argonaute RISC Catalytic Component 2 (Ago2) couples with RNA-induced silencing complex (RISC). CircCRIM1 was determined by RNA immunoprecipitation (RIP) assays that it bound explicitly with Ago2 but not IgG (Figure 4.3A). CircRNA pulldown assay using biotin-labeled circCRIM1 RNA probe targeting BSJ followed by RT-qPCR identified serval miRNA candidates that potentially bind with circCRIM1 (Fig 4.3B), as predicted by miRanda package[33]. Among these miRNAs, miR-16 was highly enriched by anti-circCRIM1 probe (Figure 4.3B). We then cloned the circCRIM1 full length into Myocd promoter luciferase reporter (Myocd) immediately after the luc2 gene to generate the MyocdcCRIM1 reporter vector (Figure 4.3C, upper panel). Myocd promoter luciferase reporter has been validated by our lab previously that had stable expression in mesenchymal progenitor 10T1/2 cells which could be induced to SMCs by Transforming growth factor beta (TGF-β)[22]. Luciferase assays showed that miR-16 mimic significantly decreased the luciferase activity of MyocdcCRIM1 in RVSMCs, as compared to the MyocdcCRIM1 transfected with scramble miRNA mimic (Figure 4.3C, lower panel), demonstrating that circCRIM1 physically bound miR-16. The previous study has elucidated that miR-16 was abundant in rat thoracic aorta and significant reduction of miR-16 was found both in PDGF-bb-induced rat aortic SMCs and

balloon-injured rat carotid arteries, indicating miR-16 may protect SMC from turning contractile phenotype to synthetic phenotype in response to PDGF-bb or injury[34]. We next determined the miR-16 expression pattern in PDGF-BB-treated HASMCs and balloon-injured rat carotid arteries (14 days post-injury), consistent with the previous findings (Figure 4.3 D&E). We then speculated that circCRIM1 might mediate PDGF-BB-induced SMC phenotypic modulation by sponging miR-16. To test this hypothesis, we performed a miR-16 mimic rescue assay by co-transfecting scramble or miR-16 mimics with control or circCRIM1 overexpression plasmid followed by vehicle or PDGF-BB treatment. As shown in Figure 4.3F (lower panel) and 4.3G, enforced circCRIM1 downregulated SMC markers, but miR-206 mimics rescued the inhibitory effects. These results indicated that circCRIM1 might modulate PDGF-BB-induced SMC phenotypic switching via sponging miR-16.

CircCRIM1 Encodes a Protein via Continuous Loop-translation

Besides sponging miRNAs, cytoplasmic circRNAs can also act as translation template[16]. CircRNA translation can be special since the circularized formation gives rise to a splicing junction region which may produce novel peptides or proteins. Additionally, continuous loop-translation may occur if there is no stop codon on a circRNA and the length is a multiple of three. We next used an accurate predictor-Coding-Potential Assessment Tool (CPAT) to predict the coding probability of circCRIM1. Fickett score was applied to distinguish protein-coding RNA and ncRNA based on the combinational effect of codon usage bias and nucleotide composition. At the same time, hexamer score determines the relative degree of hexamer usage bias in a particular sequence. After running CPAT by inputting the DNA sequence of circCRIM1, we predicted the combined coding probability of circCRIM1 was 99.65%

(Supplemental Figure S4.3A). Interestingly, a putative open read frame (ORF) was detected by CPAT with the start codon located at 144nt to 146nt while no stop codon was found (Supplemental Figure S4.3B). We then hypothesized that circCRIM1 might have the coding potential to encode a protein through continuous loop-translation. Polyribisome (polysome) is an essential factor for RNA translation[35]. RNA associated with many ribosomes form large polysomes that are predicted to be actively translated, while RNAs associated with few or no ribosomes are expected to be translated poorly[27]. Polysome fractioning assay was performed and found in puromycin-treated 293T cells, positive control hypoxanthine-guanine phosphoribosyltransferase (HPRT), and circCRIM1 shifted to lighter polysomes (Figure 4.4A). In contrast, negative control circPMS1, which has been proven untranslatable, showed no expression in heavy polysomes fractions (Figure 4.4A). These results suggested that circCRIM1 was associated with large polysomes and may have coding potential. We previously have constructed the circCRIM1 overexpression vector and revealed that the production of this vector was perfect in correspondence with the endogenous circCRIM1. By taking advantage of this expression vector, we inserted 1×FLAG-coding sequence immediately downstream of the start codon (c-Flag); thus, a flag tag protein could be expressed only upon the translation of c-Flag (Figure 4.4B). We then transfected control and c-Flag vectors into 293T cells, respectively, following Flag IP assay, due to Flag antibody gave rise to too much unspecific signal which buried the positive signal (Supplemental Figure S4.3C). As shown in Figure 4.4C, as compared with control lane in the blotting, two specific Flag bands were detected, which were located at the size of 35 KDa and 70 KDa, which was consistent with the size of one-loop and two-loop translational products. To further validate the amino acid sequences of these two bands, we performed the Flag-IP in Figure 4.4C again and subjected two Flag-IP elution Liquid

Chromatography-Mass Spectrometer (LC/MS). LC/MS analysis successfully detected the c-Flag protein specifically appeared in the c-Flag transfected Flag-IP sample (Figure 4.4D) (Supplemental Figure S4.3D). Moreover, a peptide specifically covered the junction site (one-loop tail and two-loop head) of this protein was detected (Figure 4.4E). Interestingly, multiple translation initiation factors (eIFs) and elongation factors (eEFs) were identified uniquely presented in c-Flag transfected Flag-IP sample (Supplemental Figure S4.3E). However, no translation termination factor (eRF) was found in this sample, indicating c-Flag may undergo continuous translation without being terminated as other linear mRNAs (Supplemental Figure S4.3E). Our results showed that circCRIM1 could perform continuous loop-translation (at least two loops) to produce a protein.

CircCRIM1 Translation is Driven by N^6-Methyladenosine (m^6A) Modification

Translatable circRNAs usually undergo m^6A driven translation or internal ribosome entry sites (IRESs) driven translation[36-38]. We suspected that the translation of circCRIM1 was driven either by m^6A modification or IRES elements. A prediction of IRES revealed no IRES element was found on circCRIM1 (Supplemental Figure S4.4A). In contrast, multiple m^6A sites were predicted on circCRIM1 (Supplemental Figure S4.4B). We then performed methylated RNA immunoprecipitation (MeRIP) and found circCRIM1 not only contained m^6A modification but also the level of m^6A was highly enriched by PDGF-BB treatment in HASMCs (Figure 4.5A). To further determine whether circCRIM1 translation was modulated by m^6A modification, we generated several m^6A substitution vectors based on the c-Flag vector by substituting A site to T site (Figure 4.5B). Based on the m^6A prediction, only m^6A sites with high confidence and upstream of the start codon within 100nt could be selected for substitution (Supplemental Figure

S4.4B). As shown in Figure 4.5C and 4.5D, single substation had limited inhibition on c-Flag translation, but combined substitution exhibited high-level suppression on c-Flag translation, especially when the first and second m^6A sites were substituted to T together. These results suggested that multiple m^6A modifications might drive circCRIM1 translation. A previous study has reported that m^6A modification-driven circRNA translation was done by recruiting an m^6A reader YTH N6-methyladenosine RNA binding protein 3 (YTHDF3), which directly interacts with translation initiation factor eIF4G2. To reveal whether YTHDF3 mediated circCRIM1 translation, we next transfected control, c-Flag and c-Flag-s-1+2 vectors into 293T cells, respectively, following pulling down circCRIM1 and Flag in all three samples. As shown in Figure 4.5E and 4.5F, overexpression circCRIM1 containing Flag tag sequence significantly increased the interaction between YTHDF3 and circCRIM1, while m^6A site 1 and 2 combo substitution alleviated this effect. The same phenomenon was observed in the Flag co-IP assay. Our results indicated that circCRIM1 translation was driven by m^6A modifications and initiated by YTHDF3.

Discussion

CircRNAs have been proven to be a promising regulator in multiple disease progressions[14, 39-41]. CircRNAs exert functions usually through acting as miRNA sponges, protein scaffolds, and templates of translation. However, little is known about the role of circRNAs in SMC phenotypic modulation. In this study, we determine circCRIM1 is highly induced in PDGF-BB-treated SMCs and neointimal hyperplasia. By conducting a series of loss- and gain- of function studies,

we demonstrate that circCRIM1 regulates SMC phenotypic modulation via binding with miR-16. Although circCRIM1 showed a relatively low level of expression in normal healthy arterial SMCs, circCRIM1 was highly increased in the neointimal SMCs in rat balloon-injured arteries, demonstrating that circCRIM1 may promote vascular remodeling by stimulating SMC phenotypic modulation. Moreover, we, for the first time, reveal that circCRIM1 can undergo continuous loop-translation driven by m^6A modification and identify a novel protein encoded by circCRIM1, which fulfills the knowledge gap of the endogenous RNA molecule can perform continuous loop-translation.

SMC phenotypic modulation is a crucial step for vascular restenosis following injury[5, 10]. Thus far, only sporadic circRNAs have been discovered to play a role in SMC phenotypic modulation, such as circANRIL[42], circACTA2[43], and circMAP3K5[44]. In our study, circCRIM1 was detected from RNA-Seq data having high expression in PDGF-BB-treated HASMCs. Our results showed that circCRIM1 regulated PDGF-BB induced SMC phenotypic modulation via physically sponging miR-16. MicroRNA has been studied for decades and revealed to be a key player in multiple biological processes, including SMC phenotypic modulation[45]. MiR-16 previously has been reported to promote the contractile phenotype of SMC by targeting YAP and inhibiting angiotensin II (Ang II) mediated VSMC proliferation[34, 46]. The miR-16 level is significantly down-regulated after PDGF-BB stimulation and vascular injury, which is consistent with our findings. However, whether the downregulation of miR-16 in PDGF-BB treated SMCs, and injured vessels are caused by elevated circCRIM1 level is still unknown. Other studies have reported ectopic expression of circRNAs impacts miRNA expression, although the general understanding believes circRNAs only reserve miRNA and prevent it from degrading its downstream target[47]. This question still needs to be further validated.

CircRNA translation is an intriguing mechanism and may not be a rare phenomenon. A recent study using mass spectrometry to screen circRNA candidates with IRES-like sequence has found that nearly 50% of these circRNAs encode proteins[48]. Thus far, a considerable number of translatable circRNAs (more than 200) have been identified, including those expressed from vectors and endogenous circRNAs[49]. For example, circZNF609, circMbl3, circβ-catenin, and circ-SHPRH are found to have IRES and encode novel proteins or peptides[36, 38, 50, 51]. Yang et al. identified 19 circRNAs with m^6A modification using search tandem mass spectrometry (MS/MS). Even though several studies have been elucidated that circRNA can be continuously translated in a rolling-cycle manner by using synthetically engineered plasmids either contain IRES elements or Kozak sequence, there is still no natural derived circRNA found has this exciting feature[37, 52]. With a combination of bioinformatic tools, our study predicted circCRIM1 might have coding potential, and following polysome fractioning analysis revealed circCRIM1 was associated with heavy ribosomes. There is only a start codon on circCRIM1, and the number of nucleotides composing the infinite open reading frame is a multiple of three. CircCRIM1 can be characterized as a circRNA that undergoes continuous loop-translation. By modifying the overexpression vector system described in Figure 4.2B, we generated a c-Flag vector that contains Flag tag sequencing right after the start codon. Expression of c-Flag vector in 293T cells generated two circCRIM1 translated products, with 35 KDa and 70 KDa. Amino acid validation of these two products by LC/MS also confirmed the continuous loop-translation of circCRIM1. Although overexpression vector can produce a mimic of endogenous circCRIM1, it is still not solid to conclude endogenous circCRIM1 can produce proteins via continuous loop-translation. In the future, we can knock-in tag sequence using CRISPR/Cas9 system, such as Flag or His, into CRIM1 genomic loci to detect if endogenous circCRIM1 can undergo the exact translation

mechanism. Besides, to detect the existence of endogenous protein derived from circCRIM1, we plan to generate a specific antibody. It is still unknown whether circCRIM1 protein has biological functions, which will be investigated in the future. Considering the continuous loop-translation, If the product has no or limited biological function, it may lead to the aggregation of proteins which may cause protein misfolding and eventually generating pathogenic condition intracellular.

As above-mentioned, m^6A modification can modulate circRNA translation. By applying m^6A substitution c-Flag expression vectors and bi-directional pulldown assays, we further determined that circCRIM1 translation was driven by m^6A modifications upstream of the start codon through recognition by YTHDF3, which recruited translational initiation factors to circCRIM1. The efficiency of m^6A driven circRNA translation can be affected by the m^6A level on circRNA[37, 38, 48]. In our results, modulating single, double, and triple m^6A sites on circCRIM1 could reduce but not eliminate the efficiency of continuous loop-translation of circCRIM1, indicating that other m^6A sites may still essential for this translation, or there are translation mechanisms we do not know compensates the translation. Moreover, because m^6A-driven circRNA translation has been validated relatively weak compared with IRES-driven circRNA translation and canonical translation, it is reasonable for us only detected two-loop translational products (35KDa and 70KDa)[48].

In conclusion, this study revealed a novel mechanism underlying SMC phenotypic modulation, injury-induced neointima formation, and continuous loop-translation. Therefore, targeting circCRIM1 may be a promising strategy to hinder injury-induced vascular remodeling in proliferative vascular diseases, and circCRIM1 can be a qualified model for future studies about circRNA translation.

Reference

1. Mittal, R. *et al.* Recent treatment modalities for cardiovascular diseases with a focus on stem cells, aptamers, exosomes and nanomedicine. *Artif Cells Nanomed Biotechnol* **46**, 831-840 (2018).

2. Al-Lamee, R.K. *et al.* Dobutamine Stress Echocardiography Ischemia as a Predictor of the Placebo-Controlled Efficacy of Percutaneous Coronary Intervention in Stable Coronary Artery Disease: The Stress Echocardiography-Stratified Analysis of ORBITA. *Circulation* **140**, 1971-1980 (2019).

3. Yang, F. *et al.* miR-22 Is a Novel Mediator of Vascular Smooth Muscle Cell Phenotypic Modulation and Neointima Formation. *Circulation* **137**, 1824-1841 (2018).

4. Owens, G.K., Kumar, M.S. & Wamhoff, B.R. Molecular regulation of vascular smooth muscle cell differentiation in development and disease. *Physiol Rev* **84**, 767-801 (2004).

5. Shi, N. & Chen, S.Y. Smooth Muscle Cell Differentiation: Model Systems, Regulatory Mechanisms, and Vascular Diseases. *J Cell Physiol* **231**, 777-787 (2016).

6. Gabbiani, G. *et al.* Vascular smooth muscle cells differ from other smooth muscle cells: predominance of vimentin filaments and a specific alpha-type actin. *Proc Natl Acad Sci U S A* **78**, 298-302 (1981).

7. Madsen, C.S. *et al.* Smooth muscle-specific expression of the smooth muscle myosin heavy chain gene in transgenic mice requires 5'-flanking and first intronic DNA sequence. *Circ Res* **82**, 908-917 (1998).

8. Duband, J.L., Gimona, M., Scatena, M., Sartore, S. & Small, J.V. Calponin and SM 22 as differentiation markers of smooth muscle: spatiotemporal distribution during avian embryonic development. *Differentiation* **55**, 1-11 (1993).

9. van der Loop, F.T., Schaart, G., Timmer, E.D., Ramaekers, F.C. & van Eys, G.J. Smoothelin, a novel cytoskeletal protein specific for smooth muscle cells. *J Cell Biol* **134**, 401-411 (1996).

10. Gomez, D. & Owens, G.K. Smooth muscle cell phenotypic switching in atherosclerosis. *Cardiovasc Res* **95**, 156-164 (2012).

11. Shi, N., Mei, X. & Chen, S.Y. Smooth Muscle Cells in Vascular Remodeling. *Arterioscler Thromb Vasc Biol* **39**, e247-e252 (2019).

12. Tang, R. *et al.* LncRNA GAS5 regulates vascular smooth muscle cell cycle arrest and apoptosis via p53 pathway. *Biochim Biophys Acta Mol Basis Dis* **1865**, 2516-2525 (2019).

13. Tang, R. *et al.* LncRNA GAS5 attenuates fibroblast activation through inhibiting Smad3 signaling. *Am J Physiol Cell Physiol* **319**, C105-C115 (2020).

14. Chen, L.L. The expanding regulatory mechanisms and cellular functions of circular RNAs. *Nat Rev Mol Cell Biol* **21**, 475-490 (2020).

15. Jeck, W.R. & Sharpless, N.E. Detecting and characterizing circular RNAs. *Nat Biotechnol* **32**, 453-461 (2014).

16. Li, X., Yang, L. & Chen, L.L. The Biogenesis, Functions, and Challenges of Circular RNAs. *Mol Cell* **71**, 428-442 (2018).

17. Ji, P. *et al.* Expanded Expression Landscape and Prioritization of Circular RNAs in Mammals. *Cell Rep* **26**, 3444-3460 e3445 (2019).

18. Zhang, Y., Yang, L. & Chen, L.L. Characterization of Circular RNAs. *Methods Mol Biol* **1402**, 215-227 (2016).

19. Daugherty, A. *et al.* Response by Daugherty et al to Letter Regarding Article, "Consideration of Sex Differences in Design and Reporting of Experimental Arterial Pathology Studies: A Statement From the Arteriosclerosis, Thrombosis, and Vascular Biology Council". *Arterioscler Thromb Vasc Biol* **38**, e101-e102 (2018).

20. Luo, J. *et al.* A protocol for rapid generation of recombinant adenoviruses using the AdEasy system. *Nat Protoc* **2**, 1236-1247 (2007).

21. Liang, D. & Wilusz, J.E. Short intronic repeat sequences facilitate circular RNA production. *Genes Dev* **28**, 2233-2247 (2014).

22. Xie, W.B., Li, Z., Miano, J.M., Long, X. & Chen, S.Y. Smad3-mediated myocardin silencing: a novel mechanism governing the initiation of smooth muscle differentiation. *J Biol Chem* **286**, 15050-15057 (2011).

23. Tang, R., Zhang, G., Wang, Y.C., Mei, X. & Chen, S.Y. The long non-coding RNA GAS5 regulates transforming growth factor beta (TGF-beta)-induced smooth muscle cell differentiation via RNA Smad-binding elements. *J Biol Chem* **292**, 14270-14278 (2017).

24. Engreitz, J.M. *et al.* RNA-RNA interactions enable specific targeting of noncoding RNAs to nascent Pre-mRNAs and chromatin sites. *Cell* **159**, 188-199 (2014).

25. Engreitz, J.M. *et al.* The Xist lncRNA exploits three-dimensional genome architecture to spread across the X chromosome. *Science* **341**, 1237973 (2013).

26. Azzam, M.E. & Algranati, I.D. Mechanism of puromycin action: fate of ribosomes after release of nascent protein chains from polysomes. *Proc Natl Acad Sci U S A* **70**, 3866-3869 (1973).

27. Panda, A.C., Martindale, J.L. & Gorospe, M. Polysome Fractionation to Analyze mRNA Distribution Profiles. *Bio Protoc* **7** (2017).

28. Schwartz, S.M., deBlois, D. & O'Brien, E.R. The intima. Soil for atherosclerosis and restenosis. *Circ Res* **77**, 445-465 (1995).

29. Suzuki, H. *et al.* Characterization of RNase R-digested cellular RNA source that consists of lariat and circular RNAs from pre-mRNA splicing. *Nucleic Acids Res* **34**, e63 (2006).

30. Werfel, S. *et al.* Characterization of circular RNAs in human, mouse and rat hearts. *J Mol Cell Cardiol* **98**, 103-107 (2016).

31. Rybak-Wolf, A. *et al.* Circular RNAs in the Mammalian Brain Are Highly Abundant, Conserved, and Dynamically Expressed. *Mol Cell* **58**, 870-885 (2015).

32. Glazar, P., Papavasileiou, P. & Rajewsky, N. circBase: a database for circular RNAs. *RNA* **20**, 1666-1670 (2014).

33. Enright, A.J. *et al.* MicroRNA targets in Drosophila. *Genome Biol* **5**, R1 (2003).

34. Xu, F. *et al.* MicroRNA-15b/16 Attenuates Vascular Neointima Formation by Promoting the Contractile Phenotype of Vascular Smooth Muscle Through Targeting YAP. *Arterioscler Thromb Vasc Biol* **35**, 2145-2152 (2015).

35. Zuccotti, P. & Modelska, A. Studying the Translatome with Polysome Profiling. *Methods Mol Biol* **1358**, 59-69 (2016).

36. Legnini, I. *et al.* Circ-ZNF609 Is a Circular RNA that Can Be Translated and Functions in Myogenesis. *Mol Cell* **66**, 22-37 e29 (2017).

37. Yang, Y. *et al.* Extensive translation of circular RNAs driven by N(6)-methyladenosine. *Cell Res* **27**, 626-641 (2017).

38. Pamudurti, N.R. *et al.* Translation of CircRNAs. *Mol Cell* **66**, 9-21 e27 (2017).

39. Aufiero, S., Reckman, Y.J., Pinto, Y.M. & Creemers, E.E. Circular RNAs open a new chapter in cardiovascular biology. *Nat Rev Cardiol* **16**, 503-514 (2019).

40. Lei, M., Zheng, G., Ning, Q., Zheng, J. & Dong, D. Translation and functional roles of circular RNAs in human cancer. *Mol Cancer* **19**, 30 (2020).

41. Akhter, R. Circular RNA and Alzheimer's Disease. *Adv Exp Med Biol* **1087**, 239-243 (2018).

42. Shi, P. *et al.* circANRIL reduces vascular endothelial injury, oxidative stress and inflammation in rats with coronary atherosclerosis. *Exp Ther Med* **20**, 2245-2251 (2020).

43. Sun, Y. *et al.* A Novel Regulatory Mechanism of Smooth Muscle alpha-Actin Expression by NRG-1/circACTA2/miR-548f-5p Axis. *Circ Res* **121**, 628-635 (2017).

44. Zeng, Z. *et al.* Circular RNA CircMAP3K5 Acts as a MicroRNA-22-3p Sponge to Promote Resolution of Intimal Hyperplasia Via TET2-Mediated Smooth Muscle Cell Differentiation. *Circulation* **143**, 354-371 (2021).

45. Samanta, S. *et al.* MicroRNA: A new therapeutic strategy for cardiovascular diseases. *Trends Cardiovasc Med* **26**, 407-419 (2016).

46. Gu, Q., Zhao, G., Wang, Y., Xu, B. & Yue, J. Silencing miR-16 Expression Promotes Angiotensin II Stimulated Vascular Smooth Muscle Cell Growth. *Cell Dev Biol* **6** (2017).

47. Gasparini, S., Licursi, V., Presutti, C. & Mannironi, C. The Secret Garden of Neuronal circRNAs. *Cells* **9** (2020).

48. Xiaojuan Fan, Y.Y., Chuyun Chen, Zefeng Wang Pervasive translation of circular RNAs driven by short IRES-like elements. *bioRxiv* (2020).

49. Li, H. *et al.* riboCIRC: a comprehensive database of translatable circRNAs. *Genome Biol* **22**, 79 (2021).

50. Zhang, M. *et al.* A novel protein encoded by the circular form of the SHPRH gene suppresses glioma tumorigenesis. *Oncogene* **37**, 1805-1814 (2018).

51. Liang, W.C. *et al.* Translation of the circular RNA circbeta-catenin promotes liver cancer cell growth through activation of the Wnt pathway. *Genome Biol* **20**, 84 (2019).

52. Abe, N. *et al.* Rolling Circle Translation of Circular RNA in Living Human Cells. *Sci Rep* **5**, 16435 (2015).

Figure Legends

Figure 4.1. CircCRIM1 expression pattern in vascular smooth muscle cells (SMCs). **A**, Spliced reads per billion mapped reads (SRPBM) of circCRIM1 from RNAseq data was upregulated by PDGF-BB (20 ng/mL). *P<0.05 vs Vehicle group, n=5. **B**, Diagram of circCRIM1 formation. CircCRIM1 was derived from CRIM1 pre-mRNA via back-splicing. The region of back-splicing junction is shown. **C**, Divergent primers only amplified circCRIM1 in cDNA, but not the genomic DNA (gDNA) (upper panel). Sanger sequencing confirmed the head-to-tail junction (lower panel). The red solid line shows the back-splicing junction site. **D,** Cyclophilin (CYP) and CRIM1 linear RNAs, but not circCRIM1, were digested by RNase R, as detected by RT-qPCR. *P<0.05 vs Mock group, n=3; N.S. non-significant. **E,** CircCRIM1 was mainly located in cytoplasm of human aortic smooth muscle cells (HASMCs). Cytoplasmic and nuclear RNAs of HASMCs were isolated, and CircCRIM1 was assessed by RT-qPCR. *P<0.05 vs cytoplasmic portion, n=3. **F,** CircCRIM1 was time-dependently induced by PDGF-BB (20 ng/mL) as assessed by RT-qPCR. *P<0.05 vs vehicle group (0 h), n=3. **G**, In situ hybridization for circCRIM1 in vehicle- or PDGF-BB-treated HASMCs. circCRIM1 was detected by biotin-labeled anti-circCRIM1 probe (green). Nuclei stained by DAPI (blue). Random probe served as negative control (NC). Bar: 10 μm. **H**, CircCRIM1 was induced in injured rat carotid arteries. The control or injured arteries (for 14 days) were stained for circCRIM1 by RNA-FISH. M: media; L: lumen; Bar: 100 μm. **I**, CircCRIM1 were time-dependently induced by balloon injury. CircCRIM1 levels in injured rat carotid arteries were detected by RT-qPCR. *P<0.05 vs uninjured (Ctrl) rat carotid arteries (n=5).

Figure 4.2. CircCRIM1 regulates phenotypic modulation of HASMCs. A, Schematic representation of the knockdown strategy used for circCRIM1 knockdown (left

panel).CircCRIM1 expression level was knocked down by shRNA in HASMCs (right panel). HASMCs were treated with adenoviral scramble shRNA (shScramble) and circCRIM1 knockdown adenovirus (shcircCRIM1), and expression of circCRIM1 in each group was measured by RT-qPCR. *P<0.05 vs shScramble group, n=3. **B**, Schematic representation of the overexpression strategy used for circCRIM1 overexpression, intronic complementary sequence (ICS) was shown as arrow (left panel). CircCRIM1 expression level was overexpressed by circCRIM1 overexpression vector (circCRIM1) in HASMCs (right panel). HASMCs were transfected with circRNA control vector (circCtrl) and circCRIM1 overexpression vector, and expression of circCRIM1 in each group was measured by RT-qPCR. *P<0.05 vs circCtrl group, n=3. **C**, Knockdown of circCRIM1 reversed PDGF-BB induced downregulation of SMC marker genes. **D**, Quantification of SMC marker genes protein level shown in C by normalizing to GAPDH. *P<0.05 vs scramble shRNA (shScramble)-transduced cells; #P<0.05 vs shScramble-transduced cells with PDGF-BB (n=3); NS: Non-siginificant. **E**, Forced expression of circCRIM1 further suppressed PDGF-BB induced downregulation of SMC marker genes. **F,** Quantification of SMC marker genes protein level shown in E by normalizing to GAPDH. *P<0.05 vs circCtrl-transfected cells; #P<0.05 vs circCtrl-transfected cells with PDGF-BB (n=3); NS: Non-siginificant.

Figure 4.3. CircCRIM1 regulates SMC phenotypic modulation via sponging miRNA-16. A, HASMCs was immunoprecipitated (IP) using Ago2 or IgG antibody. circCRIM1 was detected by RT-qPCR, *P<0.05 vs IgG IP group (n = 3). **B**, CircCRIM1-interacting molecules were pulled down by biotin-labelled anti-circCRIM1 probe. Potential circCRIM1-binding microRNAs (miRNA) were screened by RT-qPCR. *P<0.05 vs control (Ctrl) probe pull-down group (n=3). **C**, Schematic representation of the circCRIM1 luciferase vector (MyocdcCRIM1) was shown

(upper panel).CircCRIM1 sponging miRNA-16 as shown by luciferase assay. Rat vascular SMCs (RVSMCs) were co-transfected control luciferase vector (Myocd) or MyocdcCRIM1 (containing circCRIM1 sequence after luc2 gene) with negative control (miR-NC) or miR-16 mimics. Luciferase activity was detected 48 h after the transfection, *P < 0.05 vs cells transfected with MyocdcCRIM1 with miR-NC (n=3). **D**, The expression level of miR-16 was downregulated by PDGF-BB treatment. HASMCs were treated with PDGF-BB (20ng/ml) for 48 hours, and miR-16 was assessed by RT-qPCR. *P < 0.05 vs vehicle group (0 h), n=3. **E**, The expression level of miR-16 was downregulated in rat carotid artery balloon injury (14 days after injury). The expression level of miR-16 in healthy (Ctrl) or injured arterial vessels (Injury) were measured by RT-qPCR. *P < 0.05 vs Ctrl (n=5). **F**, CircCRIM1 mediated SMC phenotypic modulation via inhibiting miRNA-16 activity. Upper panel: putative miR-16 binding sites on the circCRIM1. Lower panel: control circRNA (circCtrl) or circCRIM1 overexpression vector were co-transfected into HASMCs with miR-NC or miR-16 Mimics followed by vehicle or PDGF-BB treatment for 48 hours. CNN1 and SM22α protein levels were detected by Western blot. **G**, Quantification of CNN1 and SM22α levels shown in F by normalizing to GAPDH. *P<0.05 vs circCRIM1-transfected cells with miR-NC; #P<0.05 vs circCRIM1-transfected cells with miR-NC with PDGF-BB treatment (n=3).

Figure 4.4. CircCRIM1 loop-translates protein. A, CircCRIM1 associated with polysomes and had coding ability. Polysome gradient profiles of 293T cytoplasmic extracts after treatment with native (light blue) or puromycin (light orange) were shown as the chart background, analyzed by absorbance of 253nm of each fraction. The fraction number from top/light to bottom/heavy was indicated as 1 to 22. Ribosomal RNA 80s peak was labeled. The relative distribution of the % mRNA of HPRT, circPMS1, and circCRIM1 in native group (solid blue)

and puromycin group (solid orange) over the sucrose gradient were presented and studied by RT-qPCR of the RNA in each of the 22 fractions. Calculation of percentage recovered RNA was followed by ΔCT method. Data are representative of three independent experiments. The arrow indicated the shift peaks of HPRT and circCRIM1. **B**, Schematic representation of the circCRIM1-Flag vector (c-Flag) construction. Start codon of circCRIM1 was indicated by red rounded rectangle, Flag-tag was indicated by green rounded rectangle, and intronic complementary sequence (ICS) was shown as arrow. Arrow with dashed line indicated translation direction. **C**, CircCRIM1 translated a protein. Control vector and c-Flag vector were transfected into 293T cells for 48 hours, and cells were harvested and processed to Flag co-immunoprecipitation (co-IP). CircCRIM1 translated protein was detected by anti-Flag antibody. GAPDH was served as internal control. Black arrows indicated the circCRIM1 translated protein. **D**, Flag co-IP Samples in C were sent for liquid chromatography-mass spectrometry (LCMS). CricCRIM1 protein sequence coverage by LCMS in Flag sample was shown. The blue lines represented identified peptides. **E**, The peptide (TCSNPFEFPSQDMDYKDDDDK) covered the head-to-tail junction was shown, supporting at least two loops of translation of circCRIM1 occurred.

Figure 4.5. CircCRIM1 translation is driven by N^6-Methyladenosine (m^6A) modification. A, CircCRIM1 contained m^6A modification and the m^6A level was induced by PDGF-BB treatment. HASMCs were treated with vehicle and PDGF-BB (20ng/ml) for 48 hours and RNA were processed to methylated RNA immunoprecipitation (MeRIP), following RT-qPCR detection of circCRIM1 expression level. Data was presented as expression of methylated circCRIM1 / expression of total circCRIM1 in input. *$P < 0.05$ vs vehicle (n=3). **B**, Schematic representation of the different modified circCRIM1-Flag vector (c-Flag) construct (A to T

substitution). Start codon of circCRIM1 was indicated by red rounded rectangle, Flag-tag was indicated by green rounded rectangle, intronic complementary sequence (ICS) was shown as arrow, and m^6A modification was shown as a brown dot attached with line. **C**, CircCRIM1 translation was driven by multiple m^6A modifications. Control vector and c-Flag vector were transfected into 293T cells for 48 hours, and cells were harvested and processed to Flag co-immunoprecipitation (co-IP). CircCRIM1 translated protein was detected by anti-Flag antibody. GAPDH was served as internal control. Black arrows indicated the circCRIM1 translated protein. **D**, Quantification of Flag levels at 35 KDa and 70 KDa shown in C by normalizing to GAPDH. **E**, CircCRIM1 translation was initiated by YTHDF3. Control vector, c-flag and c-Flag-s-2 were transfected respectively into 293T cells for 48 hours, and cells were harvested and processed to RNA-pulldown assay by using anti-circCRIM1 probe and Flag co-immunoprecipitation (co-IP). YTHDF3 protein was detected by anti-YTHDF3 antibody. GAPDH was served as internal control. **F**, Quantification of YTHDF3 level were shown in D by normalizing to YTHDF3 level in input and then to GAPDH. *P<0.05 vs Ctrl; #P<0.05 vs c-Flag-transfected cells (n=3).

Supplemental Figure S4.1: Conservation of circCRIM1 in humans, mice and rats. **A**, alignment of circCRIM1 in humans, mice and rats was performed by using ClustalW 2.1. **B**, Percentage of pairwise identity and identical sites in A was calculated by ClustalW 2.1. **C**, distances of each circCRIM1 sequence in A were calculated by Geneious prime.

Supplemental Figure S4.2: Knockdown and overexpression of circCRIM1 did not affect CRIM1 level. **A**, CircCRIM1 expression level was knocked down by two siRNAs in a dose-dependent manner in HASMCs. 100 nM siRNA1 showed a better knockdown efficiency. CircCRIM1 expression was quantified by RT-qPCR. The expression was normalized to

cyclophilin. *p < 0.05 vs non-target siRNA treated cells (n = 3). **B**, circCRIM1 knockdown and overexpression did not impact CRIM1 protein expression. **C**, Quantification of CRIM1 protein expression in B by normalizing to α-Tubulin levels. NS: Non-significant.

Supplemental Figure S4.3: CircCRIM1 encodes a protein via continuous loop-translation. **A**, Coding potential of circCRIM1 was predicted by CPAT (Coding-Potential Assessment Tool). **B**, DNA sequence of circCRIM1 and schematic representation of the continuous loop-translation. Start codon of circCRIM1 was indicated by red rounded rectangle. The direction of translation was indicated by dashed-line with arrow. **C**, Western Blot of Flag tag using whole cell lysate from control and c-Flag vector-transfected 293T cells. **D**, Sequence of "TCSNPFEFPSQDMDYKDDDDK" mass spectrometry spectrum and ion table. The blue and red values represent ions that were identified. **E,** Translation factors uniquely identified in c-Flag Flag-IP elution sample using LC/MS**.**

Supplemental Figure S4.4: CircCRIM1 encodes protein via N^6-Methyladenosine (m^6A) modification, but not IRES element. **A**, circCRIM1 did not contain IRES element. The probably of IRES was calculated by IRESpy. **B**, CricCRIM1 might contain multiple m^6A sites. The prediction was proceeded by SRAMP (sequence-based RNA adenosine methylation site predictor).

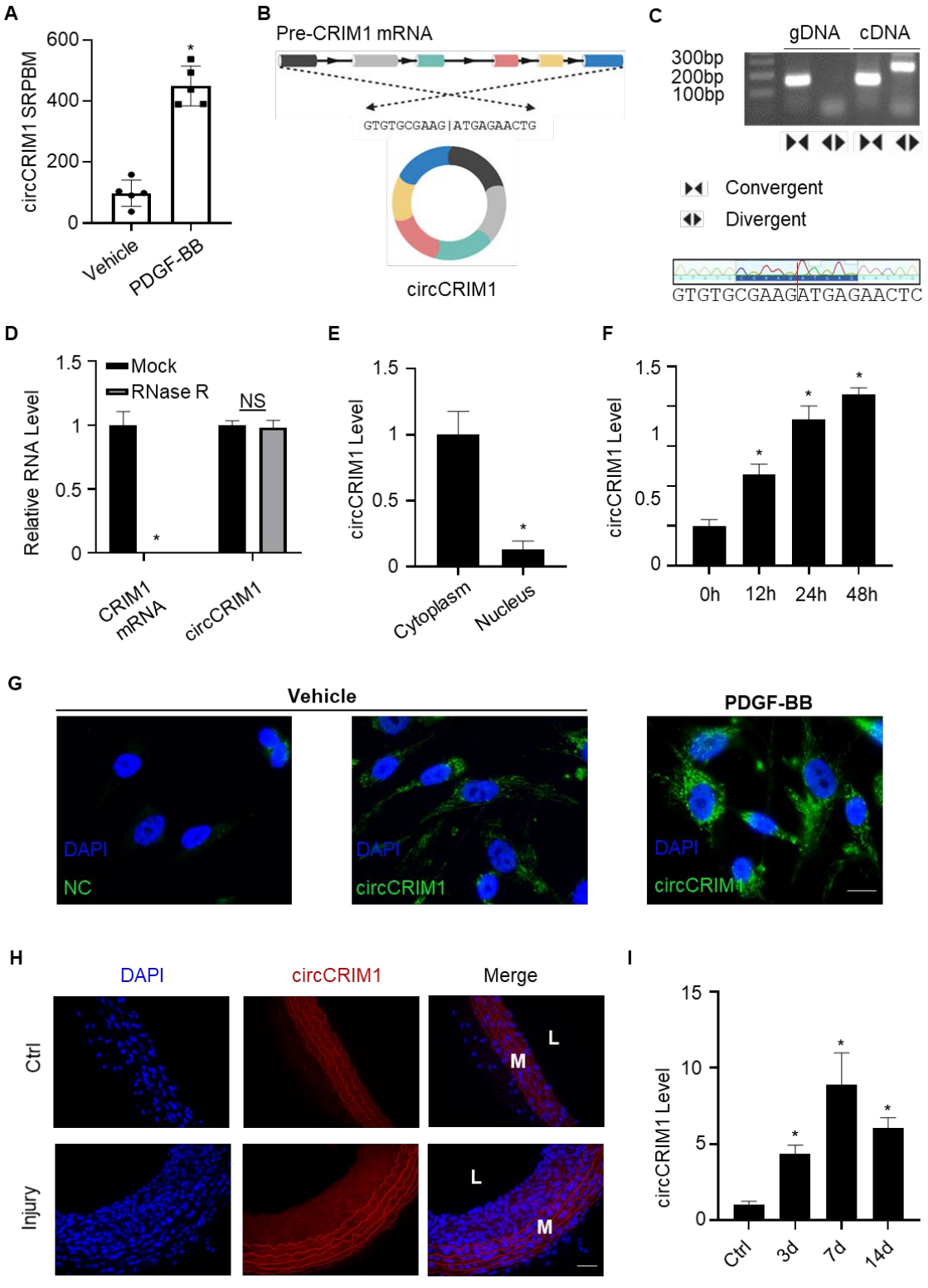

Figure 4.1. CircCRIM1 expression pattern in vascular smooth muscle cells (SMCs).

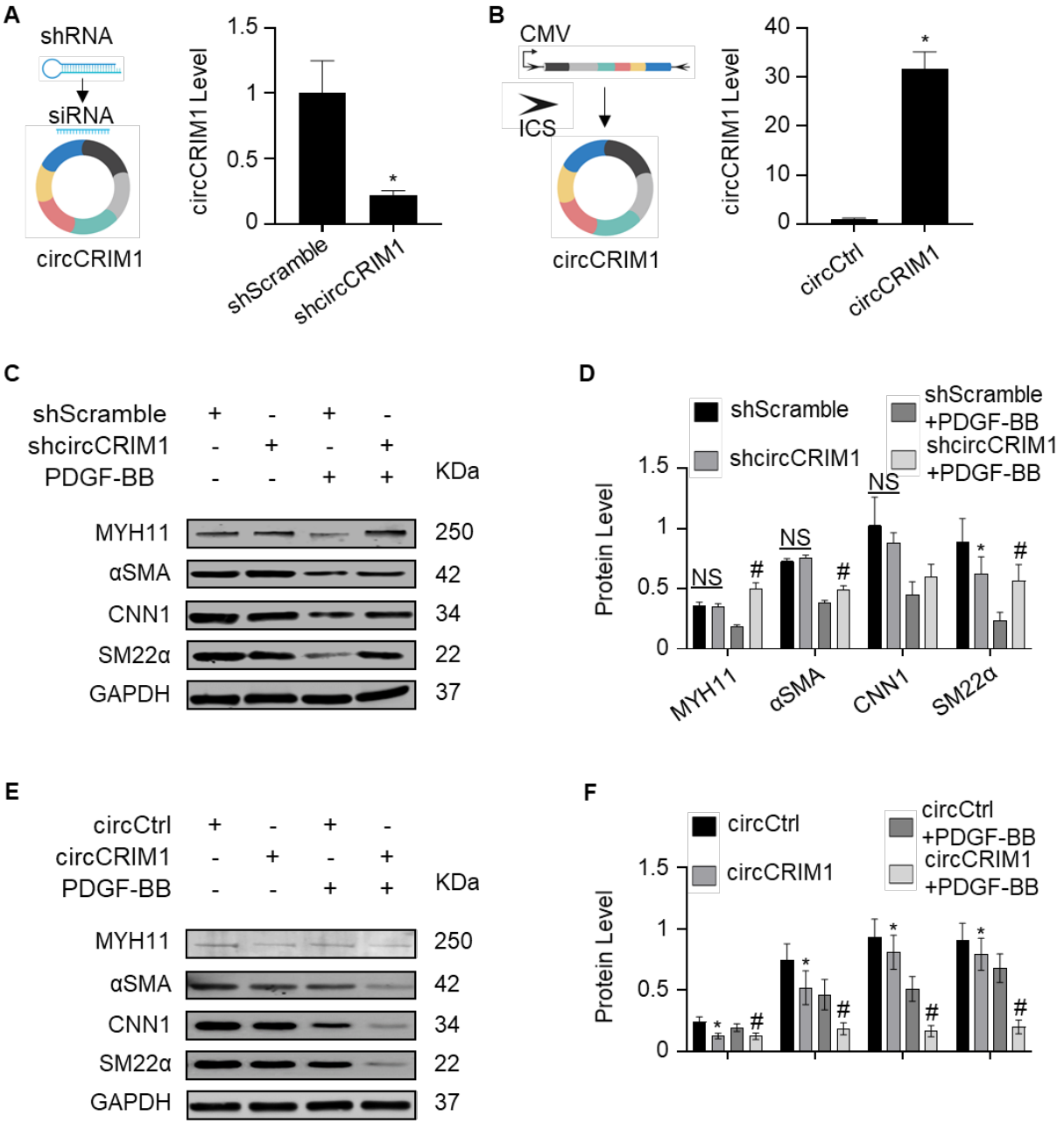

Figure 4.2. CircCRIM1 regulates phenotypic modulation of HASMCs.

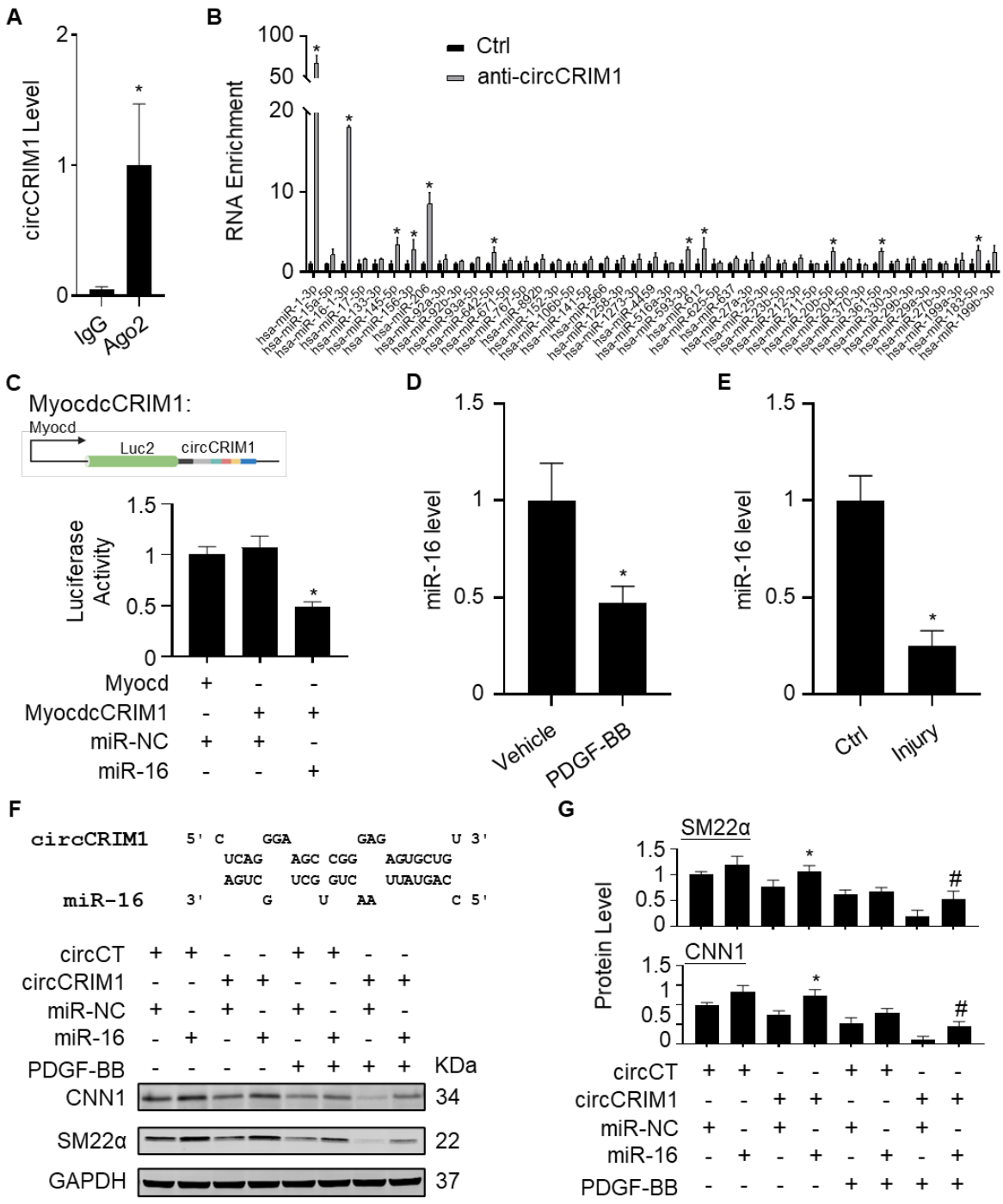

Figure 4.3. CircCRIM1 regulates SMC phenotypic modulation via sponging miRNA-16.

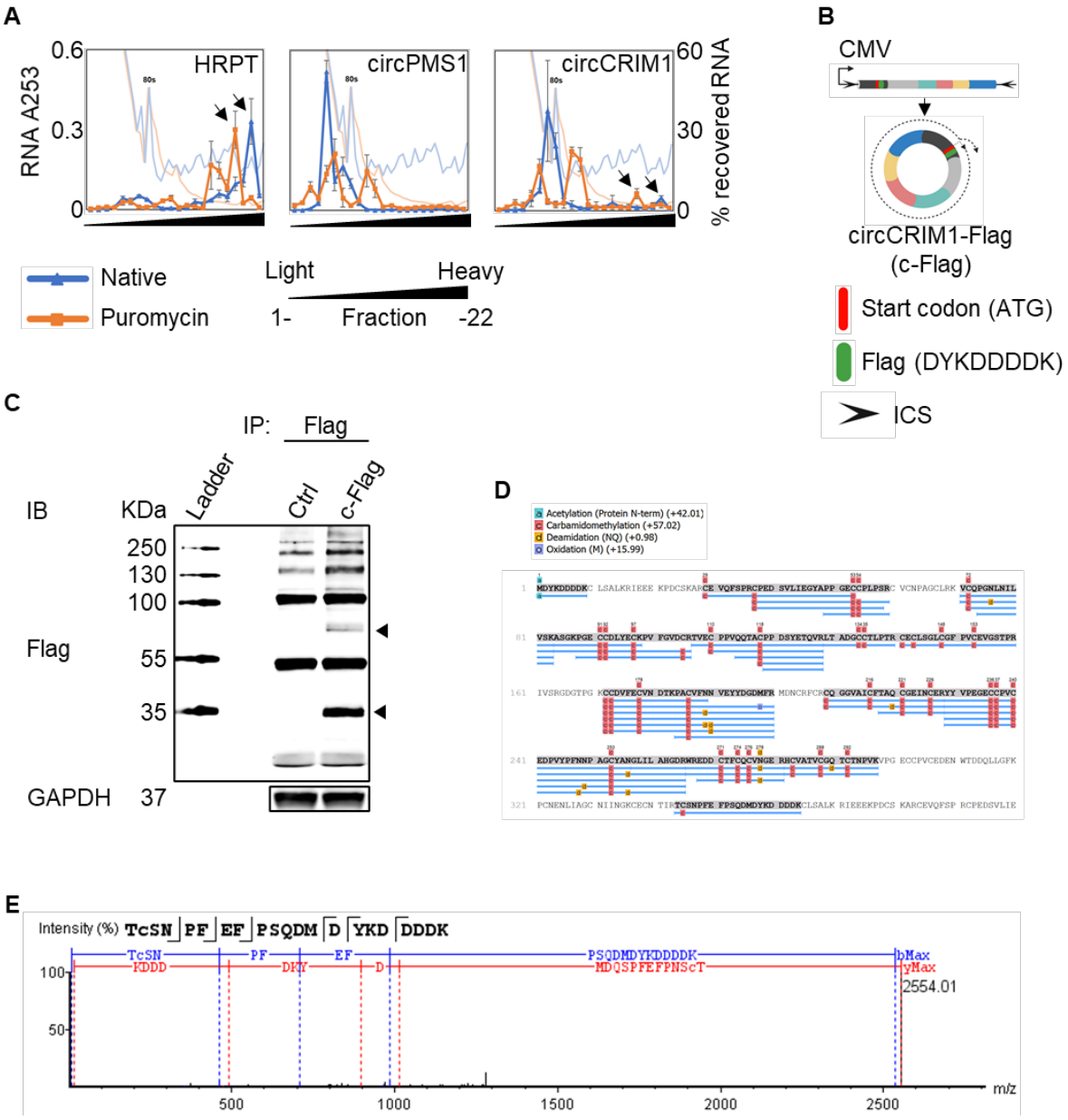

Figure 4.4. CircCRIM1 loop-translates protein.

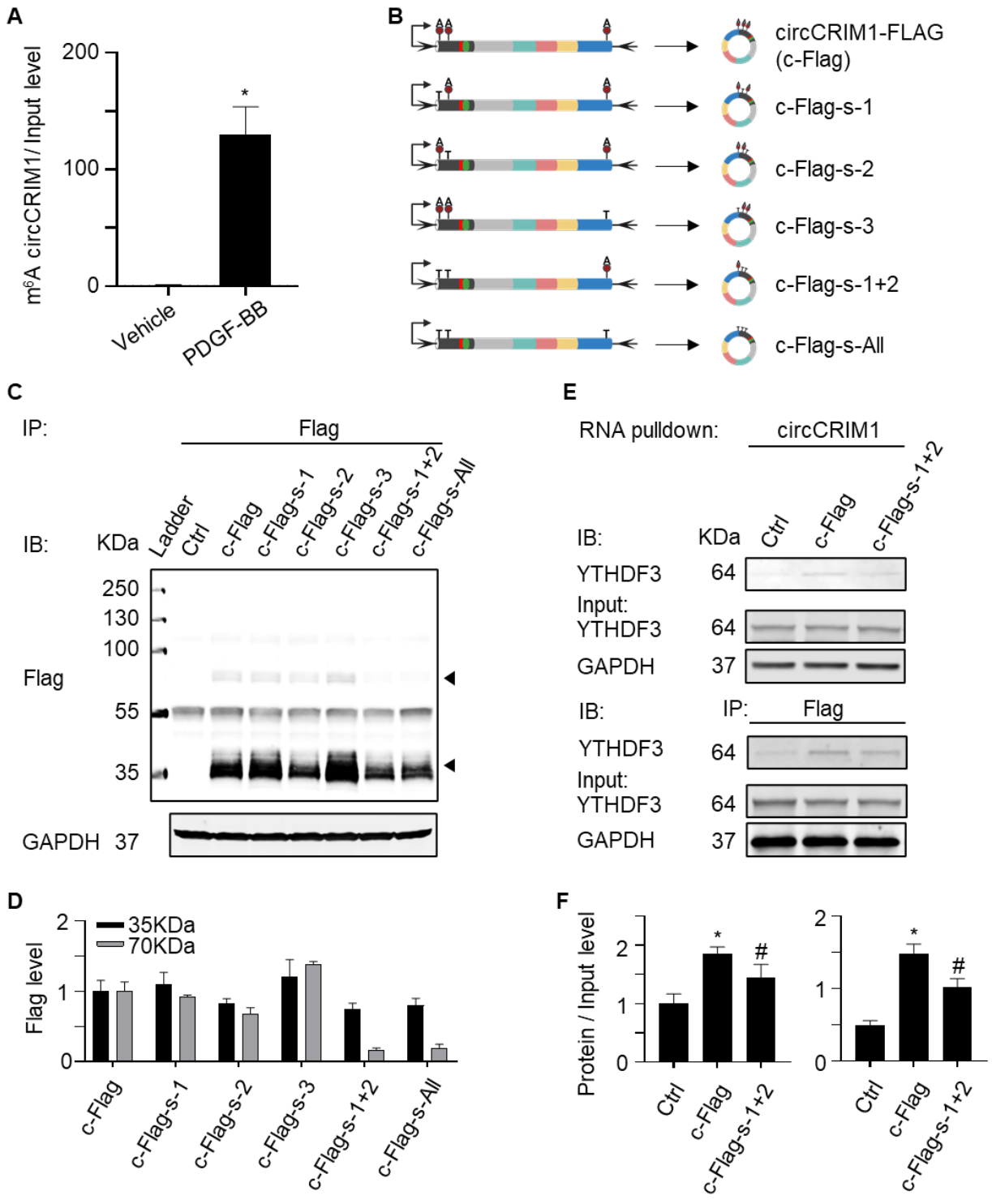

Figure 4.5. CircCRIM1 translation is driven by N^6-Methyladenosine (m^6A) modification.

A

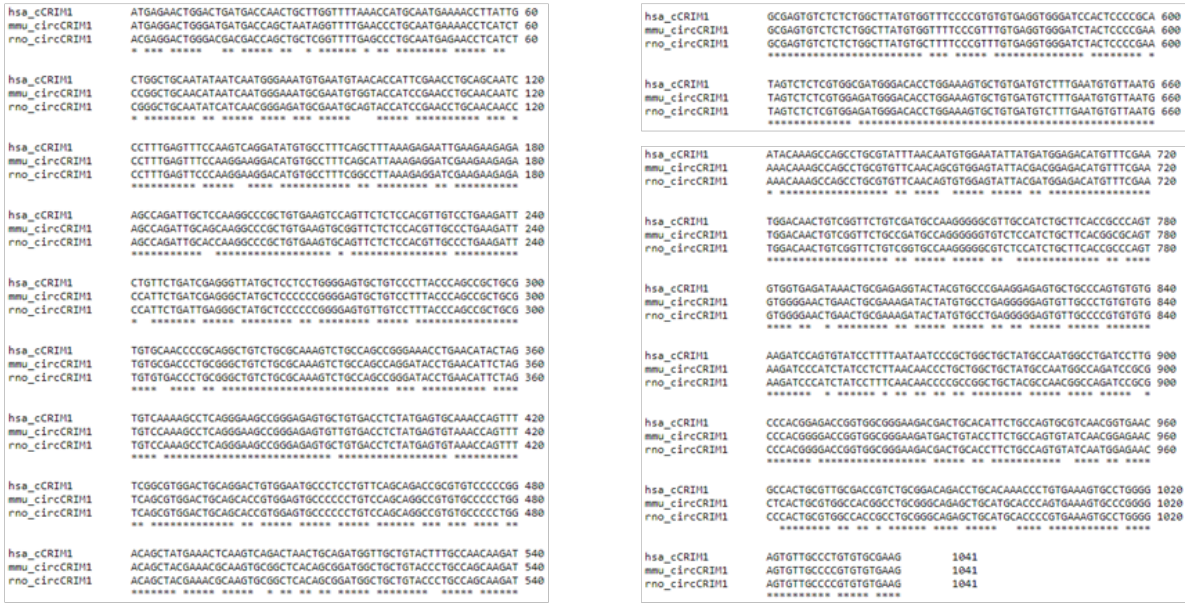

B

% Pairwise Identity	% Identical sites
90.0	85.2

C

%	rno_circCRIM1	mmu_circCRIM1	hsa_cCRIM1
rno_circCRIM1		95.293	87.32
mmu_circCRIM1	95.293		87.32
hsa_cCRIM1	87.32	87.32	

Supplementary Figure S4.1. Conservation of circCRIM1 in humans, mice and rats.

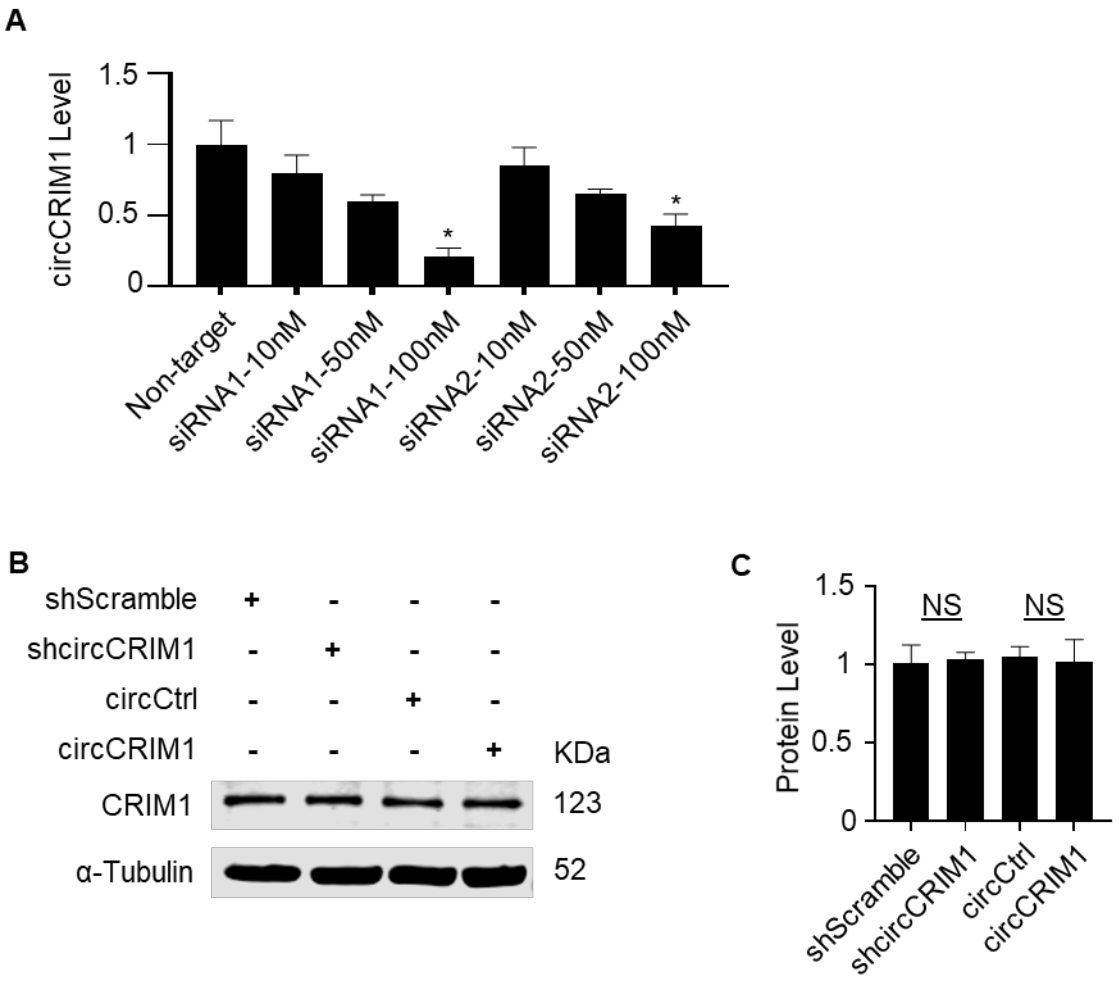

Supplementary Figure S4.2. Knockdown and overexpression of circCRIM1 did not affect CRIM1 level.

A

Sequence Name	RNA size	ORF size	Ficket Score	Hexamer Score	Coding Probability
circCRIM1	1041	897	0.9375	0.178858766	0.996544981

B

C

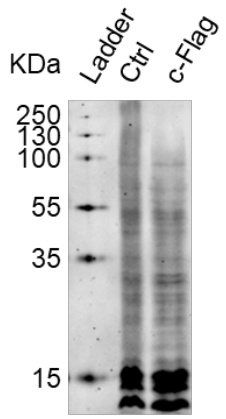

D

#	Immonium	b	b-H2O	b-NH3	b (2+)	Seq	y	y-H2O	y-NH3	y (2+)	#
1	74.06	102.06	84.04	85.03	51.53	T					21
2	133.04	262.09	244.08	245.06	131.54	C(+57.02)	2452.95	2434.94	2435.93	1226.98	20
3	60.04	349.12	331.11	332.09	175.06	S	2292.92	2274.91	2275.90	1146.96	19
4	87.06	463.16	445.15	446.13	232.08	N	2205.89	2187.88	2188.86	1103.45	18
5	70.07	560.21	542.20	543.19	280.61	P	2091.85	2073.84	2074.82	1046.42	17
6	120.08	707.27	689.27	690.26	354.13	F	1994.80	1976.79	1977.77	997.90	16
7	102.06	836.32	818.31	819.30	418.66	E	1847.73	1829.72	1830.70	924.36	15
8	120.08	983.39	965.38	966.39	492.19	F	1718.68	1700.67	1701.66	859.84	14
9	70.07	1080.45	1062.44	1063.42	540.72	P	1571.62	1553.61	1554.59	786.31	13
10	60.04	1167.48	1149.47	1150.45	584.24	S	1474.56	1456.55	1457.54	737.78	12
11	101.07	1295.54	1277.53	1278.51	648.27	Q	1387.53	1369.52	1370.50	694.27	11
12	88.04	1410.56	1392.55	1393.54	705.78	D	1259.47	1241.46	1242.45	630.24	10
13	104.05	1541.60	1523.59	1524.58	771.30	M	1144.45	1126.44	1127.42	572.72	9
14	88.04	1656.63	1638.62	1639.60	828.82	D	1013.41	995.40	996.38	507.20	8
15	136.08	1819.69	1801.68	1802.67	910.35	Y	898.39	880.37	881.35	449.69	7
16	101.11	1947.79	1929.78	1930.76	974.39	K	735.32	717.30	718.29	368.16	6
17	88.04	2062.82	2044.81	2045.79	1031.91	D	607.22	589.21	590.19	304.11	5
18	88.04	2177.84	2159.83	2160.82	1089.42	D	492.19	474.12	475.17	246.60	4
19	88.04	2292.87	2274.86	2275.84	1146.94	D	377.17	359.16	360.14	189.08	3
20	88.04	2407.90	2389.89	2390.87	1204.45	D	262.14	244.13	245.11	131.57	2
21	101.11					K	147.11	129.10	130.09	74.06	1

E

Phase:	**Initiation**			**Elongation**	**Termination**
Factors:	**eIFs**			**eEFs**	**eRFs**
	eIF1	eIF3A	eIF4A1	eEF1A1	None
	eIF172	eIF3B	eIF4A3	eEF1A2	
	eIF1AX	eIF3C	eIF4E	eEF1B	
	eIF2A	eIF3D	eIF4E2	eEF1D	
	eIF2A	eIF3E	eIF4G1	eEF1G	
	eIF2B	eIF3F	eIF4G2	eEF2	
	eIF2B1	eIF3G	eIF4G3		
	eIF2B2	eIF3H	eIF4H		
	eIF2B3	eIF3J	eIF6		
	eIF2G	eIF3K	eIFCL		
	eIF2P	eIF3L	eIFS		
	eIF31	eIF3M	eIFSA1		

Supplementary Figure S4.3. CircCRIM1 encodes a protein via continuous loop-translation.

A

Name	IRES probably	Result
circCRIM1	0.079695046	potential not IRES

B

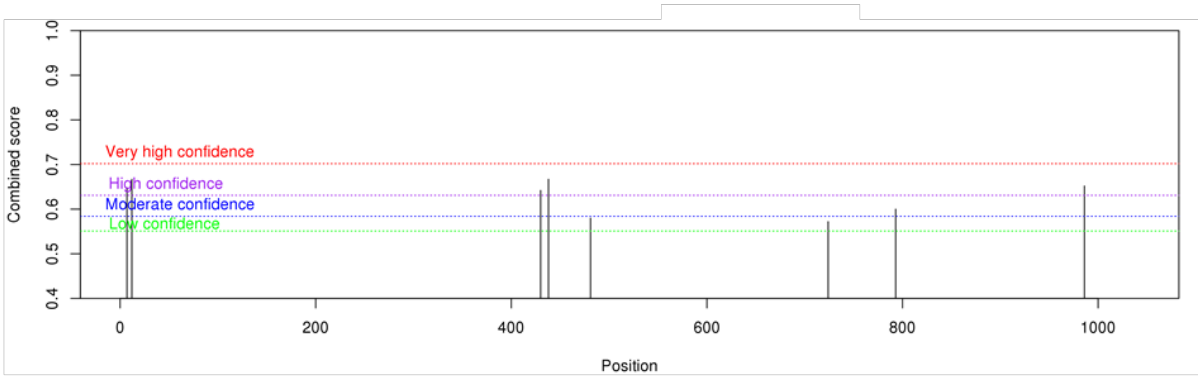

Position	Sequence context	Score(combined)	Decision
7	----------ATGAGAACTGGACTGATGACCAACTGCTT	0.648	m6A site (High confidence)
12	----------ATGAGAACTGGACTGATGACCAACTGCTTGGTTT	0.667	m6A site (High confidence)
430	TGCAAACCAGTTTTCGGCGTGGACTGCAGGACTGTGGAATGCCCT	0.642	m6A site (High confidence)
438	AGTTTTCGGCGTGGACTGCAGGACTGTGGAATGCCCTCCTGTTCA	0.667	m6A site (High confidence)
481	CAGCAGACCGCGTGTCCCCCGGACAGCTATGAAACTCAAGTCAGA	0.58	m6A site (Low confidence)
724	GATGGAGACATGTTTCGAATGGACAACTGTCGGTTCTGTCGATGC	0.572	m6A site (Low confidence)
793	ACCGCCCAGTGTGGTGAGATAAACTGCGAGAGGTACTACGTGCCC	0.6	m6A site (Moderate confidence)
986	ACTGCGTTGCGACCGTCTGCGGACAGACCTGCACAAACCCTGTGA	0.652	m6A site (High confidence)

Supplementary Figure S4.4. CircCRIM1 encodes protein via N^6-Methyladenosine (m^6A) modification, but not IRES element.

Supplementary Table S4.1: Primer sets used in shRNA vector construction.

Primer name	sequence (5' to 3')
Hsa-shCCRIM1-F	CGCGTCGCCCTGTGTGCGAAGATGAGAACTGGATTCAAGAGATC CAGTTCTCATCTTCGCACACAGGGCTTTTTTCCAAA
Hsa-shCCRIM1-R	AGCTTTTGGAAAAAAGCCCTGTGTGCGAAGATGAGAACTGGATC TCTTGAATCCAGTTCTCATCTTCGCACACAGGGCGA

Supplementary Table S4.2: Primer sets used in mutagenesis and infusion cloning.

Primer name	sequence (5' to 3')
Circmini-cCRIM1-infusion-F	TTTATACTTCAGGATCATGAGAACTGGACTGATGAC
Circmini-cCRIM1-infusion-R	TTACCTCCGCGGGTTAACCTTCGCACACAGGGCAACAC
Circmini-cCRIM1-mut-5'-F	AATGACTTTTTTTTTATACTTCAGGAGATGTTACAGCCCAGATAGC
Circmini-cCRIM1-mut-5'-R	TGGTCATCAGTCCAGTTCTCATCTGAAGTATAAAAAAAAAGTCATTA
Circmini-cCRIM1-mut-3'-F	GTTGCCCTGTGTGCGAAGGTAAGAAGCAAGGAAAAG
Circmini-cCRIM1-mut-3'-R	CTTTTCCTTGCTTCTTACCTTCGCACACAGGGCAAC
Circmini-cCRIM1-1xFlag-F	AATCCCTTTGAGTTTCCAAGTCAGGATATGGATTACAAGGATGACGACGATAAGTGCCTTTCAGCTTTAAAGAGAATTGAAGAA
Circmini-cCRIM1-1xFlag-R	TTCTTCAATTCTCTTTAAAGCTGAAAGGCACTTATCGTCGTCATCCTTGTAATCCATATCCTGACTTGGAAACTCAAAGGGATT
Circmini-cCRIM1-m6a-1-1xFlag-F	TTTTTATACTTCAGATGAGATCTGGACTGATGACCAACTGC
Circmini-cCRIM1-m6a-1-1xFlag-R	AGTTGGTCATCAGTCCTCATGATATCCTGAAGTATAAAAAAAAAGTC
Circmini-cCRIM1-m6a-2-1xFlag-F	GCAGTTGGTCATCAGTCCAGATCTCATCTGAAGTATAAAAA
Circmini-cCRIM1-m6a-2-1xFlag-R	AAGCAGTTGGTCATCAGACCAGTTCTCATCTGAAG
Circmini-cCRIM1-m6a-3-1xFlag-F	CGACCGTCTGCGGTCAGACCTGCACAA
Circmini-cCRIM1-m6a-3-1xFlag-R	TTGTGCAGGTCTGACCGCAGACGGTCG
Circmini-cCRIM1-m6a-1+21xFlag-F	TTTTATACTTCAGATGAGATCTGGTCTGATGACCAACTGCTTGG
Circmini-cCRIM1-m6a-1+21xFlag-R	CCAAGCAGTTGGTCATCAGACCAGATCTCATCTGAAGTATAAAA
Myocd-cCRIM1-infusion-F	GCCGTGTAATTCTAGAATGAGAACTGGACTGATGACCAAC
Myocd-cCRIM1-infusion-R	CCGCCCCGACTCTAGACTTCGCACACAGGGCAACAC

Supplementary Table S4.3: siRNAs used in knockdown of circCRIM1. *

siRNA name	Sequence
siRNA1	Sense - 5' GCCCUGUGUGCGAAGAUGAGAdTdT 3’ Antisense - 5' UCUCAUCUUCGCACACAGGGCdTdT 3'
siRNA2	Sense - 5' UGUGCGAAGAUGAGAACUGGAdTdT 3’ Antisense - 5' UCCAGUUCUCAUCUUCGCACAdTdT 3'

* 3’ dTdT hangover was added to each strand to increase nuclease resistance of siRNAs in the cell culture medium and within transfected cells.

Supplementary Table S4.4: Primer sets used in circRNA related RT-qPCR

Primer name	sequence (5' to 3')
circSOD2-Div-F	ATTCTGCCAGTGCGTCAAC
circSOD2-Div-R	CTGCAGGTTCGAATGGTGTT
circSOD2-Con-F	AGAGAAGCCAGATTGCTCCA
circSOD2-Con-R	TCCCTGAGGCTTTTGACACT
hsa-HPRT-F	GCTATAAATTCTTTGCTGACCTGCTG
hsa-HPRT-R	AATTACTTTTATGTCCCCTGTTGACTGG
hsa-cPMS1-F	GATCTCCTCATGAGCTTTGGTATCC
hsa-cPMS1-R	GACTAGTGAAAGAGTGGTCTGC
human-CYP-F	GACCCAACACAAATGGTTCC
human-CYP-R	TCGAGTTGTCCACAGTCAGC

Supplementary Table S4.5: Primer used in miRNA RT-qPCR

Primer name	sequence (5' to 3')
hsa-miR-106b-5p-q	ACACTCCAGCTGGGTAAAGTGCTGACAGT
hsa-miR-106b-5p-RT	CTCAACTGGTGTCGTGGAGTCGGCAATTCAGTTGAGATCTGCAC
hsa-miR-133a-3p-q	ACACTCCAGCTGGGTTTGGTCCCCTTCAAC
hsa-miR-133a-3p-RT	CTCAACTGGTGTCGTGGAGTCGGCAATTCAGTTGAGCAGCTGGT
hsa-miR-141-5p-q	ACACTCCAGCTGGGCATCTTCCAGTACAGT
hsa-miR-141-5p-RT	CTCAACTGGTGTCGTGGAGTCGGCAATTCAGTTGAGTCCAACAC
hsa-miR-145-5p-q	ACACTCCAGCTGGGGTCCAGTTTTCCCAGGA
hsa-miR-145-5p-RT	CTCAACTGGTGTCGTGGAGTCGGCAATTCAGTTGAGAGGGATTC
hsa-miR-149-5p-q	ACACTCCAGCTGGGTCTGGCTCCGTGTCTTC
hsa-miR-149-5p-RT	CTCAACTGGTGTCGTGGAGTCGGCAATTCAGTTGAGGGGAGTGA
hsa-miR-152-3p-q	ACACTCCAGCTGGGTCAGTGCATGACAGA
hsa-miR-152-3p-RT	CTCAACTGGTGTCGTGGAGTCGGCAATTCAGTTGAGCCAAGTTC
hsa-miR-15a-5p-q	ACACTCCAGCTGGGTAGCAGCACATAATGG
hsa-miR-15a-5p-RT	CTCAACTGGTGTCGTGGAGTCGGCAATTCAGTTGAGCACAAACC
hsa-mir15b-3p-q	ACACTCCAGCTGGGTAGCAGCACATCATGG
hsa-mir15b-3p-RT	CTCAACTGGTGTCGTGGAGTCGGCAATTCAGTTGAGTGTAAACC
hsa-mir16-1-3p-q	ACACTCCAGCTGGGCCAGTATTAACTGTGC
hsa-mir16-1-3p-RT	CTCAACTGGTGTCGTGGAGTCGGCAATTCAGTTGAGTCAGCAGC
hsa-miR-17-5p-q	ACACTCCAGCTGGGCAAAGTGCTTACAGTGC
hsa-miR-17-5p-RT	CTCAACTGGTGTCGTGGAGTCGGCAATTCAGTTGAGCTACCTGC
hsa-miR-183-5p-q	ACACTCCAGCTGGGTATGGCACTGGTAGAA
hsa-miR-183-5p-RT	CTCAACTGGTGTCGTGGAGTCGGCAATTCAGTTGAGAGTGAATT
hsa-miR-199a-3p-q	ACACTCCAGCTGGGACAGTAGTCTGCACAT
hsa-miR-199a-3p-RT	CTCAACTGGTGTCGTGGAGTCGGCAATTCAGTTGAGTAACCAAT
hsa-miR-199b-3p-q	ACACTCCAGCTGGGACAGTAGTCTGCACAT
hsa-miR-199b-3p-RT	CTCAACTGGTGTCGTGGAGTCGGCAATTCAGTTGAGTAACCAAT
hsa-miR-204-5p-q	ACACTCCAGCTGGGTTCCCTTTGTCATCCT
hsa-miR-204-5p-RT	CTCAACTGGTGTCGTGGAGTCGGCAATTCAGTTGAGAGGCATAG
hsa-mir206-q	ACACTCCAGCTGGGTGGAATGTAAGGAAGT
hsa-mir206-RT	CTCAACTGGTGTCGTGGAGTCGGCAATTCAGTTGAGCCACACAC
hsa-miR-20b-5p-q	ACACTCCAGCTGGGCAAAGTGCTCATAGTGC
hsa-miR-20b-5p-RT	CTCAACTGGTGTCGTGGAGTCGGCAATTCAGTTGAGCTACCTGC
hsa-miR-211-5p-q	ACACTCCAGCTGGGTTCCCTTTGTCATCCT
hsa-miR-211-5p-RT	CTCAACTGGTGTCGTGGAGTCGGCAATTCAGTTGAGAGGCGAAG
hsa-miR-212-3p-q	ACACTCCAGCTGGGTAACAGTCTCCAGTC
hsa-miR-212-3p-RT	CTCAACTGGTGTCGTGGAGTCGGCAATTCAGTTGAGGGCCGTGA
hsa-miR-21-5p-q	ACACTCCAGCTGGGTAGCTTATCAGACTGA
hsa-miR-21-5p-RT	CTCAACTGGTGTCGTGGAGTCGGCAATTCAGTTGAGTCAACATC

hsa-miR-23b-5p-q	ACACTCCAGCTGGGTGGGTTCCTGGCATGC
hsa-miR-23b-5p-RT	CTCAACTGGTGTCGTGGAGTCGGCAATTCAGTTGAGAAATCAGC
hsa-miR-25-3p-q	ACACTCCAGCTGGGCATTGCACTTGTCTCG
hsa-miR-25-3p-RT	CTCAACTGGTGTCGTGGAGTCGGCAATTCAGTTGAGTCAGACCG
hsa-miR-27a-3p-q	ACACTCCAGCTGGGTTCACAGTGGCTAAG
hsa-miR-27a-3p-RT	CTCAACTGGTGTCGTGGAGTCGGCAATTCAGTTGAGGCGGAACT
hsa-miR-27b-3p-q	ACACTCCAGCTGGGTTCACAGTGGCTAAG
hsa-miR-27b-3p-RT	CTCAACTGGTGTCGTGGAGTCGGCAATTCAGTTGAGGCAGAACT
hsa-miR-29a-3p-q	ACACTCCAGCTGGGTAGCACCATCTGAAAT
hsa-miR-29a-3p-RT	CTCAACTGGTGTCGTGGAGTCGGCAATTCAGTTGAGTAACCGAT
hsa-miR-29b-3p-q	ACACTCCAGCTGGGTAGCACCATTTGAAATC
hsa-miR-29b-3p-RT	CTCAACTGGTGTCGTGGAGTCGGCAATTCAGTTGAGAACACTGA
hsa-miR-29c-3p-q	ACACTCCAGCTGGGTAGCACCATTTGAAAT
hsa-miR-29c-3p-RT	CTCAACTGGTGTCGTGGAGTCGGCAATTCAGTTGAGTAACCGAT
hsa-miR-330-3p-q	ACACTCCAGCTGGGGCAAAGCACACGGCCTG
hsa-miR-330-3p-RT	CTCAACTGGTGTCGTGGAGTCGGCAATTCAGTTGAGTCTCTGCA
hsa-miR-361-5p-q	ACACTCCAGCTGGGTTATCAGAATCTCCAG
hsa-miR-361-5p-RT	CTCAACTGGTGTCGTGGAGTCGGCAATTCAGTTGAGGTACCCCT
hsa-miR-367-3p-q	ACACTCCAGCTGGGAATTGCACTTTAGCAA
hsa-miR-367-3p-RT	CTCAACTGGTGTCGTGGAGTCGGCAATTCAGTTGAGTCACCATT
hsa-miR-370-3p-q	ACACTCCAGCTGGGGCCTGCTGGGGTGGAA
hsa-miR-370-3p-RT	CTCAACTGGTGTCGTGGAGTCGGCAATTCAGTTGAGACCAGGTT
hsa-miR-489-3p-q	ACACTCCAGCTGGGGTGACATCACATATAC
hsa-miR-489-3p-RT	CTCAACTGGTGTCGTGGAGTCGGCAATTCAGTTGAGGCTGCCGT
hsa-miR-497-5p-q	ACACTCCAGCTGGGCAGCAGCACACTGTG
hsa-miR-497-5p-RT	CTCAACTGGTGTCGTGGAGTCGGCAATTCAGTTGAGACAAACCA
hsa-miR-516a-3p-q	ACACTCCAGCTGGGTGCTTCCTTTCA
hsa-miR-516a-3p-RT	CTCAACTGGTGTCGTGGAGTCGGCAATTCAGTTGAGACCCTCTG
hsa-miR-524-5p-q	ACACTCCAGCTGGGCTACAAAGGGAAGCAC
hsa-miR-524-5p-RT	CTCAACTGGTGTCGTGGAGTCGGCAATTCAGTTGAGGAGAAAGT
hsa-miR-593-3p-q	ACACTCCAGCTGGGTGTCTCTGCTGGG
hsa-miR-593-3p-RT	CTCAACTGGTGTCGTGGAGTCGGCAATTCAGTTGAGAGAAACCC
hsa-miR-612-q	ACACTCCAGCTGGGGCTGGGCAGGGCTTCTGAG
hsa-miR-612-RT	CTCAACTGGTGTCGTGGAGTCGGCAATTCAGTTGAGAAGGAGCT
hsa-miR-625-5p-q	ACACTCCAGCTGGGAGGGGGAAAGTTCTA
hsa-miR-625-5p-RT	CTCAACTGGTGTCGTGGAGTCGGCAATTCAGTTGAGGGACTATA
hsa-miR-637-q	ACACTCCAGCTGGGACTGGGGGCTTTCGGGCT
hsa-miR-637-RT	CTCAACTGGTGTCGTGGAGTCGGCAATTCAGTTGAGACGCAGAG
hsa-miR-642a-5p-q	ACACTCCAGCTGGGGTCCCTCTCCAAATGT
hsa-miR-642a-5p-RT	CTCAACTGGTGTCGTGGAGTCGGCAATTCAGTTGAGCAAGACAC
hsa-miR-671-5p-q	ACACTCCAGCTGGGAGGAAGCCCTGGAGGGG

hsa-miR-671-5p-RT	CTCAACTGGTGTCGTGGAGTCGGCAATTCAGTTGAGCTCCAGCC
hsa-miR-767-5p-q	ACACTCCAGCTGGGTGCACCATGGTTGTCTG
hsa-miR-767-5p-RT	CTCAACTGGTGTCGTGGAGTCGGCAATTCAGTTGAGCATGCTCA
hsa-miR-892b-q	ACACTCCAGCTGGGCACTGGCTCCTTTCTG
hsa-miR-892b-RT	CTCAACTGGTGTCGTGGAGTCGGCAATTCAGTTGAGTCTACCCA
hsa-miR-92a-3p-q	ACACTCCAGCTGGGTATTGCACTTGTCCCG
hsa-miR-92a-3p-RT	CTCAACTGGTGTCGTGGAGTCGGCAATTCAGTTGAGACAGGCCG
hsa-miR-92b-3p-q	ACACTCCAGCTGGGTATTGCACTCGTCCCG
hsa-miR-92b-3p-RT	CTCAACTGGTGTCGTGGAGTCGGCAATTCAGTTGAGGGAGGCCG
hsa-miR-93-5p-q	ACACTCCAGCTGGGCAAAGTGCTGTTCGTGC
hsa-miR-93-5p-RT	CTCAACTGGTGTCGTGGAGTCGGCAATTCAGTTGAGCTACCTGC
URP	TGGTGTCGTGGAGTCG

Supplementary Table S4.6: Primer sets and probes used in RNA-FISH

Primer name	sequence (5' to 3')
eGFP-T7	TAATACGACTCACTATAGTTCTTCTGCTTGTCGGCCAT
eGFP-T3	AATTAACCCTCACTAAAGGGGCACAAGCTGGAGTACAA
anti-rnoccrim1-bio	/5Biosg/CCCAGTCCTCGTCTTCACACACGGG/3Bio/
anti-hsaccrim1-bio	BIO/TCCAGTTCTCATCTTCGCACACAGGGCAAC

CHAPTER 5

CONCLUSION

This dissertation work was dedicated to establishing novel and robust therapeutic strategies that specifically target smooth muscle cells (SMCs) in neointima formation after the cardiovascular intervention. We identified the existence and expression pattern of a novel type of RNA molecule, circular RNA, in SMCs in response to platelet-derived growth factor-BB (PDGF-BB). Moreover, we elucidated the molecular mechanisms of circular SOD2 (circSOD2) in SMC proliferation (Chapter 3) and circular CRIM1 (circCRIM1) with continuous loop-translation ability in SMC phenotypic modulation (Chapter 4).

Several conclusions can be drawn from this dissertation:

1. CircRNAs are abundantly expressed in SMCs.

Consolidated pipeline for circRNA detection and expression analysis from rRNA-depleted RNA-Seq data of normal and PDGF-BB-treated SMCs identify 7,713 circRNAs, in which 323 circRNAs are differentially expressed.

2. CircSOD2 is activated by PDGF-BB, targeting circSOD2 in SMCs suppressed SMC proliferation.

CircSOD2 is up-regulated in proliferative SMCs induced by PDGF-BB. Knockdown and ectopic expression of circSOD2 inhibit and promote PDGF-BB-induced SMC proliferation, respectively, by regulating SMCs G1 to S cell cycle transition.

3. CircSOD2 sequesters miR-206, hence regulates SMC proliferation via NOTCH3-ERK1/2-CyclinD1-CDK4/6 axis.

In SMC, circSOD2 physically sponges with miR-206, an upstream inhibitor of a pro-proliferative regulator, NOTCH3. MiR-206 mimic rescues forced expression of circSOD2 induced SMC proliferation by saturating miR-206 binding site on circSOD2, thus suppressing NOTCH3-ERK1/2-CyclinD1-CDK4/6 axis.

4. CircSOD2 mediates injury-induced SMC proliferation, results in neointima formation.

CircSOD2 is up-regulated in the rat carotid artery balloon-injury model. Blockade of circSOD2 in rat injured-arteries suppresses neointima formation as a result of the reduction of proliferative SMCs in neointima.

5. CircCRIM1 is induced by PDGF-BB and vascular injury, targeting circCRIM1 in SMCs modulates SMC phenotype.

CircCRIM1 is up-regulated in de-differentiated SMCs induced by PDGF-BB and in the rat carotid artery balloon-injury model 3, 7, and 14 days post-injury. Knockdown and

overexpression of circCRIM1 suppress and promote PDGF-BB-induced downregulation of SMC makers genes expression, respectively.

6. CircCRIM1 regulates SMC phenotypic modulation via sponging miR-16.

CircCRIM1 physically binds with miR-16 in SMCs. MiR-16 mimic application can restore overexpression of circCRIM1-induced SMC markers downregulation.

7. CircCRIM1 can perform continuous loop-translation.

Owing to the unique closed-loop structure, circCRIM1 with a start codon and infinite ORF can undergo continuous loop-translation (at least two loops) in human cells. LC/MS detects the circCRIM1 encoded protein.

8. CircCRIM1 contains N^6-Methyladenosine (m^6A) modifications that drive the continuous loop-translation via recruiting YTH domain-containing family protein 3 (YTHDF3).

The level of m^6A on circCRIM1 can be upregulated by PDGF-BB treatment in SMCs. Substitution of m^6A sites on circCRIM1 impacts the translation efficiency and the binding ability with YTHDF3.